A pore-flow-through membrane reactor for selective hydrogenation reactions

vorgelegt von
Diplom-Chemikerin
Andrea Schmidt
aus Berlin

Von der Fakultät II - Mathematik und Naturwissenschaften
der Technischen Universität Berlin
Zur Erlangung des akademischen Grades
Dr. rer. nat.

genehmigte Dissertation

Promotionsausschuss:
Vorsitzender: Prof. Dr. rer. nat. R. Süßmuth
Berichter: Prof. Dr. rer. nat. R. Schomäcker
Berichter: Prof. Dr.-Ing. R. Dittmeyer

Tag der wissenschaftlichen Aussprache: 5. März. 2007

Berlin 2007

D 83

Abstract

A membrane reactor in pore-flow-though (PFT) mode was developed for selective hydrogenation reactions with the aim to increase yield, selectivity and space-time-yield compared to conventional fixed bed or slurry reactors that represent state of the art. Mass transfer limitations like internal pore diffusion that often occur in porous catalyst pellets can be prevented by forcing the reactants through the pores of a membrane which results in increasing the effective reaction rate and suppressing side reactions.

The catalytically active membranes were prepared by chemical wet impregnation of α-Al_2O_3-membrane tubes with a noble metal precursor. Characterization included AAS, SEM, TEM and EPMA. The partial hydrogenation of 1,5-cyclooctadiene served as a model reaction for a detailed study of process parameters like flow velocity, membrane pore size and catalyst loading. Intrinsic kinetics for this reaction was studied in a wide range of operating conditions with a Pd/α-alumina powder catalyst in a slurry reactor. The selectivity for cyclooctene obtained in the membrane reactor was 95 % at complete conversion which exceeds the selectivity obtained in a fixed bed with common catalyst pellets. A mathematical model was developed for simulation of the hydrogenation of 1,5-cyclooctadiene in the membrane reactor and to predict the performance of the hydrogenation process under different operating conditions. The proposed model can predict the influence of circulation rate and Pd-content of the membranes that were verified experimentally. A scale-up from the laboratory experimental setup with a single capillary (membrane area: 20 cm^2) to a pilot plant with bundles of 27-capillaries (membrane area: 540 cm^2) was accomplished by multiplication of the volume of the liquid phase, the membrane area and the circulation rate.

The application of the membrane reactor for industrially important hydrogenation reactions was tested for the fat hardening process, the partial hydrogenation of alkynes, the selective hydrogenation of geraniol, an allylic terpenic alcohol, and the selective hydrogenation of cinnamaldehyde, an α,β-unsaturated aldehyde. For the partial hydrogenation of the alkynes higher alkene selectivities were obtained in the PFT-reactor than in a fixed bed reactor. The selective hydrogenation of geraniol to citronellol failed because of severe deactivation of the catalytic membranes. The partial hydrogenation of polyunsaturated fatty acids in sunflower oil in the PFT-reactor resulted in a significantly lower content of saturated fatty acids than in a slurry reactor but the formation of *trans* fatty acids could not be prevented. The hydrogenation of cinnamaldehyde was carried out with selectivities of 80 % for the saturated aldehyde at complete conversions but at extremely low reaction rates compared to an egg shell catalyst in a slurry reactor. Deactivation of catalytic membranes was found to be more pronounced than of the egg shell catalyst.

Abstract

Ein Membranreaktor im Porendurchflussmodus (PFT-Reaktor) wurde für selektive Hydrierungen mit dem Ziel entwickelt, Ausbeute, Selektivität und Raum-Zeit-Ausbeute gegenüber konventionellen Festbett- und Slurry-Reaktoren, die momentan den Stand der Technik repräsentieren, zu erhöhen. Stofftransportlimitierungen durch Porendiffusion, die häufig in porösen Katalysatorpellets auftreten, können vermieden werden, wenn das Reaktionsgemisch konvektiv durch die Poren einer Membran strömt. Dadurch können Nebenreaktionen vermieden und die effektive Reaktionszeit verkürzt werden.

Katalytisch aktive Membranen wurden durch nasschemische Imprägnierung von α-Al_2O_3-Röhrchen mit entsprechenden Edelmetall-Precursoren hergestellt. Die Charakterisierung umfasste AAS, REM, TEM und EPMA. Die partielle Hydrierung von 1,5-Cyclooktadien diente als Modellreaktion für die detaillierte Studie von Prozessparametern wie Fließgeschwindigkeit, Porengröße und Katalysatorbeladung. Die intrinsische Kinetik für diese Reaktion wurde in einem weiten Bereich von Reaktionsbedingungen mit einem Pd/Al_2O_3-Pulverkatalysator in einem Slurry-Reaktor untersucht. Die Selektivität für Cyclooktadien, die in dem Membranreaktor erreicht wurde, betrug bei vollständigem Umsatz 95 %. Dies übertrifft die Selektivität, die mit gewöhnlichen Katalysatorpellets in einem Festbettreaktor erzielt werden. Ein mathematisches Modell wurde entwickelt, um die Hydrierung von 1,5-Cyclookten im Membranreaktor zu simulieren und um den Ablauf der Reaktion unter verschiedenen Reaktionsbedingungen hervorsagen zu können. Das vorgeschlagene Modell bildet die experimentell beobachteten Einflüsse von Volumenstrom durch die Membran und Pd-Gehalt der Membran gut ab. Ein Scale-Up vom Labormaßstab mit einer Einzelkapillare (Membranfläche: 20 cm^2) in den Pilotmaßstab mit 27-Kapillarbündeln (Membranfläche: 540 cm^2) wurde durchgeführt, indem das Flüssigkeitsvolumen, die Membranfläche und die Durchflussrate jeweils um den Faktor 27 erhöht wurden. Die Anwendung des Membranreaktors für industriell interessante Hydrierungsreaktionen wurde für die Fetthärtung, die partielle Hydrierung von Alkinen, für die selektive Hydrierung von Geraniol und Zimtaldehyd getestet. Für die partielle Hydrierung der Alkine wurden im PFT-Reaktor höhere Selektivitäten erzielt als in einem Festbettreaktor. Die selektive Hydrierung von Geraniol zu Citronellol scheiterte im PFT-Reaktor wegen einer starken Deaktivierung der katalytischen Membranen. Für die partielle Hydrierung von mehrfach ungesättigten Fettsäuren im Sonnenblumenöl war der Gehalt von gesättigten Fettsäuren im PFT-Reaktor sehr viel geringer als in einem Slurry-Reaktor. Die Bildung von *trans*-Fettsäuren konnte im PFT-Reaktor allerdings nicht verhindert werden. Die Hydrierung von Zimtaldehyd lief im PFT-Reaktor viel langsamer als im Slurry-Reaktor, aber mit vergleichbaren Selektivitäten für den gesättigten Aldehyd ab; die Deaktivierung war in der Membran stärker ausgeprägt als mit den Katalysatorpellets.

Acknowledgement

The presented work was created with the financial support of the German Federal Ministry of Education and Research for the project CaMeRa (Catalytic Membrane Reactor) under the auspices of CoNeCat (Competence Network on Catalysis).
In particular, I would like to thank my supervisor Prof. Dr. Reinhard Schomäcker for his guidance and his helpful suggestions, which made this work possible. I would like to convey my thanks to Prof. Dr. Roland Dittmeyer for being very much interested in my work and being my advisor.
I am most grateful to Dr. Aurel Wolf and Rafael Warsitz from *Bayer Technology Services*, to Gundula Fischer and Dr. Ingolf Voigt from *Hermsdorfer Institut für Technische Keramik* and to Daniel Urbanczyck from *Karl-Winnacker-Institut* for collaboration and useful discussions.
A number of colleagues helped in getting this thesis done. Warm thanks to Gabi Vetter for all her generous help in the laboratory and to Björn Awe, Isis Santos Costa, Mehtap Özaslan and Frédéric Hasché for the contribution of their diploma theses.

Berlin, March 2007

Table of Contents

1 Introduction

Modern industrial chemistry is based on catalytic processes. For the production of organic chemicals mainly heterogeneous catalysts are applied. Common types of reaction in this field are catalytic hydrogenation reactions. For selective hydrogenations side reactions must be avoided. Oftentimes, a partially hydrogenated product is desired and the consecutive reaction to the completely hydrogenated product has to be suppressed. A very important process in food industry, e.g., is the fat hardening for the production of margarine by partial hydrogenation of polyunsaturated fatty acids in a vegetable oil. This process aims on improving the oxidation stability and increasing the melting point of the fat by decreasing the polyunsaturated fatty acid content in the oil without increasing the content of saturated fatty acid. But also, the production of many fine chemicals like pharmaceuticals, colorants, food additives, cosmetics, vitamins and photo chemicals, include at least one selective hydrogenation step. As the reactants and intermediates are often temperature-sensitive and complex-structured, the reactions are carried out under mild reaction conditions in liquid phase. In the majority of cases, the ingredients consist of more than one functional group, which can result in a spectrum of products. Hence, careful tuning of all process parameters like catalyst type and amount, solvent, temperature, pressure and stirring are required in order to maximize the yield and selectivity of the desired product. A diminishment of side products in a process is preferable from an economical and ecological point of view: feedstock is utilized efficiently and energy costs are reduced by eliminating costly and time-wasting separation of product mixtures by distillation. Generally hydrogenation reactions for fine chemicals are carried out in liquid phase in suspension reactors with fine catalyst powders or in fixed bed reactors with catalyst pellets. In suspension reactors the separation of the catalyst from the product is a severe problem. In fixed bed reactors diffusion limitations often appear which promote side reactions and decrease the selectivity for the desired product. A reactor system where no mass transfer limitations appear and the separation of the catalyst after reaction becomes unnecessary would be preferable. A promising concept that combines both demands is a membrane reactor. Different types of membrane reactors are described in literature, e.g. systems in which the membrane separates products and reactants or systems where the membrane properties prevent diffusion limitations and, by this way suppress side reactions. In the recent years, there has been a lot of research and development in the field of membrane reactors but an industrial application is still missing. Technical barriers, short membrane lifetime and investigation costs have up to now hindered the introduction of membrane reactors on a technical scale. Further development and

improvement on membrane reactors should help to remedy deficiencies and to make this new reactor system mature for industrial application.

2 Background

This chapter gives an overview of development, manufacture, characterization and deactivation of catalysts as it was part of this work to develop preparation methods for catalytically active membranes. Theoretical aspects that had to be considered in the planning of the experiments and in the interpretation of the results are discussed. The mechanism of heterogeneously catalyzed reactions will help to understand the processes that occur in porous, catalytic membranes. Several types of reactors that are commonly used for multiple phase reactions are presented and the motivation for the development of a new reactor concept, the membrane reactor, are explained. Finally, definitions and fundamentals of membranes as well as of different types of membrane reactors are demonstrated.

2.1 Catalyst development

Priorities in today's industry emphasize more efficient utilization of feedstock and energy. A catalyst plays an important role in economical and ecological production in chemical industry. A great effort is still needed in development of catalytic processes for selective conversion of materials in order to avoid waste and reduce energy costs. Therefore, great demands are posed for a catalytic system. The activity of the catalyst is a key in order to accelerate the rate of a reaction. The selectivity for the desired product becomes a factor when multiple reactions, parallel or consecutive, are present. Lifetime of a catalyst must be acceptable because deactivation has a profound effect on the engineering and economics of a process.
Most of the catalytic processes in industry are heterogeneously catalyzed because the advantage of easy separation of the catalyst from the product prevails over the disadvantage of mass transport limitations. Most commonly, heterogeneous systems consist of solid catalysts and gaseous or liquid reactants, sometimes both. Interfacial phenomena like diffusion, absorption and adsorption play critical roles in establishing the reaction rate. Common types of catalysts include pellets, extrudates, spheres and granules, used in packed bed operations. Significant factors for process design in catalyst beds are a uniform fluid flow and a pressure drop through the bed as small as possible. The particle diameter has to be chosen carefully because larger particles are generally cheaper and result in a decreased pressure drop but due to a smaller overall surface lead to smaller conversion. The mechanical crushing of the particles is another parameter that has to be taken into consideration by process designers as fine particle fractures in interstices can cause plugging, hot spots and pressure drop.

The catalyst must be a good compromise providing good fluid flow, activity and stability. These factors depend on the reaction itself, reactor design, process conditions and economics. A good fluid flow means a low pressure drop and a well distributed flow without any abrasion of the catalyst. High chemical activity and selectivity is achieved through selecting the correct chemical components and a high specific active surface, which is generally provided by porous materials as support for the catalyst. Lifetime stability requires resistance against deactivation due to poisoning, sintering and fouling.

2.1.1 Catalyst components

Most catalysts consist of an active component and a support, and sometimes also, a promoter. The active component is responsible for the principal chemical reaction; it can be a metal, semiconductor or insulator. Over 70% of known catalytic reactions involve some form of metallic components. Metals, particularly *d*-electron transition metals, promote electron transfer with adsorbed molecules by overlapping electronic energy bands. Atomic electron configurations explain trends in adsorption and catalysis. Similarities in groups within the periodic table are rationalized. For hydrogenation reaction of olefins, e.g., Ni, Pd or Pt is suitable as catalyst metal.

The most important function of the support is the maintenance of a high surface area for the active component. This is why porous materials like Al_2O_3, SiO_2 and activated carbon are commonly used as support. Moreover oxides, normally considered as ceramic materials, have high melting points (1800-3000°C) which secure from thermal growth of the material and provide a good thermal and mechanical stability. The support functions as a stable surface over which the active component, often a precious metal, is dispersed in crystallites. Sintering of the crystallites through migration over the surface followed by coalescence should be avoided because it reduces the active surface. Important factors are crystallite concentration, temperature, interaction with the support and catalyst manufacture. As the surface of the catalyst support is formed by the pore walls a good accessibility of the pores is required. For a fast mass transport of the reactants a pore diameter larger than the effective molecule diameter of the reactants is necessary. Furthermore, the selectivity for the desired product can strongly decrease when the transport of the product out of the pores is limited by diffusion and side reactions take place. For the choice of an adequate catalyst support material the knowledge of its texture (specific surface area, pore volume, pore structure) and the relation between chemical reaction, mass and heat transfer and pore structure is necessary.

2.1.2 Catalyst deactivation

All industrially applied catalysts undergo a form of aging during their operating time. Aging can be caused by physical or chemical impacts that are determined by the operating conditions of the process. The most important reasons for deactivation of a catalyst are coking, poisoning, fouling, sintering or particle failure (Tab. 2.1).

Table 2.1: Causes for deactivation

Type	cause	Results
chemical	coking	loss of surface, plugging
	poisoning	loss of active sites
mechanical	fouling	loss of surface
	particle failure	bed channelling, plugging
Thermal	sintering	loss of surface
	compound formation	loss of surface and component
	phase changes	loss of surfaces

Coking describes a process where carbonaceous residues deposit on the catalyst surface and, thereby, decrease the accessible surface area, encapsulate active components or block pores. This type of deactivation is experienced by all catalysts to some extent. When these effects become significant the coked catalyst has to be regenerated, or, if not possible, must be replaced. A catalyst poison, however, is any agent that reacts permanently with an active site, e.g. simple ions like halides or sulfide, complex molecules or other metals like Pb compounds. Fouling describes the deposition of reactor debris, corrosion products and salts from the raw material on the catalyst surface which also results in pore clogging and blocking of active surfaces. Sintering can diminish the dispersing function of the support when supported crystallites move closer together, accelerating loss of active surface. Particle failure by crushing and abrasion is particularly a problem in catalyst beds because it results in gradual deterioration of mechanical properties like channelling, pressure drop increase and hot spots which then again is associated with thermal and coking effects. Catalyst deactivation can further be caused by loss of active components through vaporization at elevated temperatures or phase change of active components in thermodynamically more stable phases. Some of these deactivation processes are reversible and a regeneration of the catalyst, e. g. in oxidizing atmosphere and subsequent reactivation, is possible [2.1, 2.2].

2.1.3 Catalyst preparation

Several preparation methods for deposition of the active component on the support are applied in catalyst production. The simplest way is to impregnate the support with a (preferably) aqueous solution of the active component under exactly defined conditions (concentration, temperature, time) [2.3]. The solubility of the salt must be sufficient in order to give convenient volumes at prescribed temperatures in the solvent. The choice of the anion is based on solubility, availability, costs and impurities of the metal salt. The nature of the anion can influence the stability or activity of the catalyst. It has to be removed by washing, volatilization during drying or calcination. After impregnation the catalyst has to be activated by reducing the metal cation to elementary metal, e.g. Pd^{2+} in Pd^{0}. As reducing agents, among others, hydrogen or solutions of $NaBH_4$ and $NaH_2PO_2 \cdot H_2O$ are applicable. Reduction can also be carried out in hydrogen flow at elevated temperatures. Drying occurs through evaporation of the solvent from the inner pores of the support. The rate of drying should be carefully considered as a very fast drying process, at too high temperatures, leads to an enrichment of the active component as a layer in the surface of the support. Calcination is a further heat-treatment that can be applied in order to remove precursor remains and in order to stabilize the bonding between the active component and the support. During calcination oxides as catalyst precursors are developed which have to be activated afterwards to catalytically active metal. Ideally, the active component should be fine dispersed in the whole pore structure of the support in order to obtain a good utilization of the expensive active component and in order to avoid sintering.

A recently developed technique for catalyst preparation is chemical vapor deposition (CVD). The catalyst precursor, a sublimable or volatile substance that contains the active component, is thermally decomposed in reactive intermediates which adsorb on the support material. An easy preparation method of Pd/alumina membranes by MOCVD (metal organic chemical vapour deposition) is described in detail by Reif [2.4]. The deposition of Pd on different support material by MOCVD is also reported by Schlüter [2.5].

2.1.4 Catalyst characterization

The characterization of the physical and chemical structure of a catalyst is necessary in order to reveal coherences between material structure and activity, selectivity and lifetime of the catalyst. Physical characterization includes determination of pore volume, pore size distribution and specific surface area. Chemical characterization uses spectroscopic or microscopic methods. From the multiplicity of characterization methods for catalysts only those will be considered here that cover the morphology and composition of the catalyst, the

dispersion and the size of the metal crystallites on the support and the amount of the loaded metal on the support.

A powerful tool for studying the overall topography of a catalyst is *scanning electron microscopy (SEM)*. It scans over a sample surface with a probe of electrons (5-50 kV). Backscattered or emitted electrons produce an image on a cathode-ray tube, scanned synchronously with the beam. Sample preparation is easy; sometimes a surface coverage with gold or carbon is necessary in order to ensure electric conductivity. This technique is limited by the resolution of the applied instrument which normally allows the identification of crystallites down to 5 nm. In Fig. 2.1 typical SEM images of an alumina membrane surface in different magnifications are illustrated. SEM images are characterized by depth of focus.

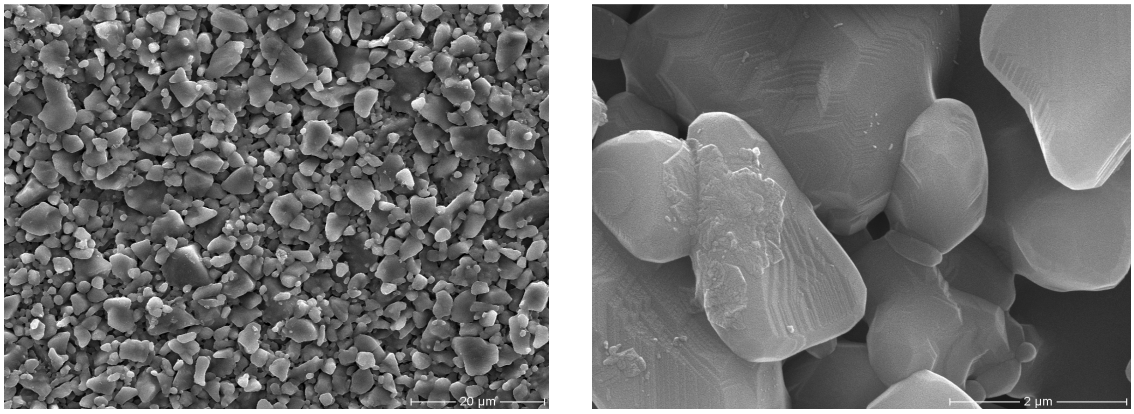

Fig. 2.1: SEM images of alumina membrane surface in different magnifications

Another imaging technique is the *transmission electron microscopy (TEM).* 100 kV or higher electrons are transmitted through a thin sample and the scattered electrons are magnified with electromagnetic optics. Improved information can be received by bright-field, dark-field or lattice imaging. Disadvantages of this method are the necessity of an extensive sample preparation (as the electron beam has to pass through the sample that must be reduced to very thin particles in the size of 50 – 100 nm). Also, high vacuum must be applied in order to avoid interaction of electrons with gas atoms. The images that are recorded and analyzed may not be representative for the average state of the catalyst.

Spectroscopic methods are applied for qualitative and quantitative identification of elemental composition of the catalyst. *Atomic absorption spectroscopy (AAS)* uses the absorption of light to measure the concentration of gas-phase atoms. The liquid sample must be vaporized in a flame or a graphite furnace. Ultraviolet or visible light is absorbed from the atoms and induces transitions to higher electronic levels. The amount of absorption allows the

determination of the concentration. Calibration of the instrument with standards of known concentrations is necessary.

Electron probe microanalysis (EPMA) is an often used, non-destructive method in which a focused electron beam impinges the sample and induces emission of secondary electrons, backscattered electrons and photons characteristic of the element. The element concentrations can be determined from the intensity of the detected wavelengths by a wavelength dispersive X-ray analysis (WDX). Backscattered electrons provide an image of the sample. With this method only punctual sample analysis is possible.

This is only a selection from a variety of analytic methods to characterize catalyst properties. *X-ray diffraction (XRD)* or *x-ray fluorescence* as well as chemisorption methods are also possible. The researcher has to select the techniques that yield the most information for the given application and know the capabilities and limitations of each method. A problem in this work, e.g., was the determination of Pd particle sizes and their dispersion in the membrane because of very low amounts of the metal loaded in the support. Instruments and techniques that have a low sensitivity failed for this application.

In Fig. 2.2 the working steps that are necessary in order to prepare a suitable catalyst for a special reaction are summarized. They include preparation, characterization and testing of the catalyst in laboratory scale, evaluation and interpretation of kinetic data, comparison to other catalysts as well as optimization and scale up.

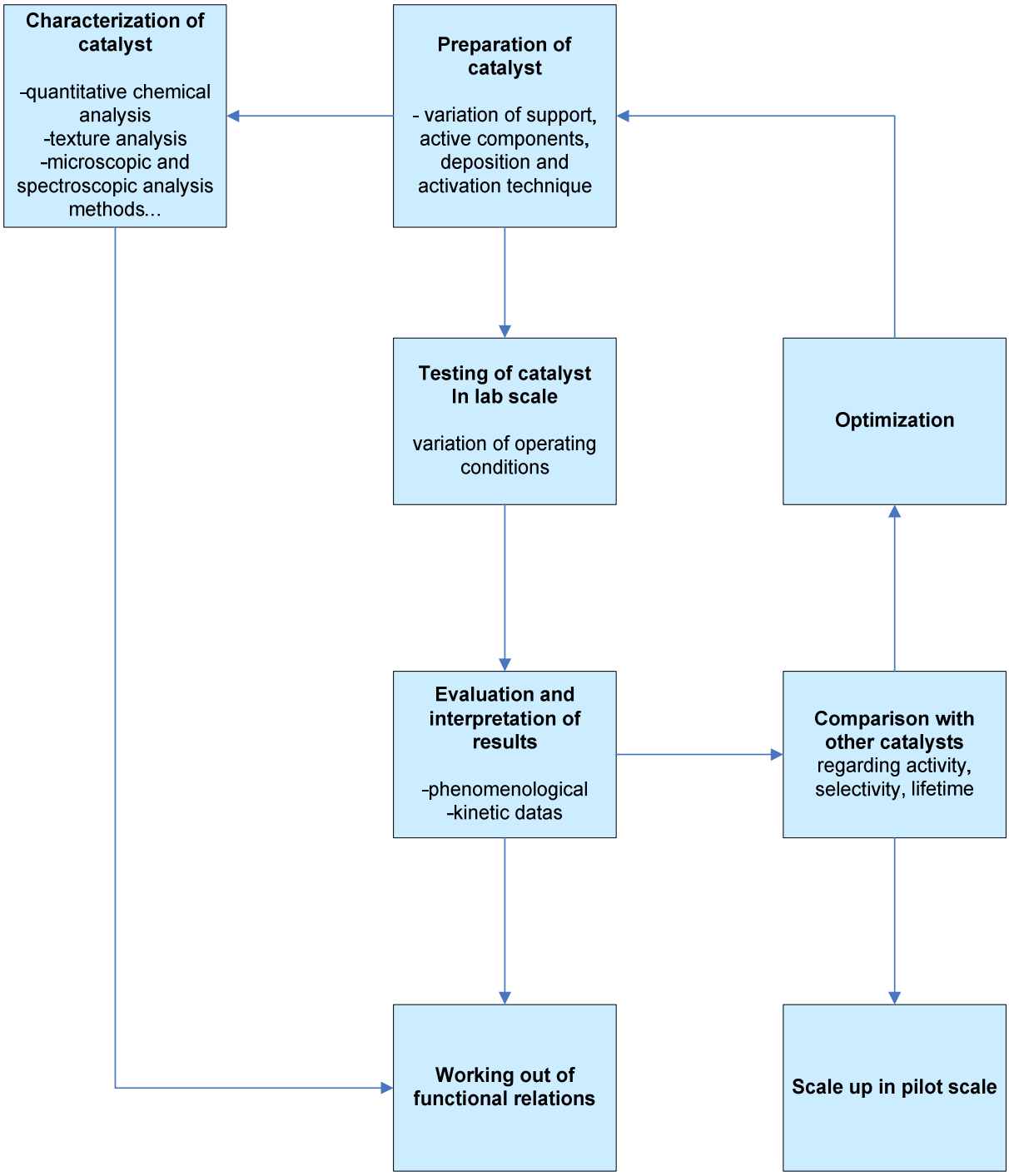

Fig. 2.2: Working steps for development of a suitable catalyst for a special reaction

2.2 Heterogeneously catalyzed three-phase reactions

Reactions involving multiple phases are frequently met in chemical industry. Examples are the hydrogenation of nitro compounds or the hydrogenation of edible oils [2.6]. Of particular interest are reactions in which a solid catalyst comes in contact with a liquid and gaseous phase. The heterogeneous catalyst does not dissolve in the gaseous or liquid reaction mixture. Consequently, the reaction occurs at or near the interface between catalyst and reactant mixture. The main problem of multiple phase reactions is that a high effective reaction rate is often not accessible because of mass transfer limitations. The reaction rate in heterogeneously catalyzed, multiple phase reactions depends on the kinetics of the chemical reaction (intrinsic kinetics, micro kinetics) and on the kinetics of mass transport at the interfaces and in the phases (macro kinetics). For the design of a reactor it is important to determine the intrinsic kinetics. With the knowledge of the maximal possible reaction rate, a catalyst can be improved and optimized for a particular process.

2.2.1 Reaction and mass transport in multiphase reactions

Mass transfer phenomena play an important role in heterogeneous catalyzed, multiple phase reactions. Dependent on the chosen process parameters, mass transfer can even be the rate determining step. The following mass transfer and reaction steps have to be considered:

1. Mass transfer of the gaseous reactant from the free gas phase into the gas-liquid-interface;
2. Mass transfer by diffusion of the dissolved gaseous reactant in the bulk of the liquid ;
3. Diffusion of the liquid reactant through the liquid-solid-interface to the catalyst;
4. Diffusion of the dissolved reactants within the pores of the catalyst to the active sites – pore diffusion;
5. Adsorption of the dissolved reactants at the catalytic active surface – chemisorption ;
6. Chemical reaction at the catalyst surface;
7. Desorption of the product;
8. Diffusion of the product out of the pores to the external surface of the catalyst particle and
9. Diffusion of the product through the external liquid interface into the bulk of the liquid.

In Fig. 2.3 the processes for a catalytic reaction at a porous catalyst pellet are illustrated schematically. The slowest step determines the effective rate of the reaction. The aim for process design should be to reduce mass transfer limitations to a minimum because they decrease the effective reaction rate and can promote side reactions.

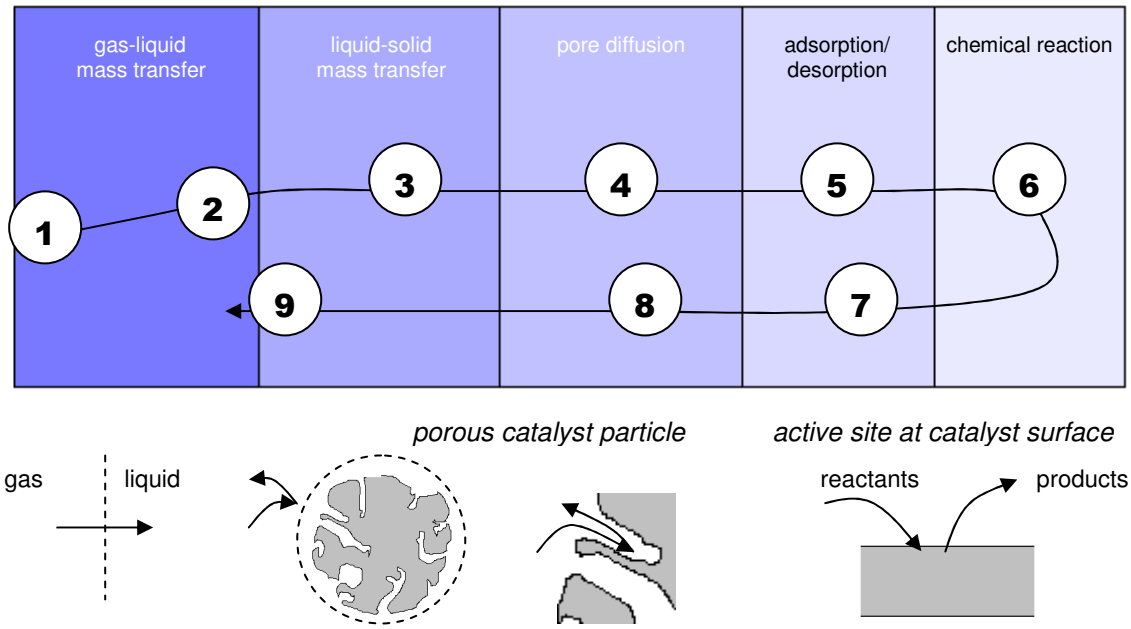

Fig. 2.3: Steps in heterogeneous catalyzed, three-phase reaction at a porous catalyst

Kinetics of a chemical reaction

The reaction *rate* describes the change of concentrations of reactants and products that occurs per unit of time. The rate of the reaction of the reactants A and B can be given by the following rate law; expressed by power law approach:

$$r = -\frac{1}{V_R} \cdot \frac{dc_A}{dt} = k \cdot c_A^a \cdot c_B^b \qquad \text{(eq. 2.1)}$$

r: reaction rate

V_R: reaction volume

c: concentration

k: rate constant

a, b: reaction orders

The temperature dependency of the rate constant *k* is described by the Arrhenius law:

$$k = k_0 \cdot e^{-\frac{E_A}{RT}} \qquad \text{(eq. 2.2)}$$

k_0: Arrhenius preexponential factor
E_A: activation energy
R: gas constant
T: temperature

The kinetics of a chemical reaction is determined experimentally by systematic variations of the impact parameters (reactant concentrations, temperature and, for catalytic reactions, concentration of the catalyst). For the determination of the intrinsic kinetics the reaction must be free of mass transfer limitations.

Gas-liquid mass transfer

The first step in multiphase reactions (gas/liquid/solid) is the transfer of the gas (in this work hydrogen) through the gas-liquid interface. Here, the gas sided or the liquid sided mass transfer, dependent on the solubility of the gas in the liquid, can be influencing. In this case, the solubility of hydrogen in the liquid phase is limited and can be described by the Henry law whereby the hydrogen concentration in the liquid phase is proportional to the hydrogen partial pressure at the interface:

$$c_{H_2,l} = H \cdot p_{H_2} = H \cdot c_g \cdot RT \qquad \text{(eq. 2.3)}$$

H: Henry constant
p: partial pressure
R: gas constant
T: temperature

The rate of mass transfer from the gas phase into the liquid can be described as follows:

$$r_{H_2,eff} = \beta_{gl} \cdot A_{gl} \cdot (c_{H_2,g} - C^*_{H_2,g}) = \beta_{ll} \cdot A_{gl} \cdot (c^*_{H_2,l} - c_{H_2,l}) \qquad \text{(eq. 2.4)}$$

β: mass transfer coefficient

A: transfer area
c*= concentration at interface

Consequently, the rate of mass transfer depends on the size of the transfer area and the hydrogen concentration. The problem of low hydrogen solubility in liquids is technically mostly solved by an increased hydrogen pressure. The gas-liquid mass transfer can be improved by intensive stirring.

Liquid-solid mass transfer

For the mass transfer from the liquid to the solid catalyst the gaseous reactant, dissolved in the liquid (H_2), as well as the liquid reactant (A) has to be considered:

$$r_{A,eff} = \beta_{ls,A} \cdot A_{ls} \cdot (c_{A,l} - C_{A,s}) \qquad \text{(eq. 2.5)}$$

$$r_{H_2,eff} = \beta_{ls,H_2} \cdot A_{ls} \cdot (c_{H_2,l} - C_{H_2,s}) \qquad \text{(eq. 2.6)}$$

This mass transfer step becomes rate determining when the gas-liquid mass transfer is relatively fast, i.e. the bulk liquid is saturated with hydrogen, and the activity of the catalyst is relatively high.

Pore diffusion

The role of mass transfer in the catalyst pores by diffusion can be quantified with two parameters, the Thiele parameter Φ and the effectiveness factor η. The Thiele parameter can be interpreted as the ratio of the intrinsic reaction rate to the diffusion rate:

$$\Phi = R\,(k^{n-1} / D_{eff})^{0.5} \qquad \text{(eq. 2.7)}$$

R: radius (for a spherical catalyst particle)
k: rate constant
D_{eff}: effective diffusion coefficient
n : reaction order

The effectiveness factor η is defined as the ratio of measured reaction rate to the reaction rate without pore diffusion influence. The effectiveness factor can be estimated from the size and the geometry of the catalyst particles, the effective diffusion coefficient, the concentration of the regarded reactant (for a reaction that is not first order) and the intrinsic reaction rate.

For a first-order reaction occurring in a spherical catalyst pellet the Thiele parameter and the effectiveness factor result in

$$\Phi = R\,(k / D_{eff})^{0.5} \qquad \text{(eq. 2.8)}$$

$$\eta = (3 / \phi)\,[1 / \tanh \phi - 1 / \phi] \qquad \text{(eq. 2.9)}$$

A plot of the effectiveness factor vs. the Thiele parameter for diffusion in a porous catalyst is illustrated in Fig. 2.4. The effectiveness factor is unity if the Thiele parameter is much smaller than one, which means the reaction is not diffusion limited. With a Thiele parameter greater than one, the effectiveness factor declines and the reaction becomes diffusion controlled. Rates of pore-diffusion controlled reactions can be increased by reduction of the catalyst particle radius.

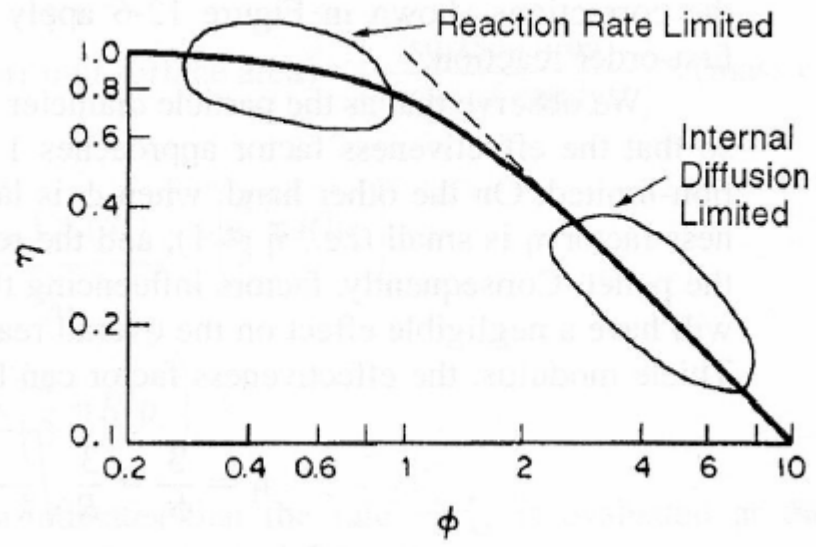

Fig. 2.4: Correlation of effectiveness factor and Thiele parameter for a reaction order of 1 and a spherical catalyst particle

Adsorption and desorption

In heterogeneously catalyzed reactions the reactants have to adsorb on the catalyst surface. In catalysis, adsorption is almost always chemisorption which results from chemical

interactions between the reactant molecule and the solid surface. Physical adsorption is driven by *Van der Waals* forces and is much weaker and unspecific.
The rate of adsorption of a reactant molecule that adsorbs at an active site on the catalyst surface depends on concentration or partial pressure *p* of the reactant and on the number of active sites [2.2]. In a dynamic equilibrium of adsorption and desorption the coverage of the catalyst surface θ_1 is given by:

$$\Theta_1 = \frac{K_1 p_1}{1 + K_1 p_1} \qquad \text{(eq. 2.10)}$$

where $K_1 = k_{ads} / k_{des}$ is the adsorption equilibrium constant. This correlation describes the *Langmuir* adsorption isotherm for molecular adsorption. For the adsorption of more than one component the equation becomes

$$\Theta_i = \frac{K_i p_i}{1 + \sum K_i p_i} \qquad \text{(eq. 2.11)}$$

For a reaction $A + B \rightarrow Products$ where both reactants are adsorbed at the catalyst surface (*Langmuir-Hinshelwood-kinetics*) the reaction rate is given by:

$$r = k \Theta_A \Theta_B \qquad \text{(eq. 2.12)}$$

and it follows with eq. 2.12

$$r = k \frac{K_A p_A K_B p_B}{(1 + K_A p_A + K_B p_B)^2} \qquad \text{(eq. 2.13)}$$

For hydrogenation reactions in the presence of metals from the VIII group of the periodic table (Fe, Ru, Os, Co, Rh, Ir, Ni, Pd, Pt) the reaction rate can be generally described by the *Langmuir-Hinshelwood kinetics* [2.1].

Activity and selectivity

Catalytic activity can be expressed in terms of reaction rates, preferentially normalized to the metal surface area for supported metal catalyst. Alternatively, the conversion *X* of the reactant, or conversion versus time plots, can be used for estimating the activity of a catalyst:

$$X = \frac{n_{i,0} - n_i}{n_{i,0}} \qquad \text{(eq. 2.14)}$$

n_i: mole number of reactant i
$n_{i,0}$: initial mole number of reactant i

The space-time-yield *STY*, expressed in units of amount of product in the reactor per unit time and unit reactor volume V_R or mass of catalyst is a readily accessible measure for activity [2.3]:

$$STY = \frac{\dot{n}}{V_R} \qquad \text{(eq. 2.15)}$$

$\dot{n}$ *= molar flow*

The selectivity *S* is defined as the amount of desired product obtained per amount of consumed reactant.

$$S = \frac{n_P \cdot (-\nu_A)}{(n_{A,0} - n_A) \cdot \nu_P} \qquad \text{(eq. 2.16)}$$

n: mole number
ν: stoichometric factor
P: product
A: reactant

Selectivity values are only useful in combination with the conversion. The selectivity indicates the relative rates of two or more competitive reactions, e.g. in parallel reactions (I, II) or in consecutive reactions (III). In case I and II the selectivity for the products P and Q is independent of the conversion of the reactants. In case III the selectivity for product P is 100% initially and decreases gradually with increasing conversion (Fig. 2.5). If P is the desired product the consecutive reaction to Q should be prevented. This can be obtained by stoppage of the process at low conversions (which is not preferable) or by choosing appropriate reactor type and reaction conditions [2.1, 2.2, 2.3].

Parallel reactions:

Case I

$$A \rightarrow P$$
$$B \rightarrow Q$$

Case II

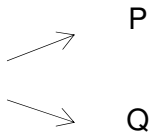

Consecutive reaction:

Case III

$$A \rightarrow P \rightarrow Q$$

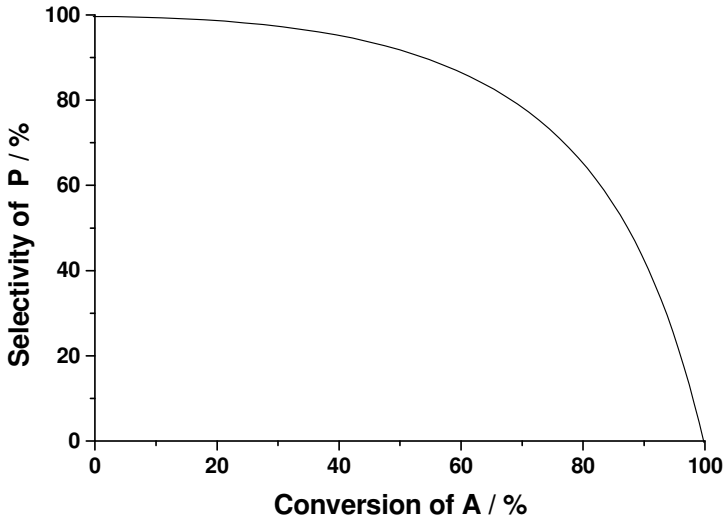

Fig. 2.5: Typical selectivity-conversion plot for a consecutive reaction (ratio of rate constants k_1:k_2= 10:1)

2.2.2 Three-phase-reactors

Three-phase reactors in industrial practice are classified as suspension or fixed-bed reactors depending on the catalyst arrangement. Fixed-bed reactors can operate in trickle bed (Fig. 2.6a) or bubble-flow mode (Fig. 2.6b). In trickle bed mode, the reactants in liquid phase are flowing downwards through the catalyst bed while the gaseous reactant flows in counter-current or co-current direction. If gaseous and liquid reactants are fed into the bottom of the

column and are flowing upwards through the fixed-bed catalyst, the reactor operates in bubble flow mode. The advantages of trickle bed reactors are:

- fast gas diffusion through the liquid film to the catalyst surface
- little back-mixing
- easy catalyst separation
- simple catalyst regeneration

However, the trickle-bed reactor has some disadvantages such as

- poor heat transfer (which is a problem for highly exothermic reactions, e.g. hydrogenation and oxidation reactions)
- unused catalyst in case of incomplete wetting
- possibility of channelling
- pore diffusion effects when size of porous catalyst pellets is too large and high pressure drop when catalyst particle size is too small

Therefore, process designers have to consider carefully catalyst shape and size, diameter/length ratio and liquid flow distribution through the catalyst bed. The particle size is limited by the pressure drop. However, diffusion problems appear when the particles are too large. Bubble flow reactors are preferred for reactions with low space velocity. With this reactor type the risk of lifting the catalyst bed by the gas flow exists. This has to be avoided by a sieve above the catalyst bed. Anyhow, extraordinary charges can lead to abrasion of the catalyst and early blocking of the sieve.

Suspension reactors include slurry reactors (stirred tank vessels, Fig. 2.6c) and bubble columns. The aim of suspension reactors is an intimate contact between the gaseous phase, dispersed in the liquid phase, and also the finely dispersed solid catalyst. The particle size of the solid catalyst is kept small (< 200 µm) in order to keep the catalyst suspended by the turbulence of the liquid. Because of the small catalyst particle size, normally no mass transfer limitations occur. However, a serious disadvantage is the difficult and expensive catalyst separation from the product. Small catalyst concentrations in the slurry reactor cause low volume related reaction rates and require large reactor volumes. Nevertheless, suspension reactors are successfully employed in chemical industry, particularly for hydrogenation reactions, because of a good heat transfer, temperature control, catalyst utilization and a simple design. Furthermore, the slurry reactors can be used as multi-purpose reactors for the production of pharmaceuticals, fine chemicals and polymers.

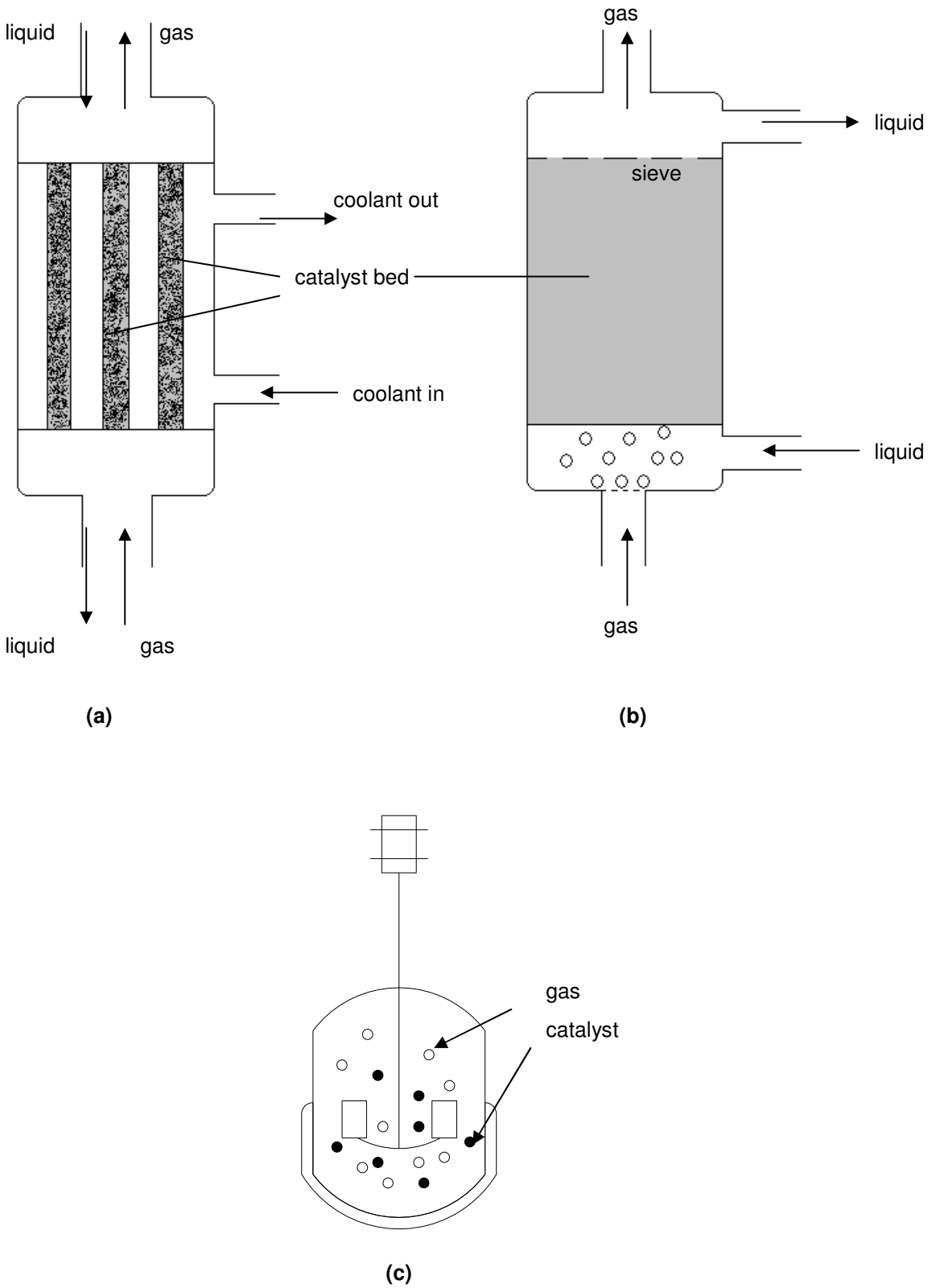

Fig. 2.6: Scheme of trickle-bed (here: tube bundle) in counter-current flow (a), bubble-column (b) and slurry reactor (c)

Two main problems for three-phase reactions in conventional reactor systems become obvious: internal pore diffusion limitations when the catalyst particles in fixed bed reactors are too large (however necessary in order to handle pressure drops) and the difficulty to separate the catalyst from the product when catalyst particles are too small, which is the case in slurry reactors [2.7]. The motivation for finding a new reactor concept that solves both problems led to the development of a membrane reactor concept.

Numerous types of membrane reactors have been proposed in recent years. Most of them couple a catalytic conversion with a separation effect provided by the integrated membrane. For example, high conversion can be achieved for equilibrium restricted reactions if the reaction product is removed from the reaction mixture through a permselective membrane. Additionally, in some catalytic reactions the control of selectivity can be improved in membrane reactors. More details about membrane reactor types will be described in the next section 2.3.

The membrane reactor investigated in this work for hydrogenation reactions operates in pore-flow through mode, using a porous membrane that has no separating functions but acts as a support for the catalyst. The catalyst is immobilized as nanoparticles in the membrane pore structure. Hydrogen is dissolved in the liquid phase in a saturation vessel, connected to the actual membrane reactor, by a gas-inducing stirrer at high rotational speed. The reactants in liquid phase are pumped through the pores of the membrane where the reaction takes place. Due to the low hydrogen solubility in the liquid phase conversions per passage are low. Therefore, the reaction system is constructed as a loop of saturation vessel and membrane module. By this way, the membrane works as a contact zone for the reactants and the catalyst. Because of fast convective flow internal diffusion limitations are reduced as the products will be immediately removed from the membrane pore which avoids a product accumulation within the membrane. As a consequence, the effective reaction rate is not influenced by mass transfer limitations and the selectivity for the desired product can be increased. The latter is particularly important for consecutive reactions, e.g. partial hydrogenation reactions. Fig. 2.7 compares the course of a consecutive reaction in a fixed-bed reactor with porous catalyst pellets and in a pore-flow-through membrane reactor. In the pores of the spherical catalyst pellets in the fixed bed reactor the residence time of the reactants and the product is increased because of internal diffusion limitation. This results in a concentration profile of the reactants in the pores of the catalyst pellet. The concentrations of the reactants A and B decrease from the shell to the core of the pellet if a fast reaction occurs. With increasing concentration of the product C the consecutive reaction to the side product D begins. By this, the selectivity of C decreases. In the membrane reactor the reactants and the product are forced through the pores. The residence time in the membrane pores is short which suppresses the consecutive reaction. By this way, the forced-through

flow concept of membrane reactors has many advantages compared to fixed-bed and slurry reactors:

- pore diffusion can be reduced
- no catalyst separation from the product necessary
- good catalyst accessibility (less catalyst metal necessary)

However, some drawbacks have to be considered thoroughly:

- the recycling of large reactant streams is necessary on the expense of energy
- the development of a new reactor design
- the pressure drop at the membrane increases with increasing flow velocity and decreasing pore diameter
- the possibility of pore blocking

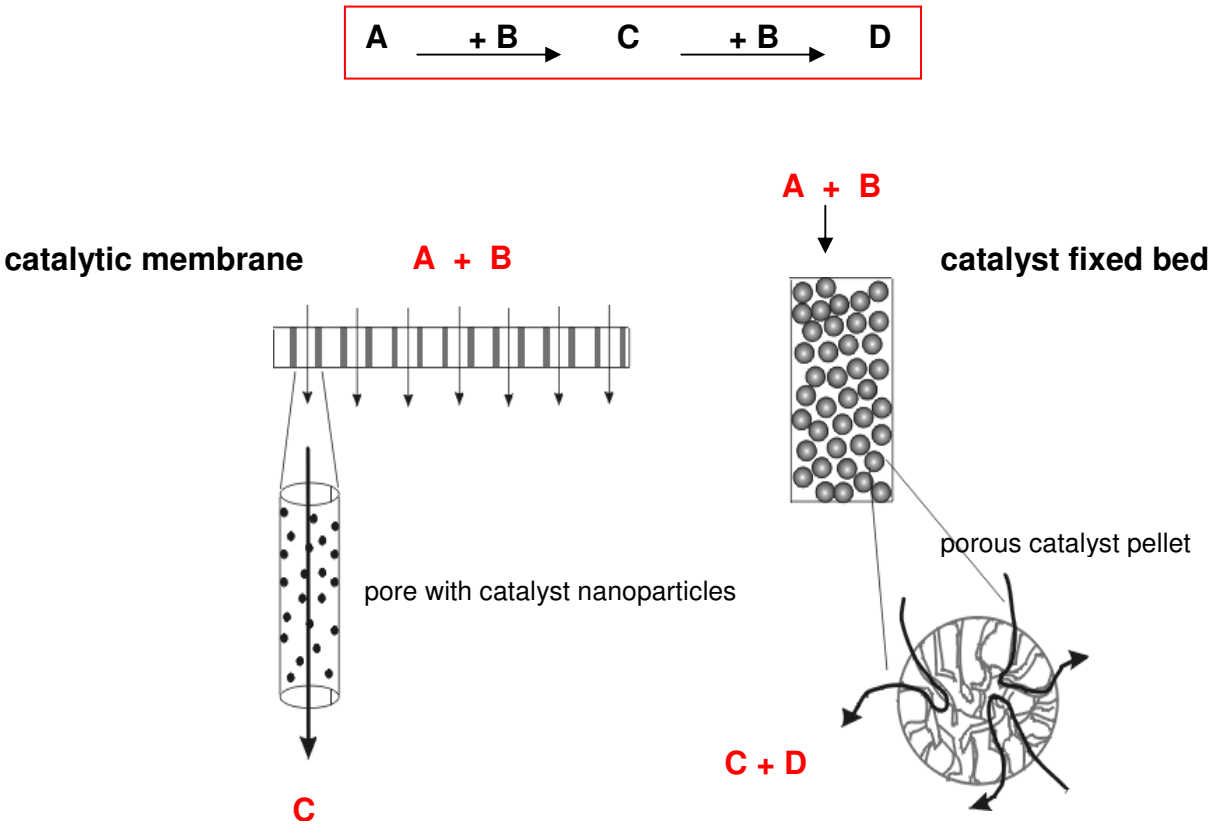

Fig. 2.7: Scheme of catalytic consecutive reaction in PFT-membrane and fixed bed reactor

If the benefits of the pore-flow-through (PFT) membrane reactor such as higher reaction rates, improved selectivity, better product quality, etc. can compensate these disadvantages, it offers interesting perspectives for an industrial application. The investigations of this work aim at advancing the development and application of such a reactor concept for

hydrogenation reactions. The potential will be demonstrated for a number of different reactions.

2.3 Membranes and membrane reactors

In this section a general and recent overview on membranes and types of membrane reactors, focused on catalytic membrane reactors, is provided. This discussion will show the different possibilities of membrane properties to influence conversion and selectivity of reactions among which the pore-flow-through concept is only one. The potential for different types of reactions is demonstrated and an outlook for industrial application is given.

2.3.1 Classification of membranes

Membranes can be classified in dense or porous membranes, by their type of material and by their structure (symmetric or asymmetric). Dense membranes are generally used for separation of gas or vapor mixtures. They are made of polymers, metals or solid oxides. Pd-membranes are specially applied for hydrogen separation; Ag-membranes are applied for oxygen separation. Solid oxide membranes consist of different types of oxygen ion conducting materials such as perovskites and modified zirconia.
Possible materials for porous membranes are polymers, ceramics (alumina, silica, titania, zirconia, zeolites, etc.) and microporous carbon. Porous membranes can be classified (according to IUPAC) in macroporous (average pore diameter > 50 nm), in mesoporous (average pore diameter between 2 and 50 nm) and microporous (average pore diameters < 2 nm) membranes.

Fig. 2.8: Examples of membranes in different geometries and of different materials: (a) Pd-polyacrylic membrane in disc geometry; (b) bundles of membrane capillaries made of α-alumina

Mass transfer through the membrane depends on several factors like specific interactions between the membrane and the fluid, the membrane structure and the operating conditions. In porous membranes mass transfer mechanisms depend mainly on the membrane average pore size and the type of diffusion. In mesoporous and macroporous membranes the predominating diffusion types are molecular and Knudsen diffusion as well as convective flow. The transport in such membranes can be described by Fick's law or a dusty gas model approach.

The membrane structure can be divided into symmetric or asymmetric. A symmetric membrane has enough mechanical strength to be self-supporting. If the mechanical stability of a membrane layer does not suffice the membrane layer can be deposited on a porous support which can be made from a different material resulting in an asymmetric membrane structure. The support provides the necessary mechanical strength but does not affect the mass transport through the membrane.

The geometry of the membrane depends on the material it is made from. Ceramic membranes are generally manufactured in tubular, multi-tubular and flat geometry whereas hollow-fiber or spiral-wound membranes are prepared from polymers. The material is also important for the membrane application. Inorganic membranes, e.g., offer the opportunity to apply the membrane in a broader range of operating conditions because they are stable at relatively high temperatures (<200°C) and possess good chemical and mechanical resistance [2.8].

2.3.2 Types of membrane reactors

According to IUPAC, in a membrane reactor, a membrane separation process is coupled with a catalytic reaction. An increasing industrial interest has been developed in membrane reactors because besides the separation function an enhanced selectivity or yield is often obtained. However, up to now membrane reactors find industrial applications only in biotechnology at low temperature levels. The membranes are there utilized as hosts for the immobilization of bacteria, enzymes, animal cells or membrane processes are coupled with biological reactions, e.g. of the fermentation type. In most cases the membrane's function is to remove one or more of the reactants or the products. This is especially interesting if the reaction is limited by thermodynamic equilibrium. The membrane can be a catalyst itself or a carrier for the catalyst [2.8]. In some catalytic applications the membrane is not even permselective but acts only as a reactive zone for the reactants. The advantage of the use of such catalytic non-permselective membrane reactor is the decrease of mass transfer limitations for multiphase reactions compared to reactions in fixed-bed or slurry reactors. This type is also called reactive *membrane contactor* because the membrane endowed with

catalytic sites provides a close contact between the liquid, gaseous and solid phase. This can be achieved by forcing the reactants to flow through the pores of the membrane or by a controlled diffusion of the gaseous and liquid phase from different sides of the membrane to the catalyst inside the membrane structure. The concept of the active *contactor in forced-through flow mode* which is studied in this work was reported so far only in a few papers. Previous investigations with Pd/polyacrylic membranes in a pore-flow-through membrane reactor showed enhanced selectivities for partial hydrogenation reactions [2.9]. The improved efficiency of the force-through flow concept was also demonstrated with Pd/α-alumina membranes for the hydrogenation of α-methylstyrene. Higher space-time-yields were obtained compared to conventional trickle-bed, bubble-column or slurry reactors [2.10]. Keil et al. presented a high performance catalytic tubular membrane reactor owing to convective flow operation for the H_2O_2 decomposition [2.11]. The influence of the catalyst preparation method and the type of membrane material (α-alumina, carbon, carbon fiber and polyethylene) was investigated and a detailed modeling for simulation of the experiments was described. Vincent et al. studied the selective hydrogenation of acetylene with thin Pd/γ-alumina membranes [2.12]. They demonstrated that ceramic membranes offer several benefits over thin metal membranes in short contact time reactors because they show high permeability, thermal stability, low-pressure-drop, efficient containment of the catalyst and enable a tailoring of the residence times and the application of more complex catalysts for specific reactions. Other applications of the forced flow concept included the epoxidation of propene with Cs-Ag and Re-Ag, immobilized in the membrane pores of a micro-porous glassy substance, resulting in an enhancement in propylene oxide selectivity [2.13]. Nishizawa et al. demonstrated that a forced-through flow membrane reactor is applicable for the transfructosylation of sucrose solution forced through an enzyme loaded membrane [2.14]. The dimerisation of isobutene to isooctane was successfully performed in a forced-flow reactor because the by-products were purged from the catalyst active sites of the membrane by a non-diffusive flow of reactants and products before for the reaction proceeded further [2.15]. For Fischer-Tropsch synthesis higher space-time-yields and selectivities towards heavy hydrocarbons and olefins were achieved in such a type of membrane reactor [2.16, 2.17]. The hydrogenation of sunflower oil was investigated by Fritsch et al. with Pt/polyethersulfone and Pd/polyamideimide membranes in a pore-flow-through-reactor with the aim to suppress the isomerization to undesired *trans* fatty acids during the hydrogenation process. The trans-isomer level of the product consisted of 25 % for an iodine value of 90 within 8 h [2.18]. The forced-through concept was also tested for the nitrate/nitrite reduction in water and the dechlorination of chlorinated hydrocarbons [2.19]. Due to a minimized pore diffusion resistance in the membrane, higher catalyst activity was obtained and increased nitrogen selectivity in the case of nitrite reduction. In comparison, the

latter reaction was also investigated in a catalytic diffuser membrane reactor. Compared to the forced-flow concept with the catalytic diffuser a lower catalyst activity is obtained but pore blocking of the membrane could be avoided. The controlled diffusion of reactants from opposite membrane sides was studied for several hydrogenation reactions. Bottino et al. pointed out the advantage of reduced mass transfer limitations and improved selectivities compared to a slurry reactor for the competitive hydrogenation-isomerization of methylenecyclohexane [2.20]. Torres et al. report about the nitrobenzene liquid phase hydrogenation to aniline [2.21, 2.22]. The membranes consist of several macroporous α-alumina layers as support, deposited with thin toplayers of mesoporous γ-alumina, containing well-dispersed Pt particles. The asymmetric geometry allowed feed the reactants either in the inner or the outer compartment of the membrane. Modeling and simulation of the catalytic membrane reactor is here also presented. Pan et al. investigated the hydrogenation of cinnamaldehyde [2.23]. They obtained a better selectivity towards hydrocinnamyl alcohol with the membrane reactor than with a slurry reactor which they explained with the absence of diffusional limitations in the membrane reactor. The hydrogenation of sunflower oil was studied by Veldsink in a range of operation conditions with a Pd/zirconia membrane as catalytic interface between hydrogen and the oil [2.24]. Under optimal conditions the consecutive reaction to the fully saturated fatty acids could be avoided but long reaction times were necessary and a severe catalyst deactivation was observed. Isomerization of *trans* isomers which should be reduced to a minimum could not be prevented completely. A general overview about the advantages of the use of membrane contactors for the study of gas-liquid and gas-liquid-solid reactions is given by Tesser et al. [2.25].

The membrane's role can also be the removal of one or more products resulting in an increased yield by shifting the equilibrium. Dehydrogenation and esterification reactions have been investigated in this type of membrane reactor, called reactive *membrane extractor*. In dehydrogenation reactions thermodynamic equilibrium conversions are often less than 20% even at high temperatures of 500°C; therefore expensive process equipment and specialized catalysts are required in order to produce acceptable olefin yields in conventional reactors. High-temperature catalytic membrane reactors which combine reaction and separation in a single unit operation may solve these problems. Chang et al. studied the propane dehydrogenation in a hydrogen permselective membrane reactor which separates hydrogen from the reaction mixture along the reaction path and, by this way, enables the operation at lower temperatures resulting in higher conversions [2.26]. In the Fischer-Tropsch synthesis a membrane reactor of this type could be used to remove water in-situ in order to increase the conversions to long-chain hydrocarbons and to reduce catalyst inhibition and deactivation [2.27].

In a catalytic *membrane distributor* the membrane controls the addition of one of the reactants. This is particularly interesting for partial oxidation of hydrocarbons because the controlled feed of the oxygen through the membrane decreases its local partial pressure within the reactor and can improve the yield of partially oxidized products. Furthermore, this type of membrane reactor has the potential to avoid thermal runaway problems which are especially associated with highly exothermic reactions like partial oxidations. An overview of partial oxidations in a catalytic membrane reactor is reported by Caro [2.28]. In Fig. 2.8 all types of reactive membranes are demonstrated schematically.

The membrane reactors described above belong all to the type of catalytic membrane reactor where the membrane acts as a catalyst. Another class of membrane reactors includes reactor systems where the membrane provides only the separation function while the reaction occurs in a packed-bed or fluidized bed of catalyst particles.

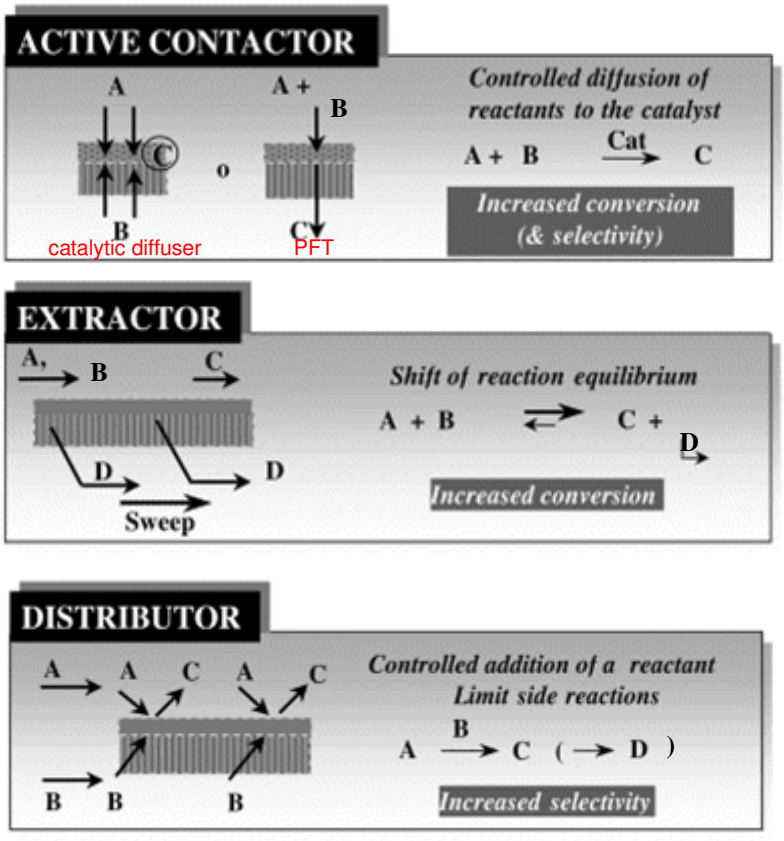

Fig. 2.9: Classes of membrane reactor types

Although the expected benefits of membrane reactors are enormous for a number of catalytic reactions and numerous investigations have been done in the last decades, large scale applications in industries are still lacking. Improvement in membrane costs and reliability are

still needed. Further research in the field of catalytic membrane reactors can help overcome the existing problems and convince the benefits of this reactor concept.

2.4 References

[2.1] J. T. Richardson, *Principles of catalyst development*, Plenum Pr., New York, 1989

[2.2] P. Kripylo, K.-P. Wendlandt, F. Vogel, *Heterogene Katalyse in der chemischen Industrie*, 1. ed., Dt. Verlag für Grundstoffindustrie, Leipzig, Stuttgart, 1993

[2.3] J. Hagen, *Technische Katalyse: Eine Einführung*, VCH, Weinheim, 1996

[2.4] M. Reif, *Herstellung, Charakterisierung und Einsatz katalytisch aktiver Membranen für Drei-Phasen-Reaktionen*, doctoral thesis at University Erlangen, 2004

[2.5] O. F.-K. Schlüter, *Die Synthese und Charakterisierung von geträgerten Pd-Katalysatoren durch die chemische Gasphasenabscheidung von metallorganischen Verbindungen im Wirbelschichtreaktor*, doctoral thesis at Ruhr University Bochum, April 2004

[2.6] M. Baerns, H. Hofmann, A. Renken, *Chemische Reaktionstechnik*, Bd. 1, 3. ed., Wiley-VCH, Weinheim, Germany, 1999

[2.7] H. Knözinger, *Heterogeneous catalysis and solid catalysts* in *Ullmann's Encyclopedia of Industrial Chemistry*, Wiley Interscience, online release 2006, 7th edition

[2.8] J. G. Sanchez Marcano, T. T. Tsotsis, *Catalytic Membranes and Membrane Reactors*, Wiley-VCH, Weinheim, Germany, 2002

[2.9] A. Schmidt, R. Haidar, R. Schomäcker, *Selectivity of partial hydrogenation reactions performed in a pore-through-flow catalytic membrane reactor*, Catalysis Today 104, 2-4 (2005) 305-312

[2.10] H. Purnama, P. Kurr, A. Schmidt, I. Voigt, A. Wolf, R. Warsitz, R. Schomäcker, *α-Methylstyrene in a flow-through membrane reactor*, AIChE Journal, 52, no.8 (2006), 2805-2811

[2.11] F. Keil, U. Flügge, *High performance catalytic tubular membrane reactors owing to forced convective flow operation*, Hungarian J. Ind. Chem. Vezprém, 33 (1) (2005), 31-42

[2.12] M. J. Vincent, R. D. Gonzalez, *Selective hydrogenation of acetylene through a short contact time reactor*, AIChE J. 48 (6) (2002) 12571267

[2.13] M. Kobayashi, J. Togawa, T. Kanno, J. Horiuchi, K. Tada, *Dramatic innovation of propene epoxidation derived from a forced flow membrane reactor*, J. Chem. Technol. Biotechnol. 78 (2003) 303-307

[2.14] K. Nishizawa, M. Nakajima, H. Nabetani, *A forced-flow membrane reactor for transfructosylation using ceramic membrane,* Biotechnol. Bioeng. 68 (2000) 92-97

[2.15] D. Fritsch, I. Randjelovic, F. Keil, *Application of a forced-flow catalytic membrane reactor for the dimerisation of isobutene*, Catal. Today, 98 (2004) 295-308

[2.16] A. A. Khassin, A. G. Sipatrov, T. M. Yurieva, G. K. Chermashentseva, V. N. Parmon, *Plug-through contactor membranes (PCM) for the Fischer-Tropsch synthesis*, Prepr. Pap.-Am. Chem. Soc., Div. Pet. Chem. 49 (2004) 2, 175-178

[2.17] A. A. Khassin, *Catalytic membrane reactor for conversion of syngas to liquid hydrocarbons*, Energeia, Center for applied energy research, vol. 16 (2005), 6

[2.18] D. Fritsch, G. Bengtson, *Development of catalytically reactive porous membranes for the selective hydrogenation of sunflower oil*, Catal. Today, 118,1-2 (2006)121-127

[2.19] M. Reif, R. Dittmeyer, *Porous, catalytically active ceramic membranes for gas-liquid reactions: a comparison between catalytic diffuser and forced through flow concept*, Catal. Today, 82 (2003) 3-14

[2.20] A. Bottino, G. Capannelli, A. Comite, A. Del Borghi, R. Di Felice, *Catalytic ceramic membrane in a three-phase reactor for the competitive hydrogenation-isomerisation of methylenecyclohexane*, Sep. Pur. Technol. 34 (2004) 239-245

[2.21] M. Torres, J. Sanchez, J. A. Dalmon, B. Bernauer, J. Lieto, *Modeling and simulation of a three-phase catalytic membrane reactor for nitrobenzene hydrogenation*, Ind. Eng. Chem. Res., 33 (1994) 2421-2425

[2.22] J. Peureux, M. Torres, H. Mozzanega, A. Giroir-Fendler, J.-A. Dalmon, *Nitrobenzene liquid-phase hydrogenation in a membrane reactor*, Catal. Today, 25 (1995) 409-415

[2.23] X. L. Pan, G. X. Xiong, S. S. Sheng, W. S. Yang, *Exploration of cinnamaldehyde hydrogenation in Co–Pt/γAl_2O_3 catalytic membrane reactors*, Catal. Lett. 66 (2000) 125-128

[2.24] J. M. Veldsink, *Selective hydrogenation of sunflower seed oil in a three-phase catalytic membrane reactor*, J. Am. Oil Chem. Soc., 78 (2001) 443-446

[2.25] R. Tesser, A. Bottino, G. Capannelli, F. Montagnaro, S. Vitolo, M. Di Serio, E. Santacesaria, *Advantages in the use of membrane contactors for the study of gas-liquid and gas-liquid-solid reactions*, Ind. Eng. Chem. Res. 44 (2005) 9451 - 9460

[2.26] J.-S. Chang, H.-S.Roh, M. S. Park, S.-E. Park, *Propane dehydrogenation over a hydrogen permselective membrane reactor*, Bull. Korean Chem. Soc., 23 (2002), 5

[2.27] M. P. Rohde, D. Unruh, G. Schaub, *Membrane application in Fischer-Tropsch synthesis to enhance CO_2 hydrogenation*, Ind. Eng. Chem. Res., 44 (2005), 9653-9658

[2.28] J. Caro, *Membranreaktoren für die katalytische Oxidation*, Chem. Ing. Tech., 78, no. 7 (2006), 899-912

3 Experimental Details

3.1 Experimental procedure

3.1.1 Preparation of catalytic membrane

Porous α-alumina membranes were in tubular geometry and had a length of 25 cm; an outer diameter of 2.9 mm and an inner diameter of 1.9 mm. 1.5 cm of the membrane tube ends were coated with glass in order to avoid breaking of the ends. This results in an active length of the membrane of 22 cm and a membrane area of 0.002 m². Only within this area the catalyst component could be deposited. The average pore diameters of the membranes were 0.6, 1.9 and 3.0 µm, respectively. The porosity was 30 %. This results in a membrane volume of $4.4 \cdot 10^{-7}$ m³ for the single tube membranes. Bundles of 27-single membrane capillaries were prepared for scale-up studies. They had an area of 0.054 m².

Pd deposition on the α-Al_2O_3–membranes was accomplished by wet impregnation with a metal precursor solution. With a simple dipping of the membranes in a Pd-salt-solution the Pd was not dispersed homogenously in the membrane structure and it was difficult to reproduce membranes with the same Pd loading. Furthermore, with this method the membranes needed at least 48 h conditioning in the impregnation solution in order to obtain acceptable Pd amounts on the support [3.1]. Better results were obtained by pumping continuously the Pd-salt-solution through the membrane for 24 h by means of a peristaltic pump (Fig. 3.1).

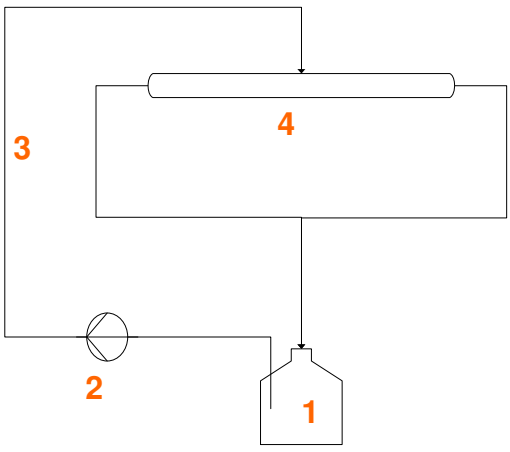

Fig. 3.1: Scheme of experimental set up for membrane impregnation: (1) vessel with precursor solution, (2) peristaltic pump, (3) silicone tubing, (4) membrane holder from glass

First impregnation experiments were carried out with a palladium (II)-acetate in toluene solution and subsequent activation by reduction to Pd in a hydrogen flow at 100°C for 2 h. By this way, Pd was located in a thin layer of about 200 µm at the membrane surface. A dispersion of Pd in the whole membrane structure could be achieved by changing the solvent of the impregnation solution from toluene to water and using $PdCl_2$ as precursor salt instead of Pd(II)- acetate (Fig. 3.2). This result can be explained by faster evaporation of the organic solvent than of the aqueous. During this drying process Pd particles were withdrawn to the membrane surface and agglomerated there resulted in a thin film of Pd. The slower this process, the better the Pd particles are dispersed in the membrane matrix. This is the case when using water as solvent for the impregnation.

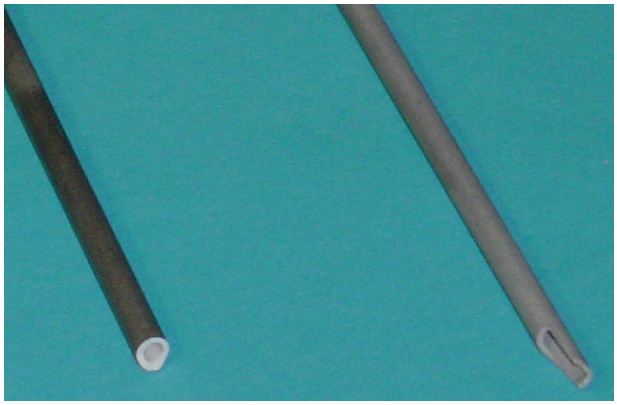

Fig. 3.2: Catalytically active membranes prepared with organic Pd-acetate-solution (left) and aqueous $PdCl_2$-solution (right)

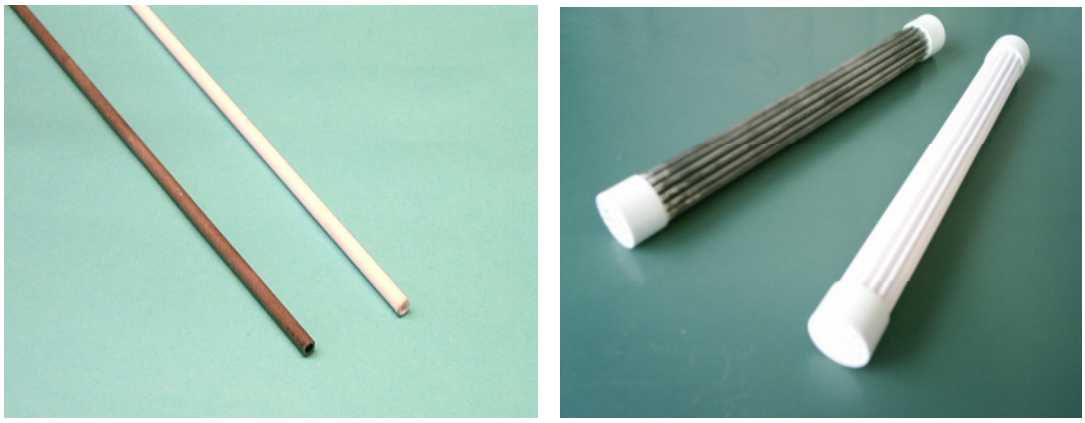

(a) **(b)**

Fig. 3.3: α-Al_2O_3 supports and Pd-containing membranes, (a) single capillary and (b) capillary bundle

The aqueous $PdCl_2$-solution was prepared by dissolving $PdCl_2$ and NaCl in a molar ratio 1 to 4 in water while stirring and heating for a minute to 80°C. A Pd content of 2 mg/mL (19 mmol/L $PdCl_2$) was obtained. After impregnation the membranes were activated by chemical reduction with an aqueous solution of $NaH_2PO_2 \cdot H_2O$ (59 mmol/L) pumped likewise through the membrane for an hour at room temperature. An instant color change from tawny to grey or black showed the immediate starting of the reduction process. The membranes were washed with water in order to remove sodium ions and then dried at room temperature. Catalytically active membranes with fine dispersed Pd were obtained (Fig. 3.3).

3.1.2 Hydrogenation experiments

Hydrogenation experiments in lab scale were performed in a reactor system constructed as a loop of saturation vessel and membrane reactor (Fig. 3.4). The membrane module accommodated up to three single capillaries (Fig. 3.5a); its temperature was controlled through a heating jacket. The stainless steel vessel had a liquid volume of 110 mL and was equipped with a gas dispersion stirrer and baffles. The vessel was mounted in an oil bath with a temperature control unit. A gear pump in the range between 50 and 350 mL/min set the circulation rate of the reaction mixture through the reactor system. The experiments were carried out in semibatch mode. Hydrogen was fed to the system from a reservoir with the desired initial hydrogen pressure. A data acquisition system monitored the decrease of hydrogen pressure in the reservoir during the reaction online. The membranes were sealed with o-rings made of viton or Kalrez. The chemical stability of the sealing material had to be tested for every involved chemical substance in order to avoid swelling and abrasion of the material in the organic solution. The reaction temperature was measured before and behind the membrane reactor with temperature sensors and was indicated by a digital thermometer.

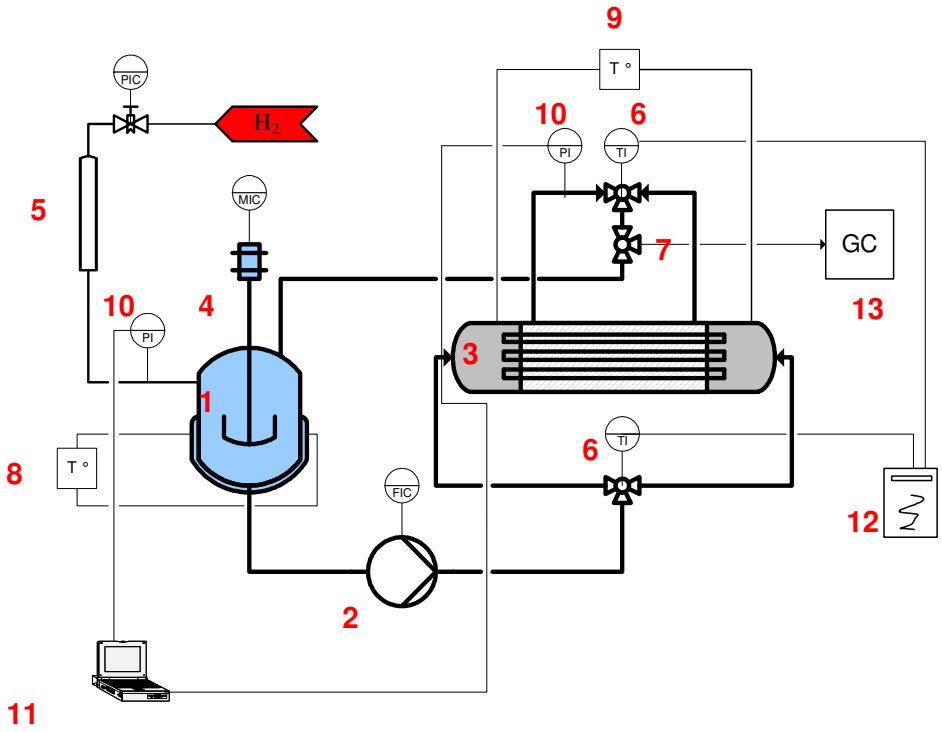

(a)

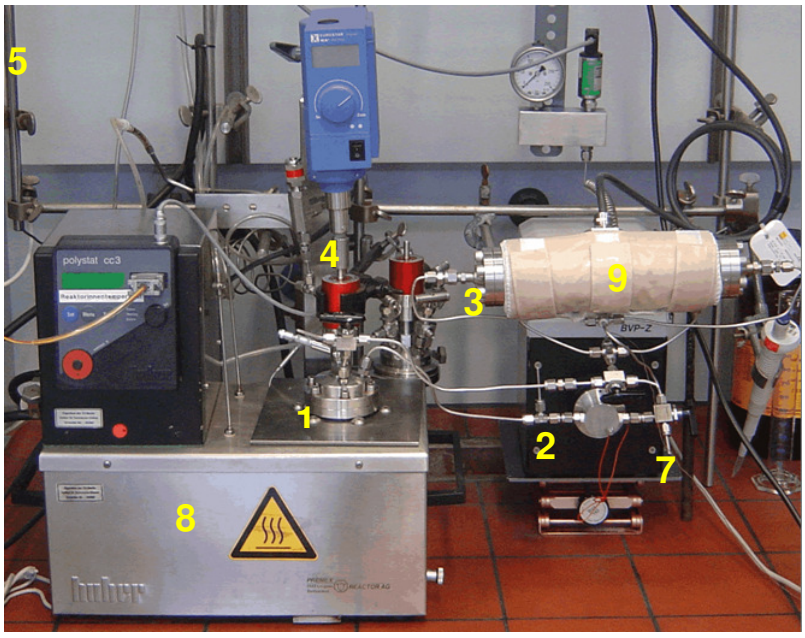

(b)

Fig. 3.4: Scheme (a) and image (b) of the PFT-membrane reactor in lab scale: (1) saturation vessel, (2) gear pump, (3) membrane reactor, (4) stirrer, (5) H_2-reservoir, (6) temperature sensors, (7) sample outlet, (8) thermostat, (9) heating jacket, (10) pressure transducer, (11) computer, (12) digital thermometer, (13) gas chromatograph

(a) (b)

Fig. 3.5: Picture of the PFT-membrane module in lab scale (a) and in pilot plant scale(b)

The reaction mixture was pumped from both capillary ends though the inner (tube side) to outer side (shell side) of the membranes. CFD (computational fluid dynamic) simulations, carried out at *Bayer Technology Services*, demonstrate the radial flow velocity along the membrane length (Fig. 3.6). It becomes obvious that a double-sided feed of the reaction mixture (a), as it is performed in the experimental set-up, results in a symmetric decrease of the flow velocity of about 18 % for the highest mass flow from the capillary ends to the middle of the membrane whereas a one-sided feed (b) would result in a decrease of the flow velocity of 65 % for the highest mass flow in one direction.

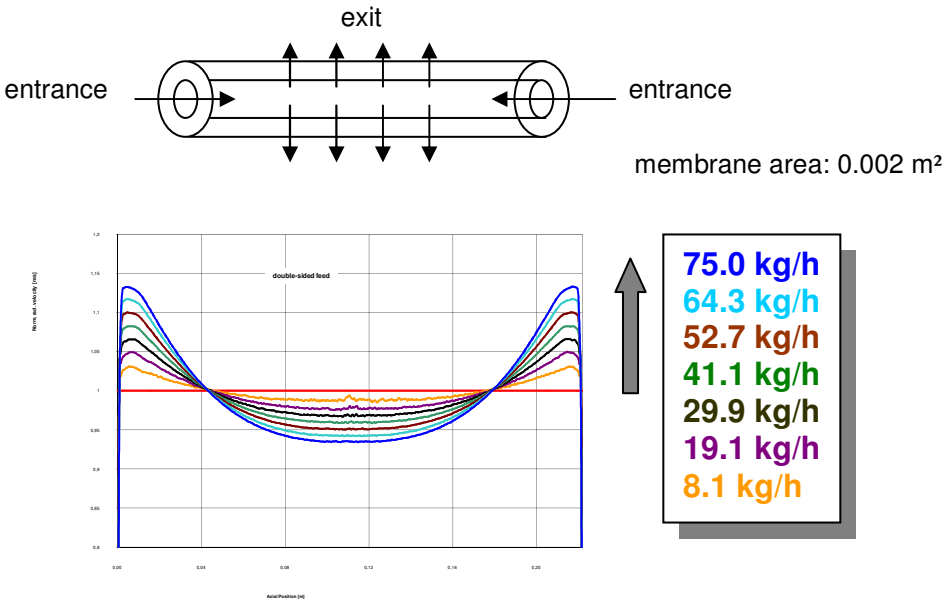

Fig.3.6a: CFD-simulations of radial flow velocity along the membrane length: double-sided feed

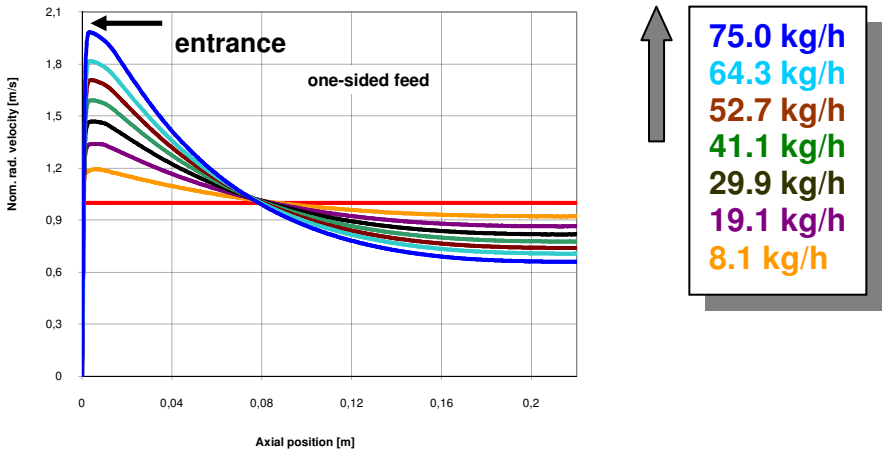

Fig.3.6b: CFD-simulations of radial flow velocity along the membrane length: one-sided feed

Hydrogenation experiments were performed with the following procedure: The catalytic membranes were assembled the membrane module. 110 mL liquid phase (solvent and substrate) were fed into the system via a syringe. The stirrer was switched on at a speed of 1600 rpm. Oil bath and heating jacket were heated to the desired temperature. The pump was started and the desired flow rate (50-350 mL/min) was adjusted. When the reaction mixture had reached the reaction temperature the reaction was started by opening the hydrogen blocking valve. During the reaction, samples of the reaction mixture were taken in constant intervals and were analyzed by gas chromatography.

Scale-up experiments were carried out in a pilot plant with *Bayer Technology Services*, Leverkusen. The plant was constructed similar to the set-up in lab scale but in a larger dimension (Fig. 3.7). The membrane module was equipped with a bundle of 27-membrane tubes (Fig. 3.5 b). The saturation vessel had a capacity of 5 L and was temperature controlled by a thermostat. All experiments were performed with a liquid inventory of about 3 L. The circulation rate of the reaction mixture was varied from 5 to 11 L/min by a gear pump. The flow velocity of the reaction mixture was controlled by a flow meter. The hydrogen pressure in the saturation vessel was kept constant during the reaction. After a saturation time of 15 minutes the reaction was started by turning on the pump. A computer monitored online temperature and hydrogen pressure in the reactor system before and behind the membrane module as well as in the saturation vessel. Samples of the reaction mixture were taken in intervals of 10 minutes and analyzed by GC.

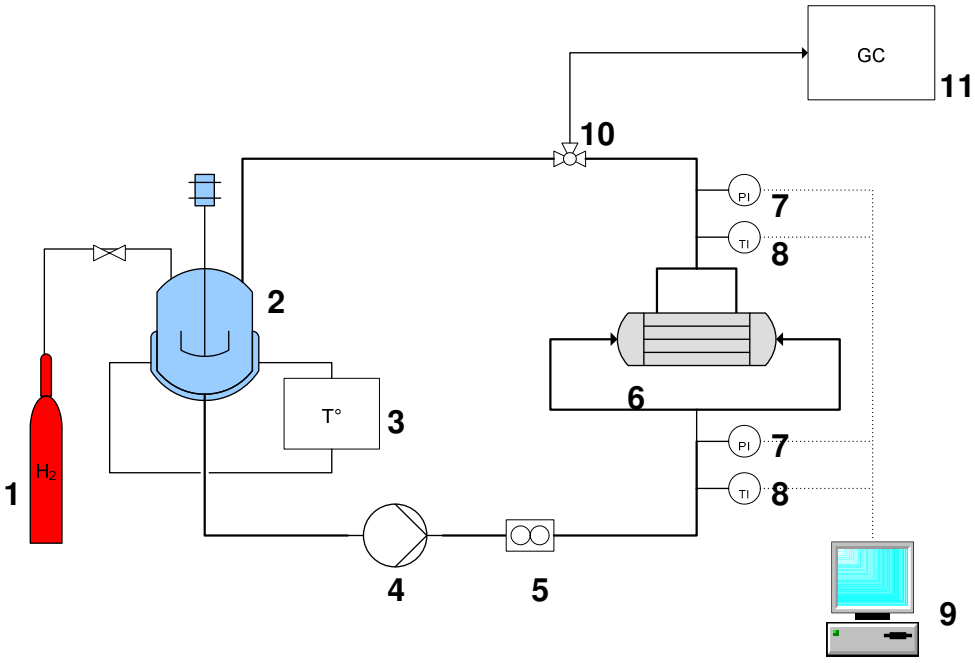

(a)

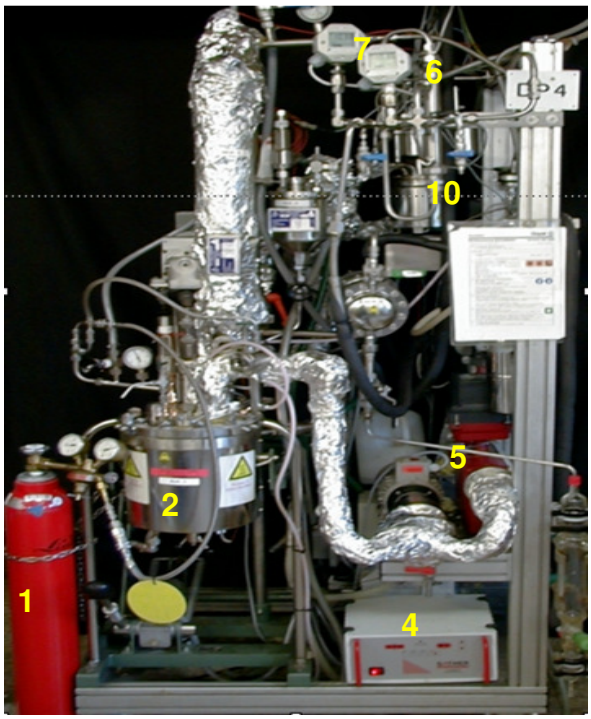

(b)

Fig. 3.7.: Scheme (a) and picture (b) of pilot plant at BTS, Leverkusen: (1) H_2-cylinder, (2) saturation vessel, (3) thermostat, (4) gear pump, (5) flowmeter, (6) membrane reactor, (7) pressure transducer, (8) temperature sensor, (9) computer, (10) sample outlet, (11) gas chromatograph

The liquid composition of the samples was analyzed by gas chromatography (Sichromat, Siemens) with a column RTX5 MS (Restek). For the analysis of the hydrogenation experiments of 1,5-cyclooctadiene, 1-octyne, phenylacetylene, geraniol and cinnamaldehyde 100 µl of the sample was diluted in 1 ml of solvent. For analysis of the experiments with sunflower oil the products had to be converted into their fatty acid methyl esters. The detailed procedure is described in chapter 8.1. A table with the temperature programs that were used for the analysis of the different product compositions is given in the appendix.

3.2 References

[3.1] P. Kurr, *Vergleich der Reaktorleistung eines Membranreaktors mit einem Festbett bzw. Rieselreaktor am Beispiel der katalytischen Hydrierung von α-Methylstyrol*, diploma thesis at TU Berlin, 2004

4 Characterization of catalytically active membranes

A characterization of the catalytic membranes is necessary in order to interpret results of hydrogenation experiments in the membrane reactor properly. Amount, particle size and dispersion of the Pd loaded on the membrane have a strong impact on the activity of the catalytic membrane. A high activity is obtained when the catalyst is dispersed homogeneously as small crystallites (nanometer range) over the whole internal surface of the membrane support.

4.1 AAS

The Pd amount in the membranes was determined by AAS (Perkin-Elmer 3500). Before AAS-measurements, the Pd was dissolved from the membrane with 10 mL of aqua regia. The AAS-measurements were accomplished for a number of Pd membranes prepared under the same conditions. The amount of Pd is found to be in the range from 0.7 to 1.5 mg per membrane capillary. An average palladium content of 1 mg per membrane (0.03 wt %) is considered in the subsequent discussion. The Pd amount of the membranes could not be increased significantly above this level, e.g. by increasing the Pd concentration of the impregnation solution or by repetition of the impregnation process. Leaching of Pd could be excluded based on AAS analyses of the product of the hydrogenation experiments (Pd detection limit: 3.6 µg/L).

The Pd amounts deposited in the membrane capillary bundles were determined by weighing before and after the impregnation and drying; typical Pd amounts of 29-35 mg were detected.

4.2 SEM

By scanning electron microscopy (SEM) the surface of a solid is scanned by a focused electron beam. Electrons emitted of the sample are detected and represent an image on a cathode ray indicator. Samples of different parts of the membrane were prepared for investigation with high-resolution SEM (Hitachi S-4000) by polishing and sputtering with a thin gold layer. A simultaneous analysis of the element composition was possible by energy-dispersive-X-ray analysis (EDX; IDFix, SamX). Pd crystallites in nanometer range were identified on the outer surface of the alumina membranes and within the structure of the pores. SEM images were recorded from several positions on the outer, the inner and the internal surface of the membrane (Fig. 4.1). Figure 4.2 a – b show typical SEM-images of

internal surfaces of the raw alumina membranes, Fig. 4.2 c-d show the Pd loaded membranes, in different magnifications. The Pd particles are well dispersed over the whole internal surface. Only some larger agglomerates of Pd in µm-range were also found. The detection of Pd was verified by EDX. In Fig. 4.3 a typical result of the element analysis is depicted for one spot on the surface. Aluminium, oxygen and palladium were detected as expected. The gold peak is due to sample preparation.

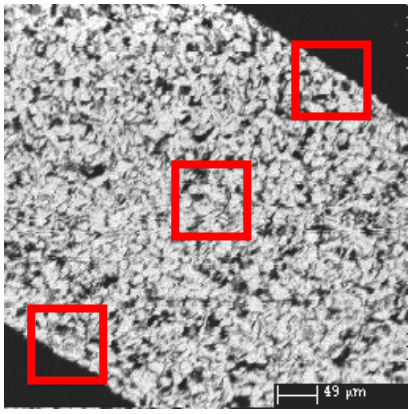

Fig. 4.1: SEM imaging, carried out at the outer, inner and internal surface of the membrane

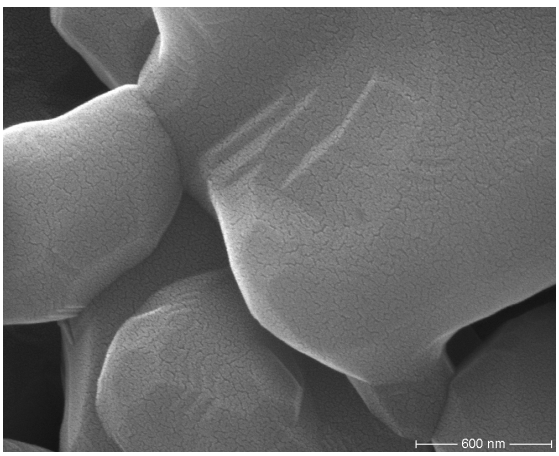

(a)

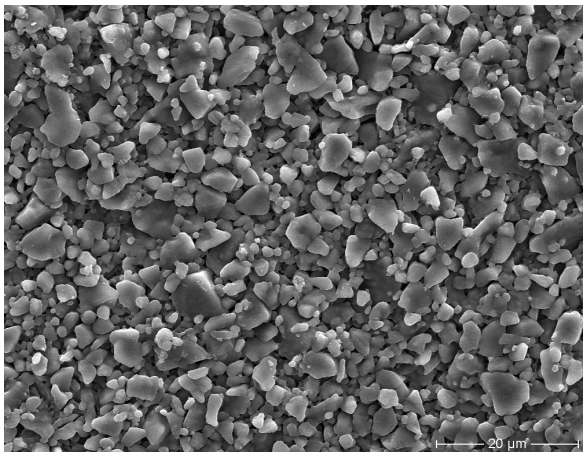

(b)

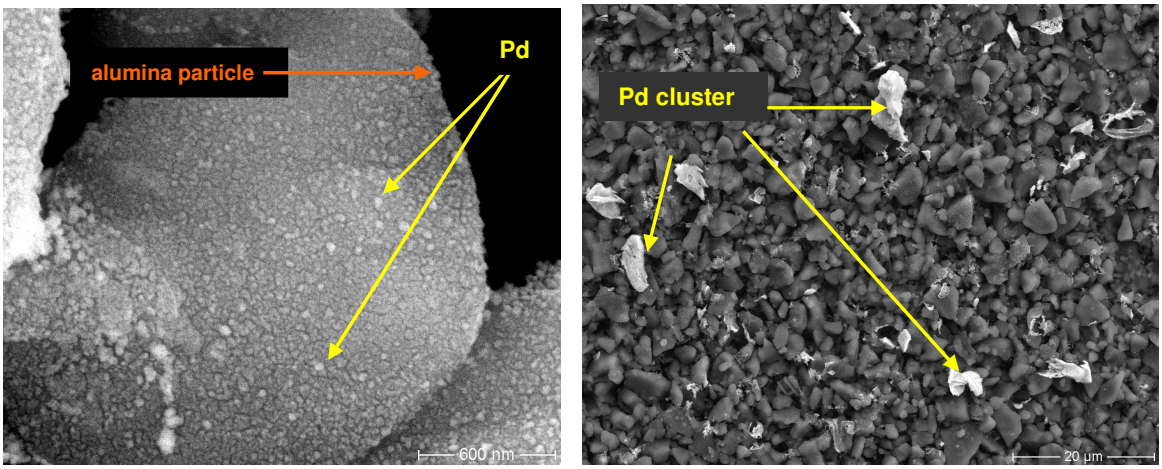

(c) (d)

Fig. 4.2: SEM images of internal membrane surface in different magnifications (a,b: α-alumina membrane; pore-ø: 1.9 µm; without Pd; c,d: α-alumina membrane; pore-ø: 1.9 µm; with Pd-nanoparticles)

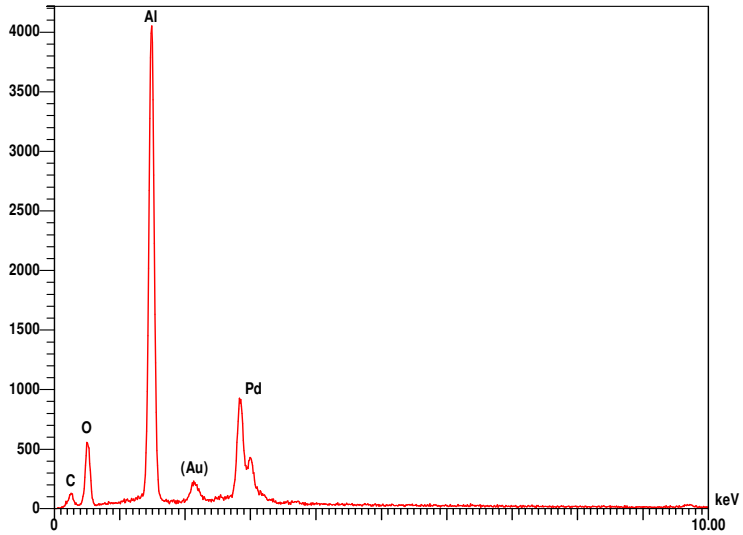

Fig. 4.3: EDX-analysis of internal membrane surface, exemplarily for one spot

4.3 TEM

The cluster size and the dispersion of the Pd in the membrane structure were studied by TEM. For TEM analysis the membrane sample needed to be reduced in particles within 50 – 100 nm size range that the electron beam is able to pass through the ceramic material. Parts of the membrane sample were grounded, suspended in ethanol and placed in an ultrasonic bath for 2 h. A drop of the suspension was placed on a copper grid, the solvent evaporated

and the sample was assembled in the transmission electron microscope. In Fig. 4.4 typical TEM images of the sample are depicted. The Pd crystallites become visible as dark spots on the alumina particle which appears the brighter, the thinner the particle. The average Pd crystallite diameters range from 8 to 15 nm. The average Pd crystallite size does not differ in membranes with different pore sizes (tab. 4.1). TEM analysis of a membrane after use for hydrogenation experiments shows the same result as fresh impregnated membranes. This indicates that the Pd particles do not undergo obvious changes during the reaction.

Tab. 4.1: Average Pd particle sizes of different membranes
(I-III prepared only for TEM, IV after hydrogenation experiment with COD)

membrane	I	II	III	IV
pore diameter of membrane [µm]	0.6	1.9	3.0	1.9
average size of Pd particles [nm]	9.4 ± 1.3	7.8 ± 2.7	9.0 ± 1.4	7.6 ± 1.4

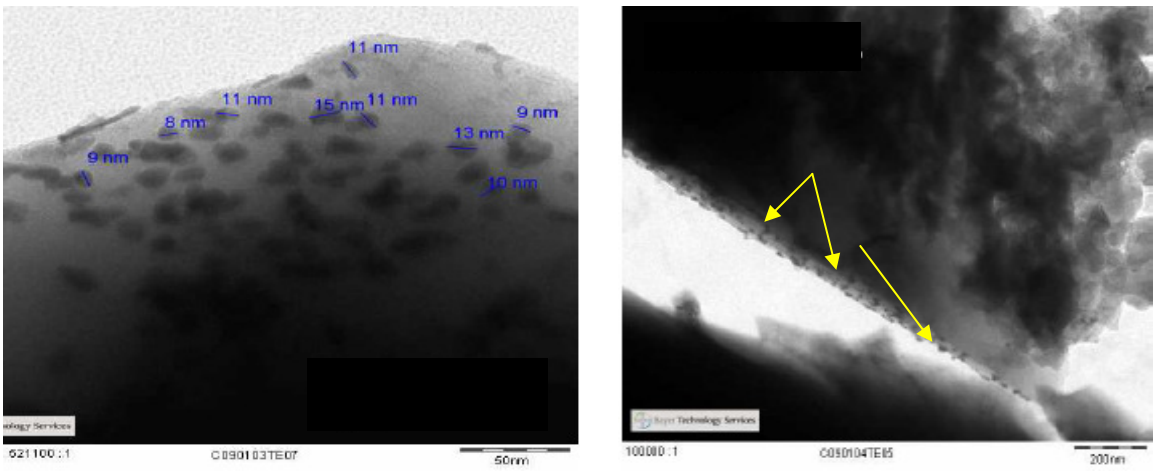

(a) **(b)**

Fig. 4.4: Typical TEM images from Pd crystallites on alumina membrane particles

4.4 EPMA

The distribution of Pd within the membrane structure was analyzed by electron probe microanalysis (EPMA). With this non-destructive method a quantitative element analysis is carried out with a focused electron beam that impinges a punctual spot on the sample and induces the emission of X-ray characteristic for the element. The element concentrations can be determined from the intensity of the detected wavelengths by wavelength dispersive X-ray

analysis (WDX). For analysis, cross sectional cuts of different parts of the membrane (from the ends and the middle) were prepared. The samples were embedded in resin, smoothed and polished.

Fig. 4.5 shows the Pd distribution (in wt. % Pd) vs. the distance from the membrane surface. The scattering of the measured values is due to the porous nature of the samples. The beam diameter of the instrument and its penetration into the specimen is at most several times the mean pore size. Therefore, from point to point of the line scan, the fraction of solids within the measuring volume may differ significantly. Since the Pd nanoparticles are deposited on the surface of the large Al_2O_3 particles and not inside, rather large variations of the local Pd/Al-ratio occur which lead to scattering of the data. EPMA measurements were usually carried out for different parts of a membrane (end and middle) with two opposite line scans in each cross section analyzed. Table 4.2 shows an example of the variation of the average Pd content derived from different line scans. It becomes obvious that the Pd is well distributed along the membrane profile and not only located at the membrane surface.

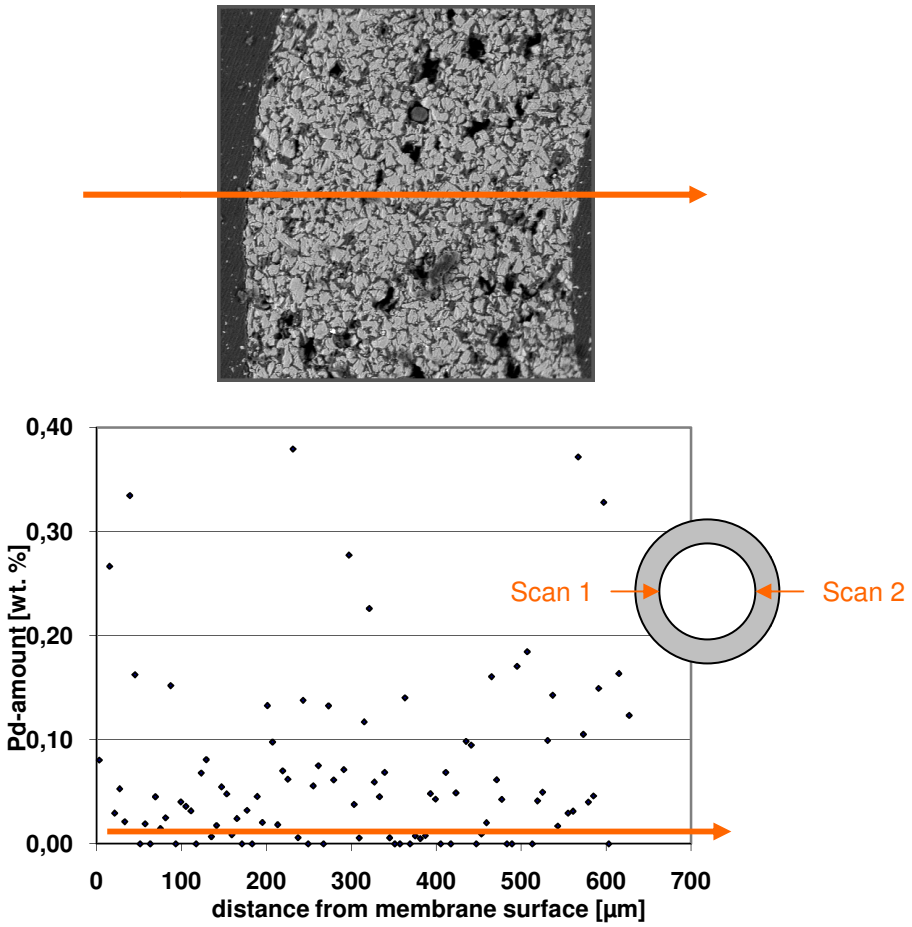

Fig. 4.5: Pd distribution in membrane profile analyzed by EPMA-line scan

Tab. 4.2: Pd amount in different parts of a membrane

	Scan 1	Scan 2	part of the membrane
	0.07	-	end
average Pd amount in wt.%	0.088	0.079	middle
	0.094	0.065	end

5 Kinetics of 1, 5 - cyclooctadiene hydrogenation on Pd/alumina

5.1 Introduction

Cyclooctene (COE) is produced by partial hydrogenation of 1,5-cyclooctadiene (COD) (Fig. 5.1). It is an important industrial intermediate product, e.g. for the manufacture of special polymers (polyoctenamer via ring opening metathesis polymerization which is used as modifier in rubbers and thermoplastics) [5.1].

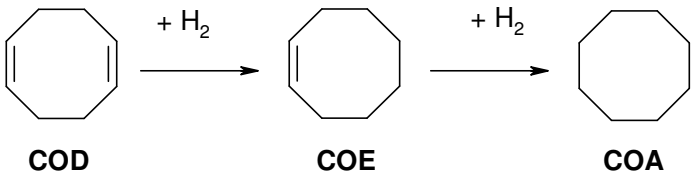

Fig. 5.1: Reaction scheme of COD hydrogenation

The hydrogenation of COD proceeds with an appreciable rate even at low temperatures and hydrogen pressures with supported Pd catalysts. With COD in liquid phase it is a typical example for a three-phase catalytic reaction. The consecutive hydrogenation to cyclooctane (COA) occurs when pore diffusion retards the removing of COE out of the catalyst pores. In order to obtain the desired product COE with a high selectivity mass transfer limitations have to be reduced. As for simulations of the membrane process the knowledge of intrinsic kinetics are required, this chapter is devoted to investigations of the intrinsic reaction kinetics of the hydrogenation of COD. Kinetic data were determined with a very fine powder of a Pd/α-alumina catalyst, in order to exclude pore diffusion influence, in a slurry reactor at different reaction temperatures, hydrogen pressures and COD concentrations. Gaube et al. studied the kinetics of this reaction in the gas phase [5.2, 5.3]. A Langmuir-Hinshelwood like model was derived and the kinetic parameter were determined. These parameters can not be applied to the three-phase hydrogenation of COD. Earlier studies of the three-phase reaction by Di Serio proposed an Eley-Rideal-model for its kinetics [5.4]. This model does not reflect the influence of the competitive adsorption of hydrogen and COD at the catalyst

surface and the consequences for the kinetics, because it does not describe the retardation of the reaction rate with increasing COD concentration. Additionally, no influence of hydrogen pressure on the reaction rate was found and leads the authors to the conclusion, that reaction order for hydrogen is zero. In the experiments following a linear dependence of reaction rate on hydrogen pressure was found. These deviations between existing kinetic models and own experimental observation made a development of a new kinetic model reasonable.

5.2 Experimental

The hydrogenation experiments were performed in a stainless steel autoclave (liquid volume 110 mL), equipped with a gas dispersion stirrer and baffles. Hydrogen was fed into the reactor at constant pressure. The autoclave was heated to the desired temperature by a heating jacket.

The purchased spherical Pd/α-Al_2O_3 catalyst, 0.5 wt. % Pd, was ground and sieved to a powder with a particle size of ~ 100 µm. A specific surface of 9 m^2/g was determined by nitrogen adsorption. The size of the palladium particles in the range of 5 to 10 nm was studied by TEM. This results in a metal specific surface of about 75 m^2/g_{Pd}. This value was only calculated, but not verified experimentally. The experiments were carried out with 1,5-cyclooctadiene in *n*-heptane as solvent in different concentrations in a range of 40-70°C, 2-10 bar hydrogen pressure and a Pd amount of 2 mg (400 mg of supported catalyst). The stirrer speed was adjusted to 1600 rpm for all experiments in order to assure fast saturation of the solution. For the calculation of the concentration of dissolved hydrogen the solvent vapour pressure at the given temperature was taken into account. Samples were taken in intervals of 2 to 10 minutes and analyzed by gas chromatography. Conversion of COD and selectivity of COE were calculated with equation 5.1 and 5.2 from the concentrations determined by GC analysis.

$$\textit{Conversion of COD:} \quad X\,(\%) = \frac{C_{COD,0} - C_{COD,t}}{C_{COD,0}} \cdot 100 \qquad \text{(eq. 5.1)}$$

$$\textit{Selectivity for COE:} \quad S\,(\%) = \frac{C_{COE,t}}{C_{COD,0} - C_{COD,t}} \cdot 100 \qquad \text{(eq. 5.2)}$$

5.3 Results and interpretation

5.3.1 Mass transfer limitations

Above a stirrer speed of 1400 rpm the measured activity was independent of the stirring rate and the experiments were considered to be free from any gas-liquid-transport limitation and external diffusion limitation [5.5]. Internal diffusion was controlled by the catalyst particle size. The Weisz modulus Ψ', considering hydrogen as the limiting reactant, was used to estimate diffusion limitations. The Weisz modulus describes the ratio of reaction rate to diffusion rate and is defined by

$$\Psi' = L^2 \cdot r_{eff} \cdot \rho_{cat} / (D_{eff,H2} \cdot C_{H2}) \qquad \text{(eq. 5.3)}$$

L: characteristic length of catalyst particle (m)

r_{eff}: measured reaction rate ($mol \cdot s^{-1} \cdot g^{-1}$)

ρ_{cat}: catalyst density ($g \cdot m^{-3}$)

D_{eff,H_2} : effective diffusivity of hydrogen ($m^2 \cdot s^{-1}$)

C_{H_2} : saturation concentration of hydrogen ($mol \cdot m^{-3}$)

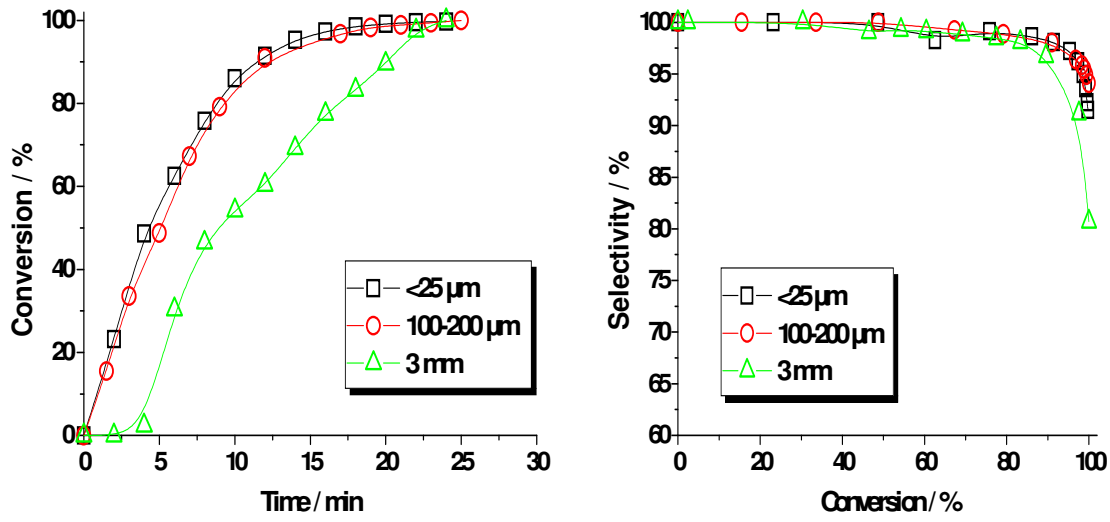

Fig. 5.2: COD conversion (a) and COE selectivities (b) with Pd/alumina catalysts with different particle sizes

The molecular diffusivity D_m of hydrogen in *n*-heptane (DETHERM databank) is 3 x 10^{-8} $m^2 \cdot s^{-1}$. With a tortuosity of 3 and a porosity of 0.4 for alumina supports the effective diffusivity of hydrogen $D_{eff,H2}$ was estimated as 4 x 10^{-9} $m^2 \cdot s^{-1}$. The catalyst density was 1.57 x 10^6 $g \cdot m^{-3}$ (considering a density of alumina of 3.92 $g \cdot m^{-3}$ and a porosity of about 0.4). With a saturation concentration of hydrogen in *n*-heptane of 58 $mol \cdot m^{-3}$ and the effective reaction rates in the range of 0.3 x 10^{-5} to 1.6 x 10^{-4} mol $s^{-1} \cdot g^{-1}$, the Weisz modulus was calculated as $\Psi' \approx 10$ which indicates that all experiments were performed under diffusion limitations. To verify this, experiments with smaller catalyst particles (<25 µm) were carried out. As can be seen from Fig. 5.2, the reaction rate and the COE selectivity obtained with a particle fraction below 25 µm was the same as with 100 µm-particles. These experiments contradict the theoretically derived prediction for the diffusion influence on the reaction. The experiment with pellets of a size of 3 mm, however, does not show exactly the expected result of a strong pore diffusion resistance but a retarded start of the reaction. This is contributed to the fact that 3 mm-pellets have not the optimal size for the slurry experiments in a stirred tank vessel. The pellets are too large for being stirred up in the reaction vessel and are partly crushed after a while by the stirrer.

Seeing that the experiments with particles of 100 µm and <25 µm did not show any difference in reaction rate and selectivity the following experiments, performed with catalyst particles of 100 µm, were considered to be free of any diffusion resistance.

5.3.2 Effect of COD concentration

The initial concentration of COD in *n*-heptane was varied in the range of 0.41 - 0.82 mol/L (5 -10 vol. % COD) at 50°C and 10 bar hydrogen pressure. Fig. 5.3a shows that with a higher initial COD concentration more time is needed for complete conversion of COD. With the lowest initial concentration COD is completely converted within 28 minutes, with 0.61 mol/L initial COD-concentration 40 minutes are needed for complete COD-conversion and with 0.82 mol/L 100 minutes are needed. The selectivity is not affected by the COD concentration. Almost the same selectivities are obtained for all studied COD concentrations (Fig. 5.3b).

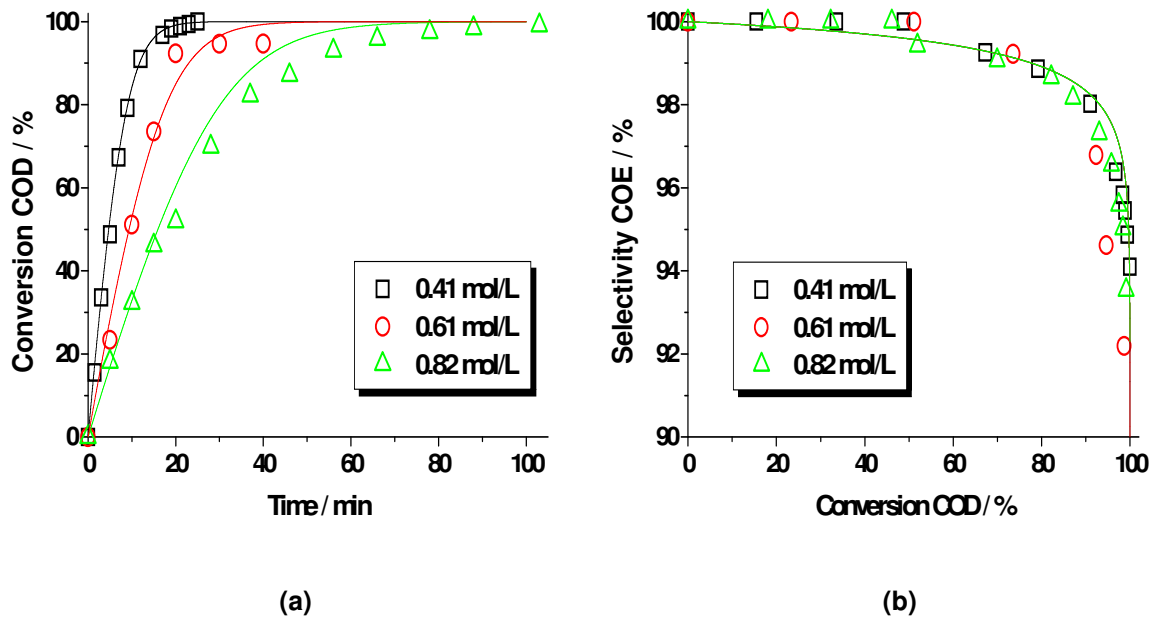

Fig. 5.3: COD conversion (a) and COE selectivities (b) at different initial COD concentrations, 50 °C and 10 bar; simulation (lines) and experimental data (symbols)

For the hydrogenation of 1,3-COD at a Pd catalyst in gas phase Haas and Gaube proposed a kinetic model of Langmuir-Hinshelwood type [5.2, 5.3] which means that both reactants, hydrogen and COD, are adsorbed on the catalyst surface. This is based on the generally accepted mechanism of olefin hydrogenation, occurring via surface adsorbed species of both reactants. In the rate law the concentrations of these adsorbed species are expressed by the surface coverage of the catalyst with these species, Θ. This model results in a derivation of the typical Langmuir-Hinshelwood type of rate law for the first and second hydrogenation reaction of COD.

$$COD + H_2 \xrightarrow{k_1} COE \qquad \text{(eq. 5.4)}$$

$$r_1 = k_1 \cdot \theta_{H_2} \cdot \theta_{COD} \qquad \text{(eq. 5.5)}$$

$$\theta_{H_2} = \frac{K_{H_2} c_{H_2}}{(1 + K_{COD} c_{COD} + K_{COE} c_{COE} + K_{H_2} c_{H_2})} \qquad \text{(eq. 5.6)}$$

$$\theta_{COD} = \frac{K_{COD} c_{COD}}{(1 + K_{COD} c_{COD} + K_{COE} c_{COE} + K_{H_2} c_{H_2})} \quad \text{(eq. 5.7)}$$

$$\theta_{COE} = \frac{K_{COE} c_{COE}}{(1 + K_{COD} c_{COD} + K_{COE} c_{COE} + K_{H_2} c_{H_2})} \quad \text{(eq. 5.8)}$$

$$r_1 = k_1 \frac{K_{COD} c_{COD} K_{H_2} c_{H_2}}{(1 + K_{COD} c_{COD} + K_{COE} c_{COE} + K_{H_2} c_{H_2})^2} \quad \text{(eq. 5.9)}$$

r: reaction rate

θ: surface coverage

k: reaction rate constant

K: equilibrium constant

c: concentration

For the consecutive reaction the reaction rate is given by

$$COE + H_2 \xrightarrow{k_2} COA \quad \text{(eq. 5.10)}$$

$$r_2 = k_2 \cdot \theta_{H_2} \cdot \theta_{COE} \quad \text{(eq. 5.11)}$$

$$r_2 = k_2 \frac{K_{COE} c_{COE} K_{H_2} c_{H_2}}{(1 + K_{COD} c_{COD} + K_{COE} c_{COE} + K_{H_2} c_{H_2})^2} \quad \text{(eq. 5.12)}$$

For the gas phase it is known that hydrogen adsorbs much stronger on Pd than COD, however the concentration of COD in liquid phase is hundredfold higher than the hydrogen concentration in liquid phase hydrogenation. From Fig. 5.3a it can be assumed that the hydrogenation of COD is first order type with respect to COD at low COD concentrations. But the reaction rate decreases substantially at high COD concentrations. This results from the competitive adsorption of COD and H_2 at the catalyst surface. The consequence is a depletion of hydrogen at the catalyst surface at high COD concentrations. This applies also to the consecutive reaction to COA as dienes adsorb more strongly than monoenes [5.6, 5.7]. Di Serio [5.4] et al. investigated the kinetics of the hydrogenation of dienes in the

presence of supported Pd catalysts. The authors observed that conjugated dienes are hydrogenated faster than non-conjugated. Therefore, the latter are firstly isomerized to conjugated ones and then hydrogenated faster than monoenes. By hydrogenation of 1,5-cyclooctadiene 1,3-cyclooctadiene is formed as an intermediate. In our model, however, we do not distinguish between 1,5 and 1,3-COD. The COD is the predominant species at the catalyst surface at a high concentration level. When the COD surface coverage decreases, the COE formed adsorbs and the consecutive reaction to COA begins.

With the following four differential equations the reaction progress can be described when the solution is always saturated with hydrogen.

$$r_{H_2} = \frac{d_{H_2}}{dt} = -r_1 - r_2 \qquad \text{(eq. 5.13)}$$

$$r_{COD} = \frac{d_{COD}}{dt} = -r_1 \qquad \text{(eq. 5.14)}$$

$$r_{COE} = \frac{d_{COE}}{dt} = +r_1 - r_2 \qquad \text{(eq. 5.15)}$$

$$r_{COA} = \frac{d_{COA}}{dt} = +r_2 \qquad \text{(eq. 5.16)}$$

The experimental data were described best by a kinetic model that also involves the adsorption of COE. Simulations were carried out with the program *Berkeley Madonna*. Equations 5.7 and 5.10 can describe the observed reaction rates and selectivities with the kinetic parameters reported in Tab. 5.1. The rate constants and equilibrium constants were obtained by manual fitting of the conversion and selectivity curves to the experimental data.

Tab. 5.1: Estimated kinetic parameters at 50°C

	Estimated parameters
k_1 [mol·mg$_{Pd}^{-1}$·s^{-1}]	1.8x10^{-3}
k_2 [mol·mg$_{Pd}^{-1}$·s^{-1}]	3.4x10^{-5}
K_{COD} [L·mol^{-1}]	17.5
K_{COE} [L·mol^{-1}]	10
K_{H2} [L·mol^{-1}]	4

5.3.3 Effect of hydrogen pressure

The reaction rate depends strongly on the hydrogen pressure because a higher pressure results in higher hydrogen solubility in the liquid phase. From Fig. 5.4 it becomes obvious that the initial reaction rate r_0 increases linearly with increasing hydrogen pressure. Fig. 5.5a shows that at higher hydrogen pressures selectivity decreases slightly faster during the reaction. This is due to a higher concentration of hydrogen at the catalyst surface which promotes the consecutive reaction of COE more than the primary reaction of COD. Still, the selectivity for COE at complete conversion of COD is 94% at 10 bar compared to 96% at 2 bar and 5 bar (Fig. 5.5b). The proposed kinetic model is in good agreement with the experimental data obtained for the three different hydrogen pressures.

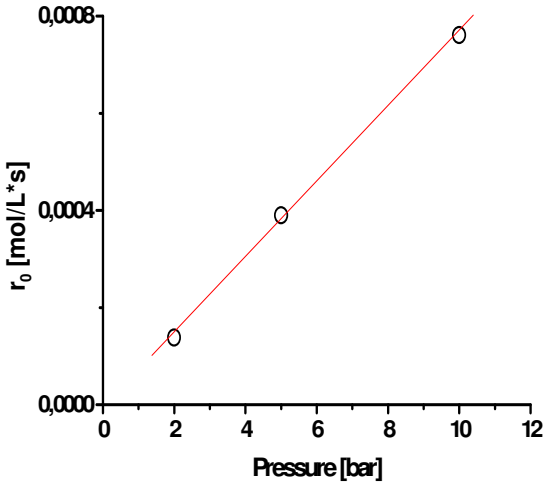

Fig. 5.4: Initial reaction rate vs. hydrogen pressure at 50°C and $c_{COD,0}$: 0.41 mol/L

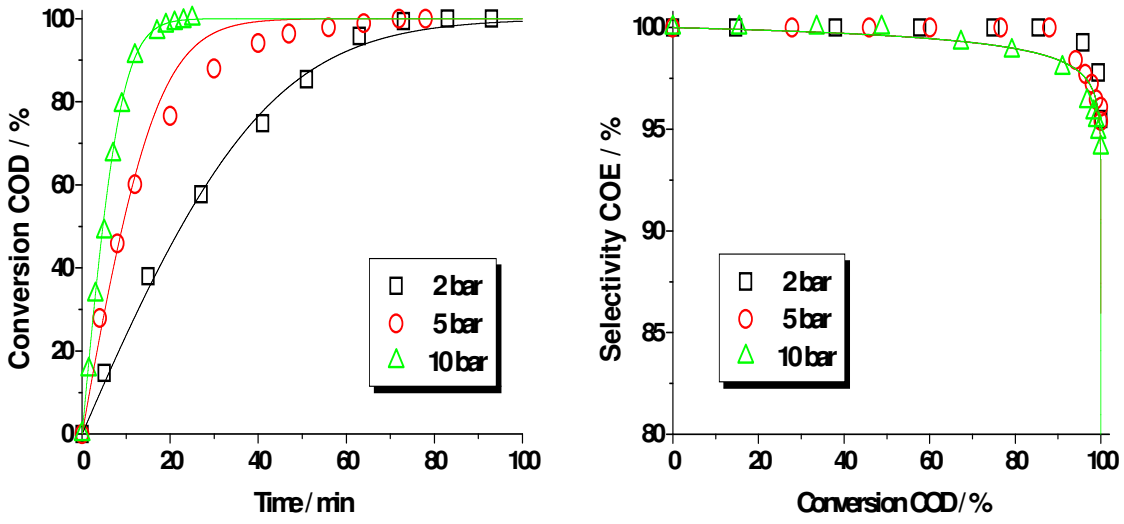

(a) (b)

Fig. 5.5: COD conversion (a) and COE selectivity (b) at different hydrogen pressures, 50 °C and $c_{COD,0}$: 0.41 mol/L; simulation (lines) and experimental data (symbols)

5.3.4 Effect of reaction temperature

The reaction rate increases with increasing reaction temperature whereas the selectivity decreases slightly with increasing reaction temperature (Fig. 5.6). The kinetic parameters k_1, k_2, K_{COD}, K_{COE} and K_{H2} at different reaction temperatures were determined by fitting the proposed kinetic model to the experimental data. In order to validate the kinetic parameters, experiments at two different initial COD concentrations (0.41 mol/L and 0.82 mol/L) for each studied reaction temperature were performed. The kinetic parameters at the different reaction temperatures are summarized in table 5.2.

Table 5.2: Kinetic parameters at different reaction temperatures

T [°C]	K_{COD} [L·mol^{-1}]	K_{COE} [L·mol^{-1}]	K_{H2} [L·mol^{-1}]	k_1 [mol·mg$_{Pd}^{-1}$·s^{-1}]	k_2 [mol·mg$_{Pd}^{-1}$·s^{-1}]
40	20.0	15.0	7.4	9.0×10^{-4}	5.8×10^{-6}
50	17.5	10.0	4.0	1.8×10^{-3}	3.4×10^{-5}
70	17.0	9.0	1.1	1.2×10^{-2}	2.3×10^{-4}

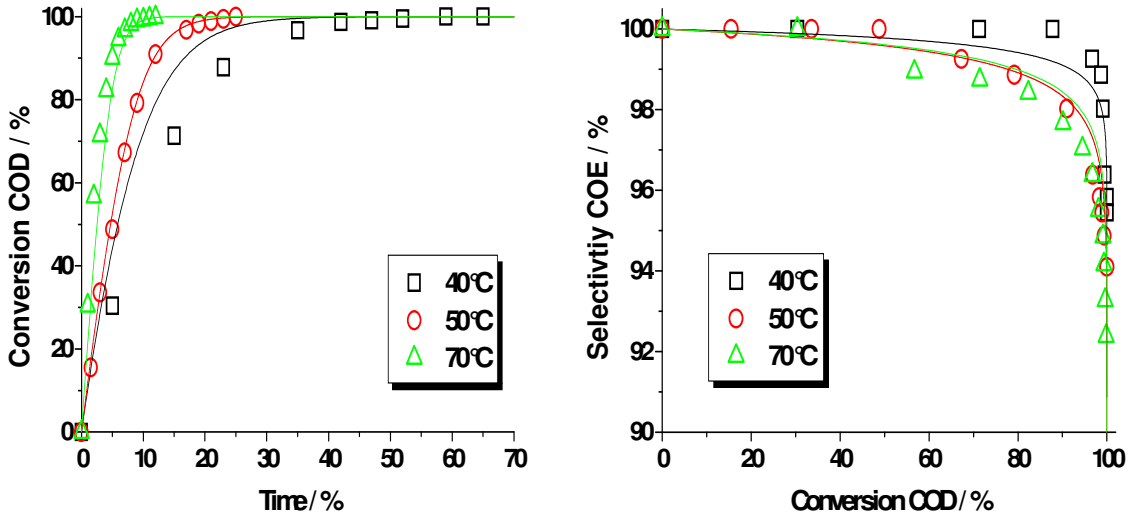

(a) (b)

Fig. 5.6: COD conversions (a) and COE selectivity (b) at different reaction temperatures, 10 bar hydrogen pressure and $c_{COD,0}$: 0.41 mol/L; simulation (lines) and experimental data (symbols)

The rate constants k_1 and k_2 for different reaction temperatures were used to determine activation energies E_A for the primary and the consecutive reaction from an Arrhenius plot (Fig. 5.7). The activation energy for the reaction of COD to COE was determined with 74 kJ/mol and for the reaction of COE to COA with 98 kJ/mol. This indicates that with increasing reaction temperature the consecutive reaction is promoted.

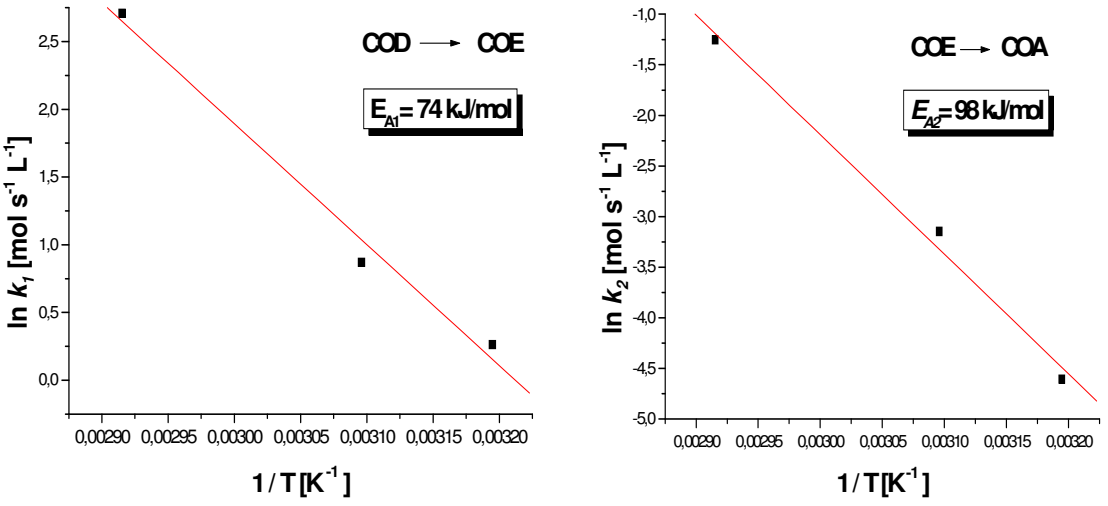

(a) (b)

Fig. 5.7 a, b: Arrhenius plot for determination of activation energy (E_A)

The hydrogenation reaction of COD on Pd/alumina is influenced by temperature, hydrogen pressure and COD concentration. The activity increases with increasing reaction temperatures, hydrogen pressures and decreasing COD concentrations. The selectivity for COE decreases slightly with increasing temperature and hydrogen pressure. The COD concentration does not affect the selectivity. The selectivities obtained are in the range of 92-95 % at complete conversion of COD. The reaction can be described by a kinetic model derived from Langmuir-Hinshelwood with COD, COE and hydrogen competitive adsorbing at the Pd-catalyst surface. The proposed model was validated by experimental data. The model parameter were determined in a wide range of experimental conditions characterized by mutual ratios of $[H_2]/m^2$ palladium surface of 5×10^{-5} to 5×10^{-2} mol $L^{-1}m^{-2}$ and [COD]/ m^2 palladium surface of 10^{-3} to 1 mol $L^{-1}m^{-2}$. This covers the whole range of experimental conditions that are reasonable for measurements in slurry reactors in order to avoid mass transfer limitations. Since the model is based on no assumptions that could be not fulfilled under certain conditions the model is expected to be reliable also for extrapolations to conditions outside the studied range of parameters. The activation energies were 74 and 98 kJ/mol for primary and consecutive reaction. The intrinsic kinetic data determined in this chapter are important for the description of the COD hydrogenation in the PFT-membrane reactor.

5.4 References

[5.1] T. Schiffer; G. Oenbrink; *Cyclododecatriene, Cyclooctadiene, and 4-Vinylcyclohexene* in: Ullmann's Encyclopedia of Industrial Chemistry, Wiley Interscience, online release 2006, 7th edition

[5.2] T. Haas; J. Gaube; *Selective Hydrogenation: Kinetic Investigation of 1,3-Cyclo-octadiene and Cyclo-octene Hydrogenation*, Chem. Eng. Technol. (1989) 12, 45-53

[5.3] H. Arnold; F. Döbert; J. Gaube; *Hydrogenation reactions* in: Handbook of heterogeneous catalysis, G. Ertl, H. Knözinger, J. Weitkamp (Eds.) Wiley- VCH, Weinheim, Vol. 3, 1995

[5.4] M. Di Serio; V. Balato; A. Dimiccoli, L. Maffucci; P. Iengo, E. Santacesaria, *Kinetic and mass transfer in the hydrogenation of polyunsaturated organic compounds in the presence of supported Pd catalysts*, Catal. Today (2001) 66, 403-410

[5.5] H. Purnama; P. Kurr; A. Schmidt;, I. Voigt; A. Wolf; R. Warsitz; R. Schomäcker; *α-Methylstyrene hydrogenation in a flow-through membrane reactor*, AIChE J. (2006), 52, 8, 2805 - 2811

[5.6] E. A. Sales; M. de Jesus Mendes; F. Bozon-Verduraz; *Liquid-phase selective hydrogenation of hexa-1,5-diene and hexa-1,3-diene on palladium catalysts*. *Effect of Tin and silver addition*, J. Catal. (2000) 195, 96-105

[5.7] L. F. Liotta; A. M. Venezia; A. Martorana; G. Deganello; *Model pumices supported metal catalysts, II. Liquid phase selective hydrogenation of 1,3-Cyclooctadiene*, J. Catal. *(*1997) 171, 177-183

6 Partial Hydrogenation of 1, 5- cyclooctadiene in PFT-membrane reactor

6.1 Introduction

Hydrogenation reactions in liquid phase are very common in chemical industry. Mostly they are heterogeneously catalyzed as a solid catalyst is easy to separate from the reaction mixture. A frequently met disadvantage of such three-phase reactions arises from mass transport limitations that reduce activity and selectivity. Firstly, the hydrogen has to be transferred from the gas phase into the liquid phase. On industrial scale this problem is most often solved by increased hydrogen pressure and intensive stirring in an autoclave. Secondly, the reactants in the liquid phase must be transported into the pores of the solid catalyst and, after reaction at the active centers, the products must be removed fast enough before side reactions occur. In the case of consecutive reactions, mass transport phenomena like pore diffusion and back mixing within the reactor increase the effective rate of the consecutive reaction and decrease the selectivity for the desired product. With a very fine catalyst powder, pore diffusion can be widely eliminated, but for an industrial application powders are often not adequate due to the difficulty to separate them from the product: costly and time-consuming filtration steps would be necessary. Egg shell catalysts have been developed to solve this problem where a support, spherical or of other shapes, is coated with a very thin layer of the catalytically active metal. In this way, effects of pore diffusion inside the catalyst particle can be minimized, but the size and geometry of egg-shell catalysts have to be adjusted to every reaction considered [6.1]. A recently developed concept to reduce the influence of pore diffusion is to pump the reaction mixture fast enough through the pores of a membrane in which the catalyst is immobilized on the pore walls. With a flow velocity of 10^{-3} m·s^{-1}, the convective flow of the reactants is at least one order of magnitude faster than the diffusion displacement of the molecules which is of the order of 10^{-5} m within 1 s. This results in residence times below one second for the reaction mixture within the membrane pores.

In the studied case, porous inorganic membranes serve as a support material for the Pd-nanoparticles as catalyst. They allow an efficient contact between catalyst and reactants but do not cause separation problems of the catalyst [6.1 – 6.4].

It is also possible to use catalytic membranes with asymmetric geometry for keeping gas and liquid phase separate, feeding both reactants from opposite sides of the membrane [6.4, 6.5].

In recent years, several studies on the performance of membrane reactors in hydrogenation reactions have been published [6.1 -6.15]. The concepts for suppressing undesired side step reactions by reaction engineering in a membrane reactor is transferable to other reactions and other membrane materials (e. g. dimerisation [6.16], Fischer-Tropsch synthesis [6.17], dehalogenation [6.4, 6.18], nitrate/nitrite reduction [6.4], dehydrogenation [6.11] and oxidation [6.19]). For partial hydrogenation reactions of polyunsaturated hydrocarbons, the application of a pore-flow-through (PFT) membrane reactor is well described. In a previous study [6.2] we reported that the selectivity for the partially hydrogenated product can be increased by using a membrane reactor compared to slurry and fixed bed reactors with catalyst pellets. Following the results of this previous work, the investigations in this chapter are focused on the partial hydrogenation of 1,5-cyclooctadiene in a pore-flow-through membrane reactor where the consecutive reaction to the fully hydrogenated product cyclooctane should be avoided. An alumina ceramic membrane in tubular geometry containing Pd was chosen because it allows an easy scale up of the reactor from one single capillary to a bundle of capillaries. Different characterization methods for the palladium distribution on the ceramic support are described. The reactor system was constructed from a saturation vessel and a membrane module connected in a loop; *n*-heptane served as a solvent. As the solubility of hydrogen in the liquid phase is modest, the reaction mixture had to be resaturated and pumped several times through the membrane in order to obtain complete conversion of the diene. The results of the hydrogenation in the membrane reactor are compared to experiments in a slurry reactor and a fixed bed reactor with a commercial Pd/alumina catalyst in order to evaluate the potential of the membrane reactor. The scale up behavior of the membrane reactor was investigated in a pilot plant with a bundle of 27-capillaries, and the results were compared to the experiments in laboratory scale with one single capillary.

6.2 Experimental

Hydrogenation experiments in the membrane reactor were performed at 50°C and 10 bar hydrogen pressure with single capillary membranes in lab scale and 27-capillary bundles in pilot scale. The initial COD-concentration was 0.41 mol/L (5 vol. % COD in *n*-heptane) in all experiments. The circulation rates were varied in the range of 80-260 mL/min for the lab scale and 5-11 L/min in the pilot plant. Pd/alumina membranes with three different pore diameters (0.6, 1.9 and 3.0 µm) were investigated. For the single capillary membranes the influence of the Pd amount on activity and selectivity was studied. The Pd amount of the single tube membranes was determined by AAS. For benchmarking the hydrogenation experiments were also performed with a commercially available egg-shell catalyst (Pd/α-

alumina, 0.5 wt. % Pd, pellet diameter: 1.5 - 2 mm) in a fixed bed reactor. For these experiments the membrane module in the laboratory set up was replaced by a fixed bed reactor. Benchmarking experiments were also carried out with a very fine powder of a Pd/αAl_2O_3 catalyst (grain size: < 25 µm) in a stirred tank reactor. The experimental conditions were the same as adjusted for the membrane experiments (50°C, 10 bar H_2-pressure, 5 vol. % COD in *n*-heptane as solvent).

6.3 Results and discussion

6.3.1 Hydrogenation in PFT-membrane reactor

The potential of the membrane reactor in pore-flow-through mode for the partial hydrogenation of COD was first tested with single tube membranes by varying the following reaction parameters: circulation rate of the reactants through the membrane, Pd amount (0.7-1.5 mg Pd) and pore size of the membrane. The influence of these parameters on the reaction rate and the selectivity for COE was investigated at 50°C, 10 bar H_2-pressure and a COD concentration of 5 vol. % in *n*-heptane as solvent. The following definitions were used for describing the performance of the membrane reactor:

$$\textit{Conversion of COD:} \quad X\,(\%) = \frac{C_{COD,0} - C_{COD,t}}{C_{COD,0}} \cdot 100 \qquad \text{(eq. 6.1)}$$

$$\textit{Selectivity for COE:} \quad S\,(\%) = \frac{C_{COE,t}}{C_{COD,0} - C_{COD,t}} \cdot 100 \qquad \text{(eq. 6.2)}$$

6.3.1.1 Influence of circulation rate

In Fig. 6.1a the conversion of COD is plotted as a function of time for 4 different circulation rates with a membrane with 1.9 µm pore size. With increasing circulation rate from 80 to 260 mL/min, the time for complete conversion of the COD decreases from 80 to 40 minutes. The same tendency can be observed with a membrane with a pore size of 3.0 µm (Fig. 6.1c). With larger pores, higher fluxes are reached because of the lower flow resistance. With increasing circulation rate, the residence time of the reactants in the membrane pores is decreased and so the fraction of hydrogen consumed per passage is lower. This gives a higher average hydrogen concentration within the membrane and consequently an increased overall reaction rate. Eliminating the mass transport limitation on the reaction rate means that the reaction depends only on the intrinsic kinetics. As a consequence the reaction rate

increases. By pumping the reaction mixture at a higher circulation rate through the reactor system, more passages per time occur and a complete conversion of the reactants will need less time. The minimum number of circulations needed for complete conversion is defined by the ratio of the initial concentration of the substrate and the saturation concentration of hydrogen (if one mole of substrate reacts with one mole of hydrogen). This minimum number cannot be realized because the hydrogen concentration within the membrane decreases below the saturation concentration. However, the flow rate is limited by the applied pump and the membrane pore size. The pressure drop at the membrane increases strongly with decreasing pore size and increasing flow rate (Fig. 6.2).

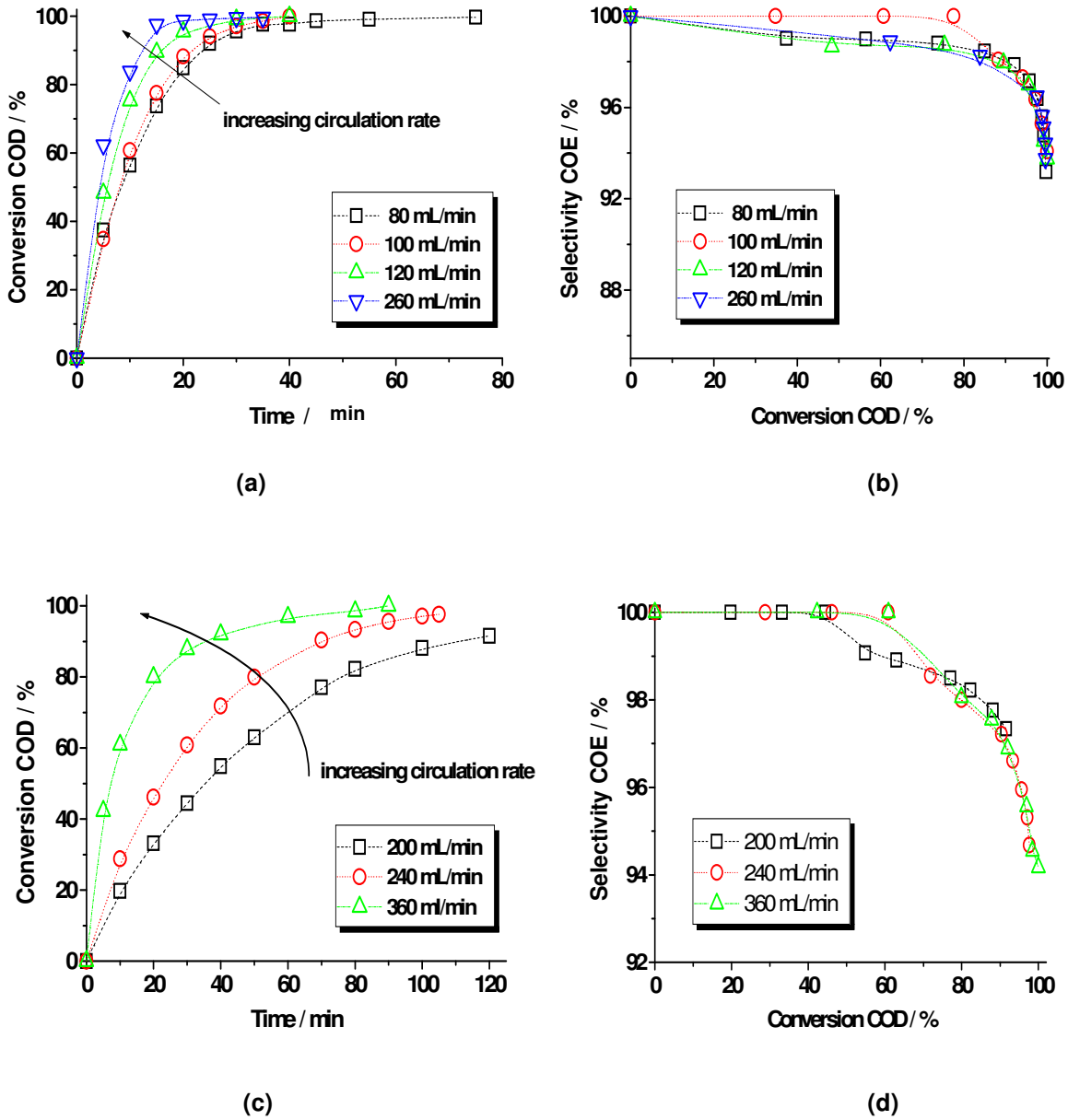

Fig. 6.1: COD-conversions and COE-selectivity at different circulation flow rates (50 °C, 10 bar H_2-pressure, 5 vol. % COD , (a, b): pore size: 1.9 µm; Pd-amount/membrane: 1.5±0.1 mg (c, d): pore size: 3.0 µm; Pd-amount: 1 ±0.1 mg)

In Fig. 6.1b and 6.1d the selectivities for COE at different circulation flow rates are plotted. The selectivity reaches 100 % for up to 60 % conversion and approximately 92-95% at complete conversion. An influence of the circulation rate on the selectivity is not observed. Already with the lowest circulation rate adjusted the removal of COE out of the membrane pores occurs sufficiently fast and an accumulation of COE does not take place. The consecutive reaction to COA does not occur until the COD concentration in the reaction mixture is very low, because the adsorption of COD at the catalyst is stronger than of COE.

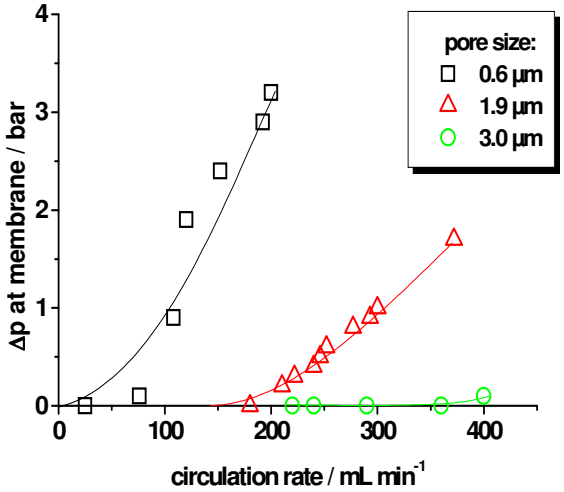

Fig. 6.2: Pressure drop at membrane for various circulation flow rates and pore sizes (*n*-heptane at 25 °C)

6.3.1.2 Influence of membrane pore size

In Fig. 6.3a the time dependent conversion for the hydrogenation with membranes with different pore sizes under the same reaction conditions are shown. The curve for the membrane with the smallest pores (0.6 µm) is slightly steeper than the two curves for the membranes with 1.9 µm and 3.0 µm pores. When using the 27-capillary bundles with different pore sizes the differences between the conversion rates become more pronounced and a clear trend is visible: the smaller the membrane pores, the higher the activity (Fig. 6.3b). A satisfactory explanation for this observation cannot be given yet. In our previous work [6.10] similar results regarding the pore size and the circulation rate were obtained for partial hydrogenation reactions with polymer membranes. The observations were explained by a better contact between reactants and the catalyst in smaller pores. In larger pores a part of the reactants flows through in a kind of bypass with fewer contacts to the catalyst at the

pore walls. However, the results of two-dimensional numerical simulations of convection and diffusion in the pores and the catalyzed reaction on the pore walls do not support this explanation for the conditions applied here. This phenomenon has to be studied deeper in further investigations. Therefore, other explanations must be considered, e.g. a different cluster size distribution of the Pd in the pores with different diameters.

No significant influence of the pore size on the selectivity for COE was observed (Fig. 6.4). The selectivities obtained at complete COD conversion are in the range of 93-95 % in the lab scale module as well as in the pilot plant.

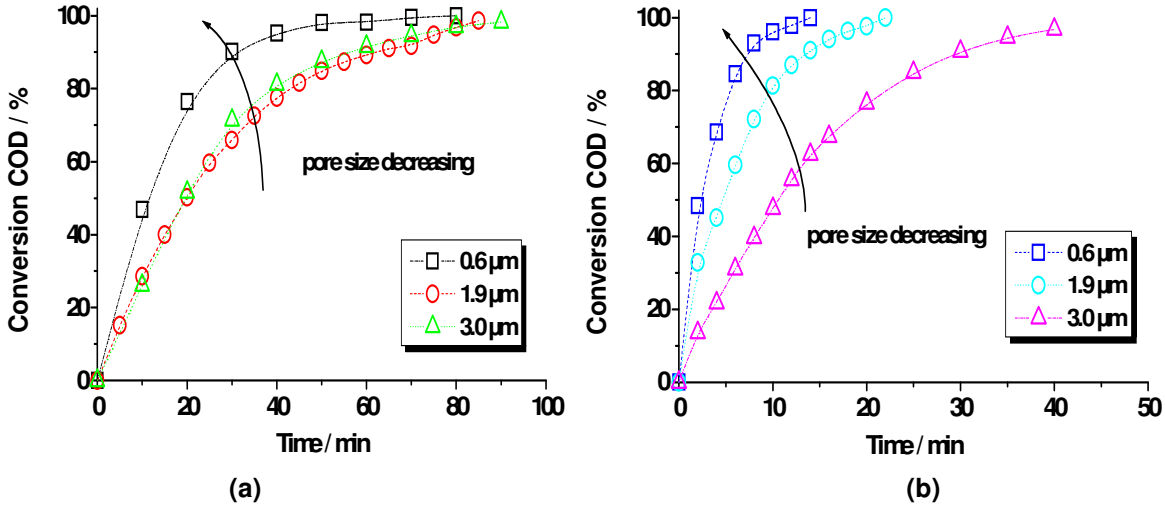

Fig. 6.3: COE-selectivity at different membrane pore sizes in lab scale and pilot plant (50 °C and 10 bar H_2-pressure, Pd amount: single capillaries: 1+/-0.1 mg, capillary bundles: 32+/-2.7 mg (0.6 µm); 35 mg +/- 2.7 mg (1.9 µm); 29 +/- 2.7 mg (3.0 µm); circulation rate in lab scale: 0.2 L/min, circulation rate in pilot plant: 8 L/min)

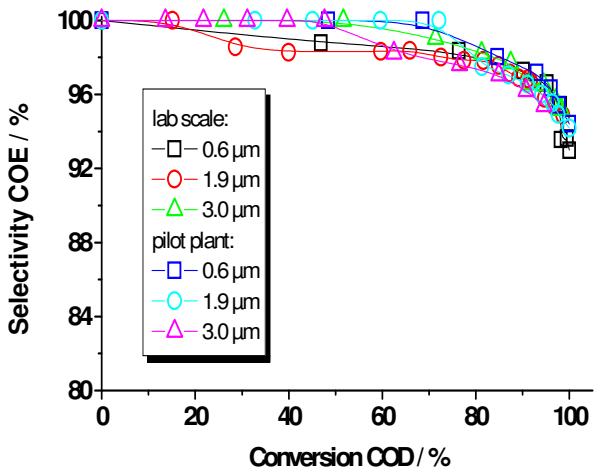

Fig. 6.4: COE selectivities at different membrane pore sizes for the partial hydrogenation of COD at 50 °C and 10 bar H_2-pressure in lab scale and pilot plant

6.3.1.3 Influence of Pd amount

From Fig. 6.5 the strong influence of the Pd amount per membrane on the reaction rate becomes obvious. Three membranes with 0.7 +/- 0.1 mg Pd, 1.0 +/- 0.1 mg Pd and 1.5 +/- 0.1 mg Pd/ per membrane are compared for the COD hydrogenation at the same circulation rate, temperature and hydrogen pressure. With the membrane with 0.7 mg Pd an initial reaction rate of 0.0204 $mol \cdot g_{Pd}^{-1} \cdot s^{-1}$ is obtained, with almost the twofold Pd amount the reaction rate is doubled (0.0422 $mol \cdot g_{Pd}^{-1} \cdot s^{-1}$). For the reaction with 1 mg Pd an initial reaction rate of 0.0226 $mol \cdot g_{Pd}^{-1} \cdot s^{-1}$. This nonlinear dependence of the observed rates is caused by different hydrogen profiles that establish within the membrane at different rates. Although the Pd amounts per membrane were relatively small, the reaction occurred in acceptable time ranges (25-80 minutes). This is due to the small Pd particle size and the homogeneous distribution of the Pd in the membrane structure as well as to a good access of the reactants to the catalytically active surface of the Pd particles. For the selectivity for COE no influence of the Pd amount was observed.

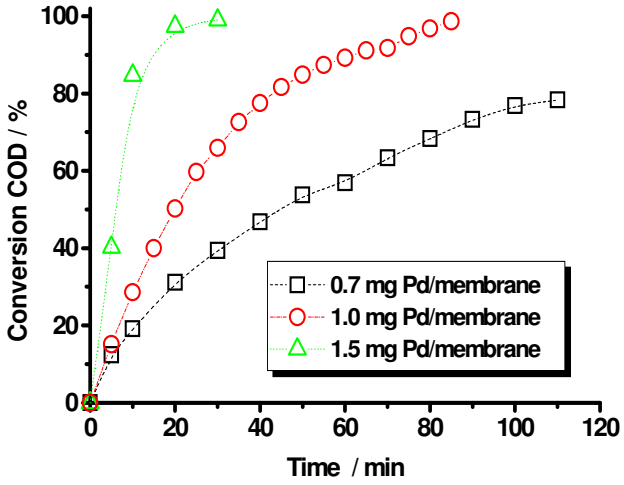

Fig. 6.5: COD-conversion rate as a function of the Pd amount of the membrane (50°C, 10 bar H_2-pressure, a pore size of 1.9 µm and a circulation rate of 200 mL/min)

6.3.1.4 Comparison of different reactor systems

In Fig. 6.6a the conversion of COD in different reactor systems with different catalysts is compared under similar reaction conditions at 50°C, 10 bar hydrogen pressure and 1 mg Pd content: membrane (0.03 wt. Pd, pore diameter: 1.9 µm), Pd/alumina egg shell catalyst (0.5 wt. Pd, particle size: 1.5 - 2 mm) in fixed-bed and Pd/alumina powder catalyst (0.5 wt.

Pd, particle size: < 25 µm) in slurry reactor. The COD hydrogenation experiments in the fixed-bed and the slurry reactor are reference experiments for benchmarking the catalytically active membranes. The Pd amount was kept at 1 mg in all experiments. With the powder catalyst the reaction rate and selectivity are expected to be unaffected by pore diffusion influence. In the slurry reactor the liquid phase is assumed to be saturated with hydrogen at any time of the reaction. This was shown by determining the volumetric gas-liquid mass transfer coefficient (k_La) [6.11]. Under these conditions an initial reaction rate of 0.039 $mol \cdot g_{Pd}^{-1} \cdot s^{-1}$ was obtained with the powder catalyst. Almost the same rate was obtained with the catalytic membrane (r_0=0.035 $mol \cdot g_{Pd}^{-1} \cdot s^{-1}$). Although the membrane reactor operates in a differential mode, which means that the hydrogen concentration of the reaction mixture decreases during every cycle through the membrane, the reaction rate is not lower than in the slurry reactor where the reaction mixture is saturated with hydrogen. This shows that with an adequately adjusted circulation rate the hydrogen concentration decay within the membrane can be compensated. With the egg shell catalyst in the fixed-bed reactor, which also operates in the differential mode, an initial reaction rate of only 0.021 $mol \cdot g_{Pd}^{-1} \cdot s^{-1}$ is obtained. The difference of the rates between membrane, powder and egg shell catalyst indicates mass transfer limitation of the reaction in the latter one caused by diffusion inside the pores of the catalyst pellet.

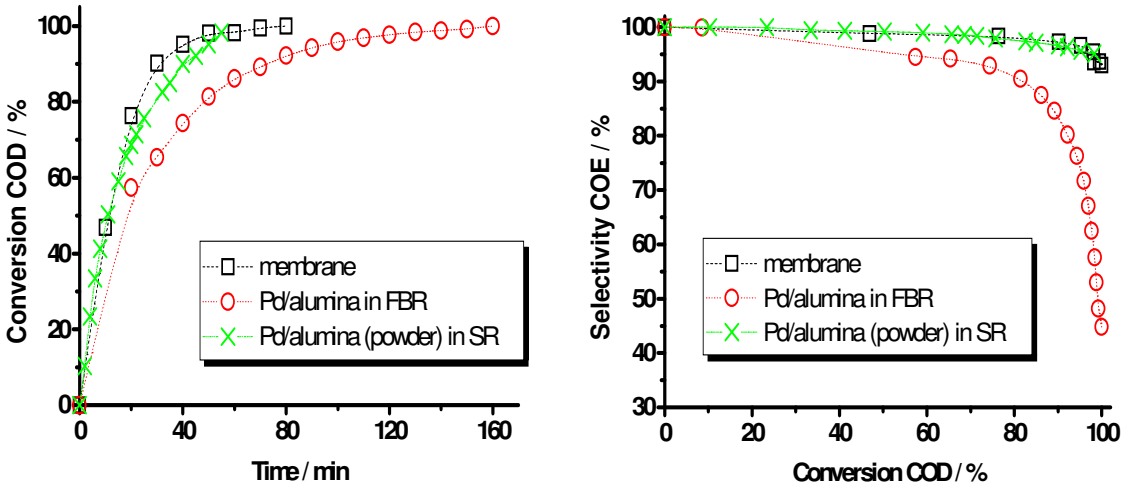

(a) (b)

Fig. 6.6: COD-conversion (a) and COE-selectivity (b) for different types of catalysts: membrane reactor (1 mg Pd, circulation rate: 200 mL/min, pore diameter: 1.9 µm), Pd/alumina powder catalyst (particle size: < 25 µm, 1 mg Pd) in slurry reactor (SR) and Pd/alumina egg shell catalyst (pellet size: 1.5-2 mm, 1 mg Pd, circulation rate: 200 mL/min) in fixed bed reactor (FBR) at 50°C and 10 bar hydrogen pressure

Fig. 6.6b and Tab. 6.1 compare the selectivity for COE obtained in the three reactor systems. With the powder catalyst a selectivity of 95 % at complete conversion is obtained, with the membrane a selectivity of 94 %. This demonstrates that the reaction in the membrane is indeed unaffected by pore diffusion. With the egg shell catalyst in the fixed bed reactor a substantially lower selectivity for COE is obtained at complete conversion (45 %). This indicates slow pore diffusion and accumulation of COE in the pores which promotes the consecutive reaction to COA. Although designed for this type of reaction, the egg shell catalyst is affected by pore diffusion while in the membrane reactor a micro kinetic control of selectivity was achieved.

Tab. 6.1: Selectivities and initial reaction rates of catalysts in different reactor types

reactor type	membrane reactor	slurry reactor (powder catalyst)	fixed bed reactor (egg shell catalyst)
COE selectivity at 100% conversion	94 ± 1 %	95 ± 1 %	45 ± 1 %
Initial reaction rate [$mol \cdot g_{Pd}^{-1} \cdot s^{-1}$]	0.035	0.039	0.021

6.3.1.5 Long-term stability of Pd- membranes

A series of measurements under the same conditions (50°C, 10 bar H_2-pressure, a flow rate of 200 mL/min) with the same membrane (pore size 1.9 µm) was carried out in order to study if there was any activity loss with increasing number of experiments. In Fig. 6.7a the time dependent conversion is plotted for six out of eleven experiments. There is some fluctuation within these results but for all experiments a reaction time of 70-80 minutes can be observed. The selectivity for COE was also barely affected in this long-term stability test; the selectivities are 92-94% at complete conversion (Fig. 6.7b).

Insofar, no significant deactivation of the catalyst is observable. AAS analysis of the product did not reveal any Pd leaching. The long-term stability was also proved for the 27-membrane bundle in the pilot plant in a series of 10 hydrogenation experiments. However, an increase of the pressure difference at the membrane from 1 to 4 bar was observed in lab scale. TOC (total organic carbon)-measurements of membranes used for hydrogenation experiments revealed an increased carbon content (0.07-0.15 wt. %) compared to new membranes (0-0.01 wt. %) which indicates some coking of the catalyst during the reaction. Although not (yet) affecting the activity of the membrane, an increase of the pressure drop is undesirable

as it increases the demand for pump energy. Therefore, measures for regenerating the membrane have to be found. The easiest way would be to rinse the membranes by flushing them with solvent. This was tested for the single capillary membranes with *n*-heptane and acetone but did not show any success. However, regeneration was possible by calcination of the membranes for 2 h at 300 °C in air and then activating them for 2 h at 250 °C in hydrogen flow. After this procedure, the membrane showed the same activity and a smaller pressure difference of 1 –2 bar in lab scale than before the calcination treatment.

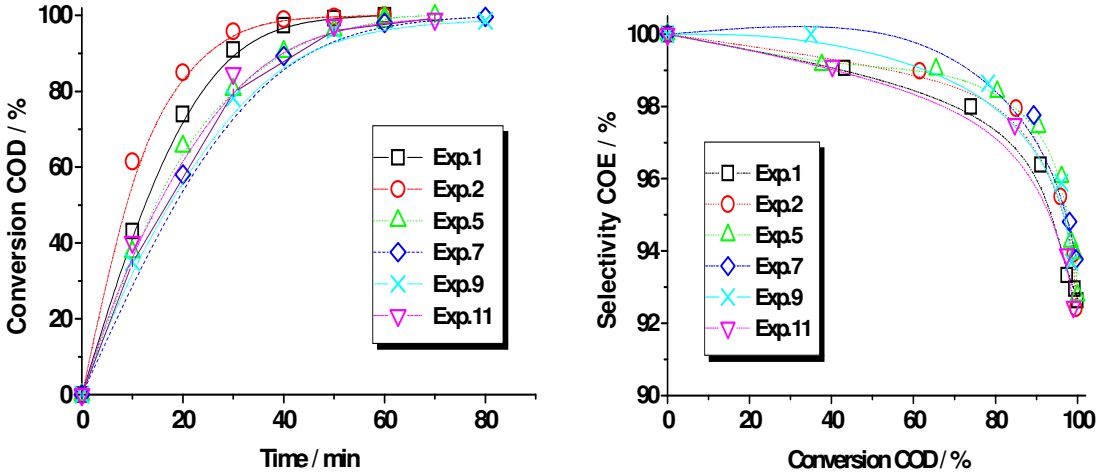

(a) **(b)**

Fig. 6.7: COD-conversion (a) and COE-selectivity (b) for a series of 11 sequenced experiments under the same conditions (50 °C, 10 bar, 5 vol. % COD, a flow rate: 200mL/min, 1 ± 0.1 mg Pd, pore size: 1.9 µm)

6.3.1.6 Scale- up of PFT-membrane reactor

For an industrial application a scale up of the reactor system to a larger dimension is necessary. For the experiments in the pilot plant bundles of 27-capillary membranes were used. Fig. 6.8a compares the results for the COD conversion in lab scale with a single capillary and in the pilot plant with a bundle of 27 capillaries under similar conditions (50 °C, 10 bar, pore diameter: 1.9 µm, mass flow: 1.48 kg/m²·s for the single capillary and 1.65 kg/m²·s for the bundle). The conversion curves for lab scale and pilot plant are in good agreement (Fig. 6.9a). For the COE selectivity also no difference could be observed: the selectivity at complete conversion is in the lab scale 93% and in the pilot plant 94% (Fig. 6.9b). The results demonstrate an easy scale up of the reactor system from lab scale to pilot

plant by simple multiplication of volume of liquid phase, membrane area and circulation rate as the up scale factor.

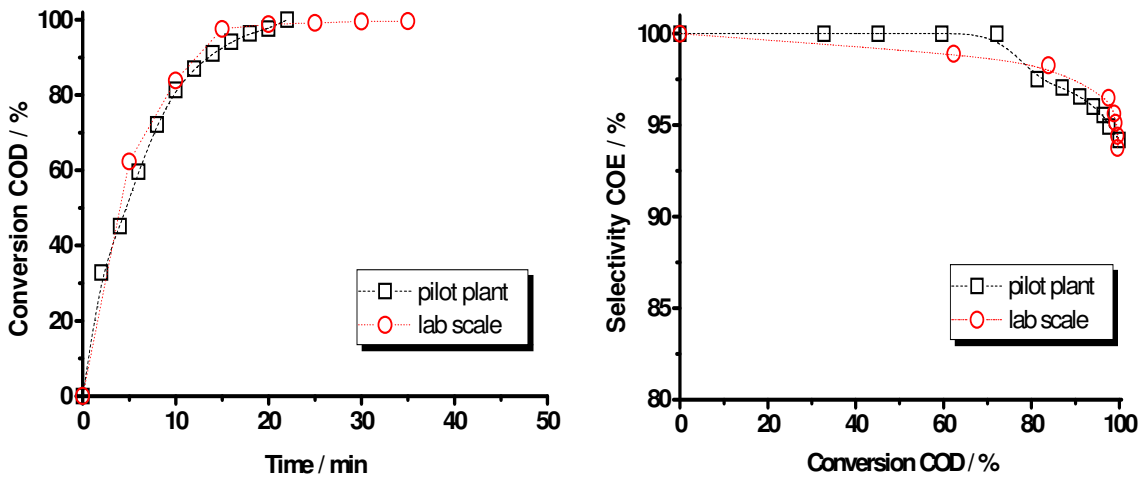

(a) **(b)**

Fig. 6.8: COD-conversion and COE-selectivity for in lab scale and pilot plant (50°C, 10 bar, 1.9 µm pore diameter, 5 vol. % COD, membrane flux: 1.65 kg/m²·s (pilot plant) and 1.48 kg/m²·s (lab scale))

Tab. 6.2: Influence of flow rate and pore size on reaction time and selectivity with membrane bundle at 50°C, 10 bar, 5 vol. % COD

pore diameter [µm]	circulation rate [kg/h·m²]	reaction time for complete conversion [min]	COE selectivity [%] at complete conversion of COD
0.6	1	16	92
(32.0 ± 2.7 mg Pd)	1.6	14	94
1.9	1	55	92
(35.0 ± 2.7 mg Pd)	1.6	22	94
3.0	1	35 (X=88%)	97 at X=88 %
(29.0 ± 2.7 mg Pd)	1.6	30 (X=88%)	97 at X=88 %
	2.4	27 (X=88%)	97 at X=88 %

Further experiments in the pilot plant validated the trends observed with a single tube in the lab scale. A higher circulation rate of the reaction mixture through the membrane increased

the conversion rate. Space-time-yields (STY) related to the module volume and to the Pd amount, respectively, were calculated at a COD-conversion of 95 %. The highest STY was obtained with the membrane bundle with the smallest pores and with the highest circulation rate of 1.65 kg/m²·s. The STY was 1.1 mol/m³ s and 5.5 mol/g_{Pd}s, respectively in this case. The selectivity for COE was hardly affected; it remained in the range of 92-94 % at complete conversion. The results are summarized in Tab. 6.2.

6.4 Summary

The partial hydrogenation of COD was studied for evaluating the potential to increase conversion and selectivity in a consecutive reaction in liquid phase by making use of the properties of a catalytic membrane in the flow-through operation mode. The reaction rate was mainly affected by the Pd amount and the circulation flow rate through the membrane. With an increasing circulation rate and higher Pd amount the rate increased. The selectivity for COE was not affected by these parameters; it was always in the range of 92-95% when COD was completely converted. The fact that the circulation rate does not affect the selectivity but changes the overall reaction rate means that both, first and second, hydrogenation reaction are influenced in the same way. The selectivity values obtained in the PFT-reactor correspond to the selectivity that was obtained in a slurry reactor with a powder catalyst where mass transport limitations can be excluded. This indicates that the reaction in the PFT-reactor was also unaffected by pore diffusion limitations. With the membrane reactor higher reaction rates und higher selectivity were obtained compared to with conventional egg shell catalyst in a fixed bed reactor. Scale-up from lab scale to a pilot plant is possible with comparable performance of the catalyst. STY can be optimized with adjusted higher circulation rates through the membranes and smaller pores. But it was also realized that the circulation rate was limited by the pressure drop at the membrane. Here, a compromise between operation costs and achievable STY must be found. For further optimization a model of this reactor is required that allows a calculation of the concentration profiles of the reactants within the membrane. Optimal utilization of the Pd and the whole membrane module should result in high STY if only weak concentration profiles of the reactants within the membrane can be adjusted. The next steps will be investigation of reactions with other substrates, metals as catalyst and supports in the membrane reactor in forced through flow mode in order to evaluate application potentials.

6.5 References

[6.1] R. Schomäcker, A. Schmidt, B. Frank, R. Haidar, A. Seidel-Morgenstern, *Membranen als Katalysatorträger*, Chem. Ing. Techn. (2005) 5: 77

[6.2] A. Schmidt, R. Haidar, R. Schomäcker, *Selectivity of partial hydrogenation reactions performed in a pore-through-flow catalytic membrane reactor*, Catal. Today (2005) 104; 2-4: 305-312

[6.3] H. Purnama, P. Kurr, A. Schmidt, I. Voigt, A. Wolf, R. Warsitz, R. Schomäcker, *α-Methylstyrene hydrogenation in a flow-through membrane reactor*, AIChE J. (2006) 52; 8: 2805-2811

[6.4] M. Reif, R. Dittmeyer, *Porous, catalytically active ceramic membranes for gas-liquid reactions: a comparison between catalytic diffuser and forced- through- flow concept*, Catal. Today (2003) 82: 3-14

[6.5] R. Dittmeyer, K. Svajda, M. Reif, *A review of catalytic membrane layers for gas/liquid reactions*, Topics in Catalysis (2004) 29; nos.1-2: 3-27

[6.6] C. Lange, S. Storck, B. Tesche, W. F. Maier, *Selective hydrogenation reactions with a microporous membrane catalyst, prepared by sol-gel dip coating*, J. Catal. (1998) 175: 280-293

[6.7] C. K. Lambert, R. Gonzalez, *Activity and selectivity of a Pd/γ-Al_2O_3 catalytic membrane in the partial hydrogenation reactions of acetylene and 1,3-butadiene*, Catal. Lett. (1999) 57: 1-7

[6.8] M. J. Vincent, R. D. Gonzalez, *Selective hydrogenation of acetylene through a short contact time reactor*, AIChE J. (2002) 48; no. 6: 1257-1267

[6.9] A. Bottino, G. Capannelli, A. Comite, A. Del Borghi, R. Di Felice, *Catalytic ceramic membrane in a three-phase reactor for the competitive hydrogenation-isomerization of methylenecyclohexane*, Sep. Pur. Technol. (2004) 34: 239-245

[6.10] I. C. Tilgner, C. Lange, H. W. Schmidt, W. F. Maier, *Three-phase hydrogenations with microporous catalytic membranes*, Chem. Eng. Technol. (1998) 21; 7:565-570

[6.11] R. Dittmeyer, V. Höllein, K. Daub, *Membrane reactors for hydrogenation and dehydrogenation processes based on supported palladium*, J. Mol. Catal. A: Chemical (2001) 173: 135-184

[6.12] G. Vitulli, A. Verrazzani, E. Pitzalis, P. Salvadori, *Pt/γ-Al_2O_3 catalytic membranes vs. Pt on γ-Al_2O_3 powders in the selective hydrogenation of p-chloronitrobenzene*, Catal. Lett. (1997) 44: 205-210

[6.13] M. Torres, J. Sanchez, J. A. Dalmon, B. Bernauer, J. Lieto, *Modeling and simulation of a three-phase catalytic membrane reactor for nitrobenzene hydrogenation*, Ind. Eng. Chem. Res. (1994) 33: 2421-2425

[6.14] L. Gröschel, R. Haidar, A. Beyer, H. Cölfen, B. Frank, R. Schomäcker, *Hydrogenation of propyne in palladium-containing polyacrylic acid membranes and its characterization*, Ind. Eng. Chem. Res. (2005) 44: 9064-9070

[6.15] J. Peureux, M. Torres, H. Mozzanega, A. Giroir-Fendler, J. A. Dalmon, *Nitrobenzene liquid-phase hydrogenation in a membrane reactor*, Catal. Today (1995) 25: 409-415

[6.16] D. Fritsch, I. Randjelovic, F. Keil, Application of a forced-flow catalytic membrane reactor for the dimerisation of isobutene, Catal. Today 2004; 98: 295-308

[6.17] A. A. Khassin, A. G. Sipatrov, T. M. Yurieva, G. K. Chermashentseva, V. N. Parmon, Plug-through contactor membranes (PCM) for the Fischer-Tropsch synthesis, Prepr. Pap.-Am. Chem. Soc., Div. Pet. Chem. 2004; 49; 2: 175-178

[16.8] D. Fritsch, K. Kuhr, K. Mackenzie, F. D. Kopinke, *Hydrochlorination of chloroorganic compounds in ground water by palladium catalysts part 1. Development of polymer-based catalysts and membrane reactor tests*, Catal. Today (2003) 82: 105-118

[6.19] F. Frusteri, A. Parmaliana, N. M. Ostrovskii, A. Iannibello, N. Giordiano, *Selective oxidation of ethylene over carbon-supported Pd and Pt catalytic membranes*, Catal. Lett. (1997) 46; nos. 1-2: 57

7 Simulation of the partial hydrogenation of 1,5-cyclooctadiene in PFT-membrane reactor

7.1 Introduction

Despite a remarkable technical attention in the last 15 years, industrial applications of membrane reactors in catalytic reaction processes are still missing. Exceptions are some low-temperature applications in biotechnology [7.1]. Technological gaps hinder further progress towards large-scale practice. Some of the major challenges concern understanding and modeling of transport mechanisms, development of criteria for choice of the optimal size of membrane reactors, flow patterns and complex modeling for large scale membrane reactors. This motivated several studies to the subject. A detailed description of a two-dimensional model for convective flux through tubular catalytic membranes is reported by Keil et al. [7.2]. The model was used for simulations of the H_2O_2 decomposition and was compared to experimental data. The authors present the residual content of H_2O_2 as a function of time and length inside the membrane tube as well as stationary profiles of H_2O_2 conversion as a function of the membrane radius and length. They conclude that the radial convective flow is a promising alternative for catalytic reactions because of the control on yield and selectivity. In a previous paper they describe the degradation of nitrate in water in the membrane reactor offering the advantage of low short-cut flows and less pressure drop compared to corresponding packed beds [7.3]. The model of a tubular, asymmetric alumina membrane is presented by Torres et al. [7.4]. The membrane consisted of a catalytically inert cylindrical wall of macroporous support of α-alumina, deposited with a thin layer of mesoporous γ-alumina, loaded with Pt as catalyst. The dynamic behavior of the closed-loop reaction system was completely modelled and simulated for the three-phase reaction of nitrobenzene hydrogenation. The model was developed coupling a numerical approach for the mass transfer mechanisms and kinetics determined experimentally without adjustable parameters. Hydrogen and nitrobenzene concentrations in the liquid phase, in the membrane and in the support were simulated. The authors showed that the mass transfer through the support and the membrane is influenced by the transmembrane pressure, the membrane thickness and the mean pore size. A model of an asymmetric membrane was also derived by Vincent et al. [7.5]. A thin Pd/γ-Al_2O_3 catalytic membrane, supported by an α-alumina macroporous membrane, was utilized for the selective hydrogenation of acetylene in a short contact time reactor. A gas-dispersion model with derived kinetics was employed in order to

describe the flow within the thin catalyst layer. The authors showed that by the forced flow situation and by short contact times mass transfer limitation can be eliminated.
In this chapter a mathematical model for the hydrogenation of COD in a membrane reactor in pore-flow-through (PFT) mode was developed in order to predict optimal operation conditions for this reaction. Concentration profiles of the reactants within the membrane give information about the optimal use of the Pd in the membrane. The model based on solving mass balances including kinetic data obtained from hydrogenation experiments in a slurry reactor with a powder catalyst (see chapter 5). The programming was carried out with the software MATLAB which allowed depiction of concentration profiles of the reactants within the membrane pore and versus the reaction time. Experimental results from the hydrogenation of COD in the membrane reactor were used to validate the model.

7.2 Reaction kinetics of COD-hydrogenation

In chapter 5 the determination of the intrinsic kinetics of the COD hydrogenation on Pd/alumina is described. The kinetics was studied with a powder catalyst (particle size: ~100 µm) at different initial COD concentrations, hydrogen pressures and reaction temperatures. A kinetic model derived from Langmuir-Hinshelwood kinetics which involves the adsorption of COD, COE and hydrogen was proposed. The kinetic parameters (k_1, k_2, K_{COD}, K_{COE} and K_{H2}) were determined by fitting the model to experimental data with the program Berkeley Madonna (Tab. 7.1). The micro kinetic reaction rates for the primary and the consecutive hydrogenation step can be predicted with the following equations:

$$r_1 = k_1 \frac{K_{COD} c_{COD} K_{H_2} c_{H_2}}{(1 + K_{COD} c_{COD} + K_{COE} c_{COE} + K_{H_2} c_{H_2})^2} \qquad \text{(eq. 7.1)}$$

$$r_2 = k_2 \frac{K_{COE} c_{COE} K_{H_2} c_{H_2}}{(1 + K_{COD} c_{COD} + K_{COE} c_{COE} + K_{H_2} c_{H_2})^2} \qquad \text{(eq. 7.2)}$$

The reaction progress is described with the following four differential equations, considering that the solution is always saturated with hydrogen:

$$r_{H_2} = \frac{d_{H_2}}{dt} = -r_1 - r_2 \qquad \text{(eq. 7.3)}$$

$$r_{COD} = \frac{d_{COD}}{dt} = -r_1 \qquad \text{(eq. 7.4)}$$

$$r_{COE} = \frac{d_{COE}}{dt} = +r_1 - r_2 \qquad \text{(eq. 7.5)}$$

$$r_{COA} = \frac{d_{COA}}{dt} = +r_2 \qquad \text{(eq. 7.6)}$$

The reaction takes place only within the volume of the membrane. As in the membrane pores the flow is assumed to be faster than diffusion, the reaction rates of the COD-hydrogenation in the PFT-reactor are described by the intrinsic kinetics.

Table 7.1: Estimated kinetic parameters for COD-hydrogenation at 50°C

	Estimated parameters
k_1 [mol·mg_{Pd}^{-1}·s^{-1}]	$1.8x10^{-3}$
k_2 [mol·mg_{Pd}^{-1}·s^{-1}]	$3.4x10^{-5}$
K_{COD} [L·mol^{-1}]	17.5
K_{COE} [L·mol^{-1}]	10
K_{H2} [L·mol^{-1}]	4

7.3 Model development

The model divides the reactor system in saturation vessel and membrane reactor (Fig. 7.1). The following assumptions and simplifications were taken into account to develop the differential equation system for the analysis.

- The saturation vessel operates as an ideal continuous stirred tank reactor (CSTR).
- All reactants form an ideal liquid mixture.
- The reaction mixture is an incompressible liquid.
- The system can be regarded as being isothermal.
- Chemical reaction takes place only inside the membrane.
- The flow is orthogonal to the membrane length.
- Potential energy has a negligible effect.
- The liquid in the saturation vessel is completely saturated with hydrogen.
- The gas-liquid solubility follows Henry's law.

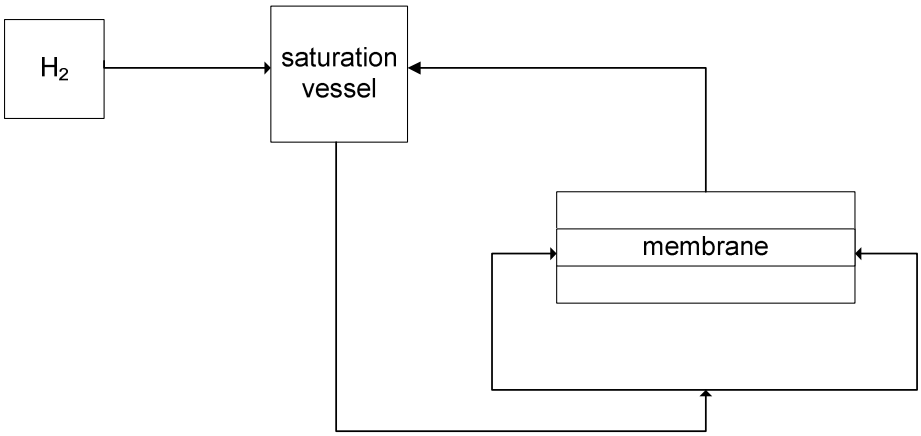

Fig. 7.1: Scheme of system configuration

The liquid flow through the membrane pores is assumed to be “plug-flow”. The conversion of COD and hydrogen while passing through the pores is described with a pseudo-homogeneous plug-flow-tube reactor model. The mass balance for the certain component within the pore under steady-state is given by:

$$dc_i / dL_{p,eff} = - R / w \qquad \text{(eq. 7.7)}$$

with c_i*: concentration of the component i*

$L_{p,eff}$*:: effective length of pore*

w: flow velocity

R: reaction rate

For calculation of the flow velocity *w* the circulation volume flow $\dot{V}$ is related to the porosity ε and the geometric surface area of the membrane *A*:

$$w = \dot{V} A / \varepsilon \qquad \text{(eq. 7.8)}$$

As it is assumed that the membrane pores are longer than the membrane wall thickness L_w, a tortuosity factor τ is included for calculation of the effective length of the membrane pores $L_{p,eff}$:

$$L_{p,eff} = L_w / \tau \qquad \text{(eq. 7.9)}$$

From the effective length of the pore and the flow velocity a residence time t_r of the reactants within the pores is obtained:

$$t_r = L_{p,eff} / w \qquad \text{(eq. 7.10)}$$

The mass balances are solved numerical by a Matlab program, provided from Karl-Winnacker- Institute, Frankfurt. The calculation is carried out quasi-stationary. The change of the concentrations while passing through the membrane pores is determined by integration of equation 7.7. The influence of the pore diameter is not included in the model.
The hydrogen supply results from the hydrogen pressure, the Henry constant, the volumetric gas-liquid mass transfer coefficient (k_La) and the hydrogen concentration in the liquid phase. The change of concentrations in the saturation vessel is calculated for a given time interval. In the saturation vessel no chemical reaction occurs and the hydrogen concentration is assumed to be constant. The mass balance for the certain component is given by eq. 7.11:

$$\frac{dc_i}{dt} = \frac{\dot{V}}{V}(c_{i,0} - c_i) \qquad \text{(eq. 7.11)}$$

$\dot{V}$: circulation volume flow
V: liquid volume
c: concentration in outlet flow
c_0: concentration in inlet flow
t: time

7.4 Module parameters

Module parameters include properties of the membrane capillaries (Tab. 7.2) and parameters of the reactor system like the employed liquid volume, the circulation rate and the k_la-value of the saturation vessel. Further input data are the initial concentrations of reactants, the reaction temperature, the hydrogen pressure and the mass of the catalyst. For the determination of the hydrogen concentration in the system the Henry coefficient is given for *n*-heptane at the corresponding temperature (DETHERM). From the input data the program calculates the membrane surface area, the cross sectional area of the pores, the number of pores per membrane, the effective length and the effective volume of the pores as well as the Pd-amount in the pore volume. With the given circulation rate the flow velocity and the residence time of the liquid in the pores is determined.

Tab. 7.2: Membrane characteristics for single tube membranes

inner diameter	1.9×10^{-3} m
external diameter	2.9×10^{-3} m
active length	0.22 m
membrane area	0.002 m²
mean pore diameter of α-Al_2O_3 support	0.6; 1.9; 3.0 x 10^{-6} m
wall thickness	0.5×10^{-3} m
effective length of a pore	1×10^{-3} m
porosity	0.3
tortuosity	2.0
membrane volume	4.4×10^{-7}m ³

7.5 Simulation and comparison with experimental results

With the derivations and input parameters above the presented model was able to calculate time dependent concentration profiles of COD, COE, COA and hydrogen as well as conversion and selectivity. Furthermore, a time dependent hydrogen concentration profile within the membrane pore is depicted. The influences of different parameters, e. g. the circulation rate and the Pd amount, on the hydrogenation reaction in the membrane reactor can be predicted. The simulated data were compared to experimental data.

Figs. 7.2a-d depict the simulated and experimental COD-conversion ($X_{COD,exp}$) and COE-selectivity curves for the hydrogenation of COD at 50°C and 10 bar hydrogen pressure for different circulation rates. As can be seen from the figures experimental and simulated curves are in good agreement. The model can represent the variations of the circulation flow as observed experimentally.

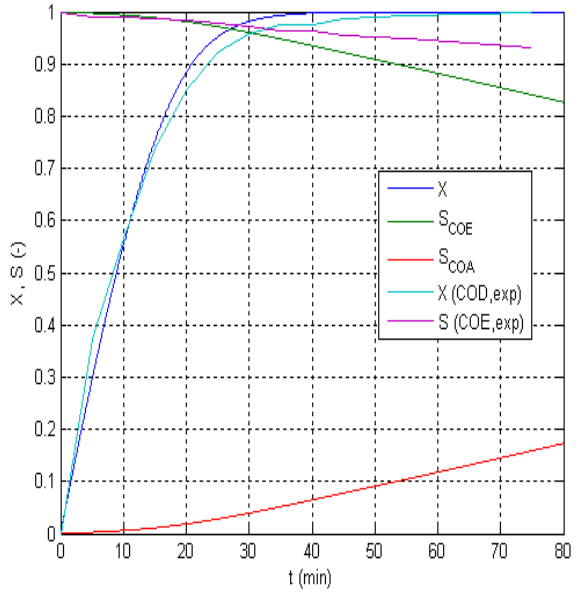

(a) 80 mL/min

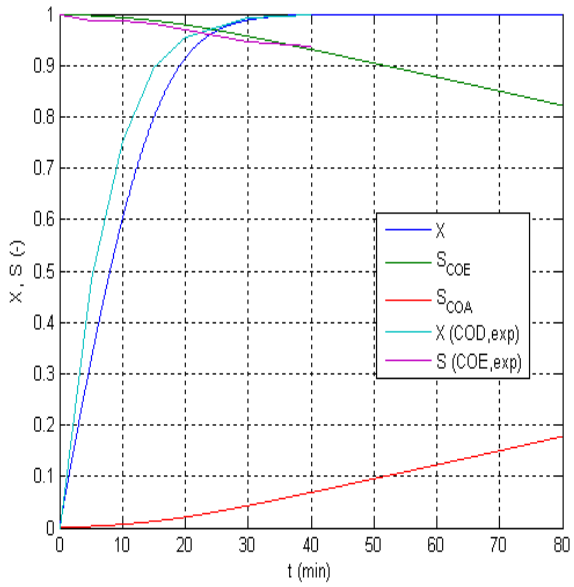

(b) 120 mL/min

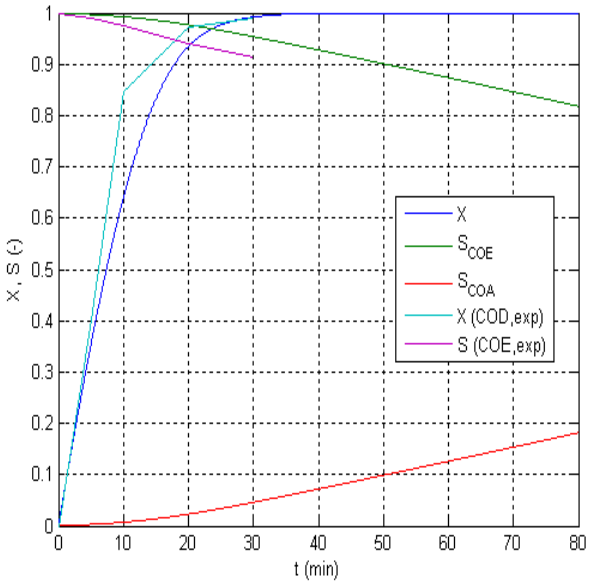

(c) 200 mL/min

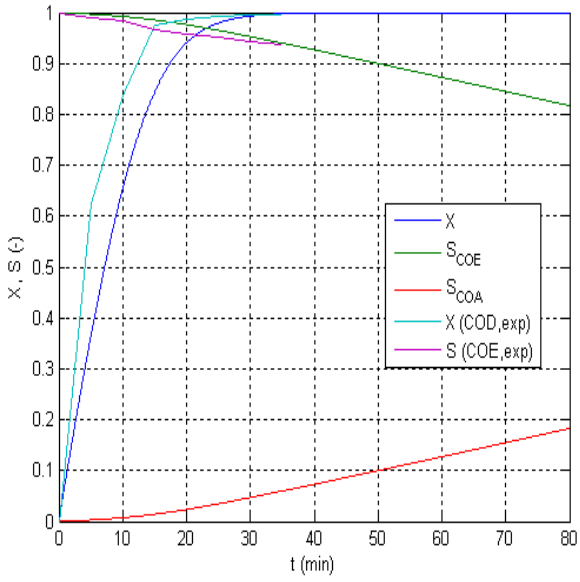

(d) 260 mL/min

Fig. 7.2: Time dependent COD conversion and COE selectivity (simulation and experimental data) at different circulation rates during hydrogenation reaction in membrane reactor at 50°C, 10 bar hydrogen pressure and a Pd-content of the membrane of 1.5 mg

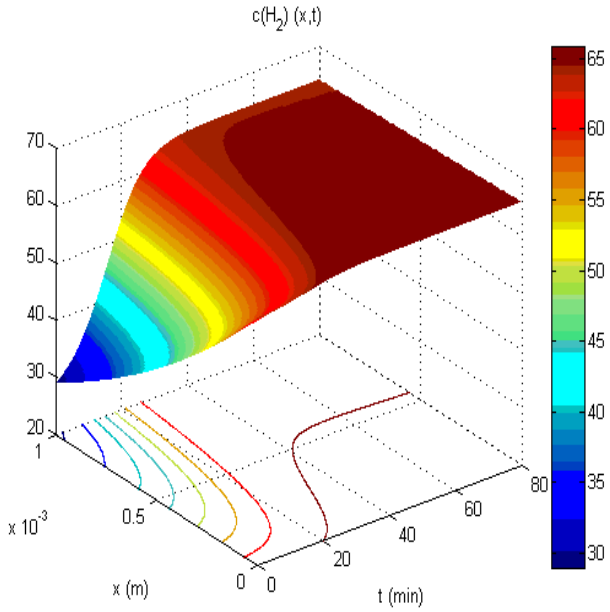

(a) 80 mL/min

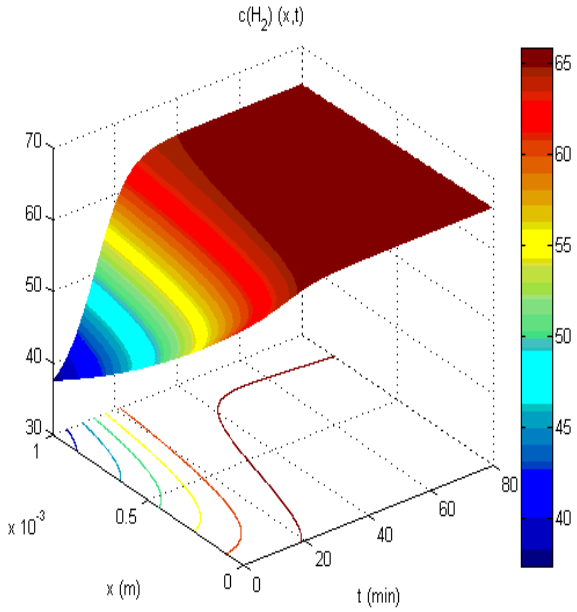

(b) 120 mL/min

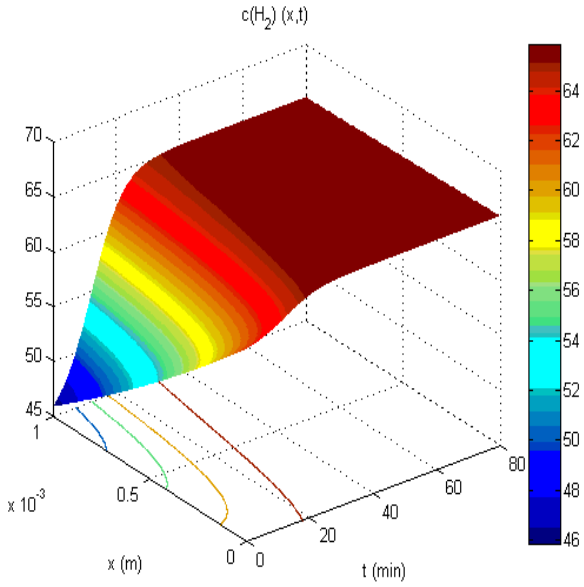

(c) 200 mL/min

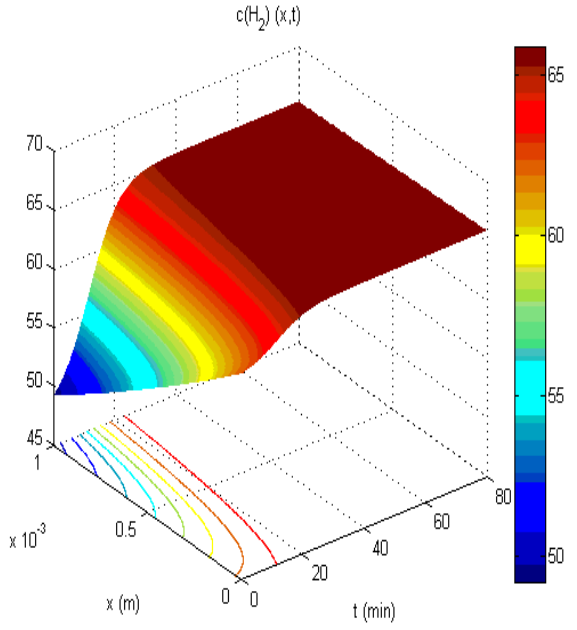

(d) 260 mL/min

Fig. 7.3: Time dependent hydrogen concentration profiles within the membrane pore at different circulation rates in PFT- membrane reactor at 50°C, 10 bar hydrogen pressure and a Pd-content of the membrane of 1.5 mg

In Figs. 7.3 a-d simulations of hydrogen consumption during the reaction are plotted versus time and versus effective membrane pore length for different circulation rates. As expected, an increased circulation rate leads to a weaker decline of the hydrogen concentration within

the membrane pore. With the lowest circulation rate (80 mL/min) the hydrogen concentration decreases from about 64 mol/m³ to about 29 mol/m³ whereas with a circulation rate of 260 mL/min the hydrogen concentration decreases from 64 mol/m³ only to 49 mol/m³. The lower hydrogen concentration decline at higher circulation rates is due to a decreasing residence time of the reactants within the membrane pore.

The simulations of the hydrogen concentration profile within the membrane pore provide important information about the progress of the particular reaction that is investigated in the PFT- membrane reactor. Three extreme cases are thinkable for different circulation rates: In case I in Fig. 7.4 the circulation rate is as low that the hydrogen concentration decreases to zero already within the membrane pore. As a result, a part of the catalyst, located at the membrane pore walls remains unused as the reactant flow pass through the pore without reacting. This situation can be optimized by increasing the circulation flow which is described in case II where the hydrogen is completely converted when the reactant leaves the membrane pore. By further increasing the circulation rate, case III is obtained which describes the situation of the COD hydrogenation in the simulations. The circulation rate is highest and hydrogen is not completely consumed within the membrane pore. From the comparison of the different possible situations it becomes obvious that the circulation rate and, if possible, the Pd content have to be carefully adjusted for an optimal utilization of the catalytic membrane. By this way, the presented model is an important tool for predicting the influences of process parameters and for optimizing reaction conditions.

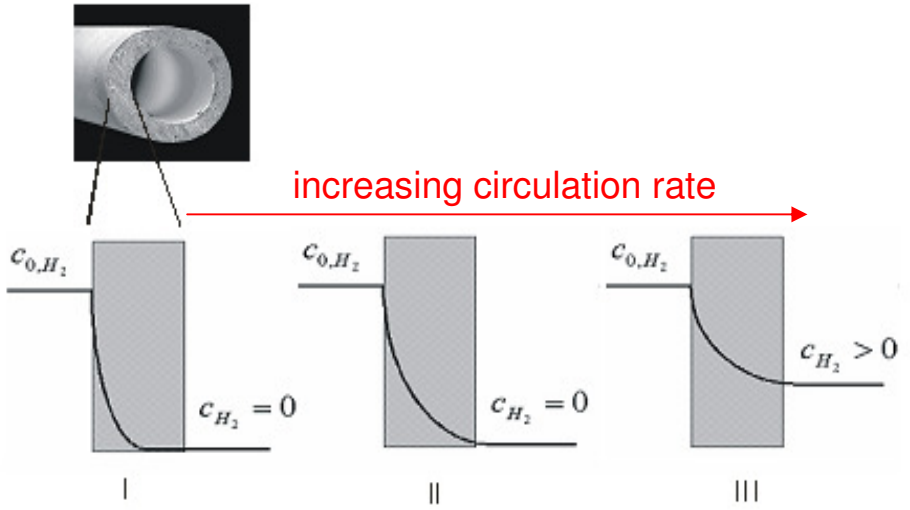

Fig. 7.4: Scheme of hydrogen conversion within a catalytic membrane pore at different circulation rates: circulation rate I <circulation rate II < circulation rate III

Simulations of the COD-conversion and COE-selectivity for the COD-hydrogenation at different Pd-contents of the membrane were also executed. Examples are presented in figs. 7.5a-c. At smaller Pd-contents (0.7 and 1mg) experimental data and simulations show no good coincidence. The simulations predict a higher reaction rate than experimentally observed. This can be explained by a nonlinear increase of Pd surface with mass of Pd deposited in the membrane pores by impregnation. It is assumed that at smaller Pd concentrations within the membrane pore structure the Pd is unevenly distributed and the Pd particle size is larger than in membranes with higher Pd content. This effect is not included in the model. However, the tendency of increasing reaction rate with increasing Pd-content in the membranes can be demonstrated with the simulations.

The simulations have demonstrated that the circulation rate of the reactants through the membrane pores and the Pd-content of the membranes play an important role for the performance of the PFT-membrane reactor. This is validated by the experimental results. A careful adjustment of the circulation rate is necessary in order to obtain an optimal utilization of the catalyst deposited in the ceramic membrane. The proposed model can be used to predict the reaction progress under certain operation conditions and to optimize the reaction parameters. This is important for the application of the PFT-reactor for other reactions and substrates. The Pd particle size distribution within the pores of membranes with different Pd contents should be investigated more detailed.

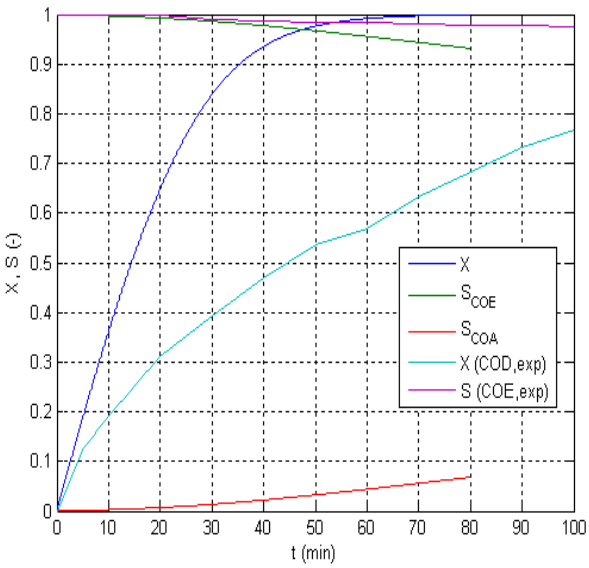

(a) Pd content: 0.7 mg

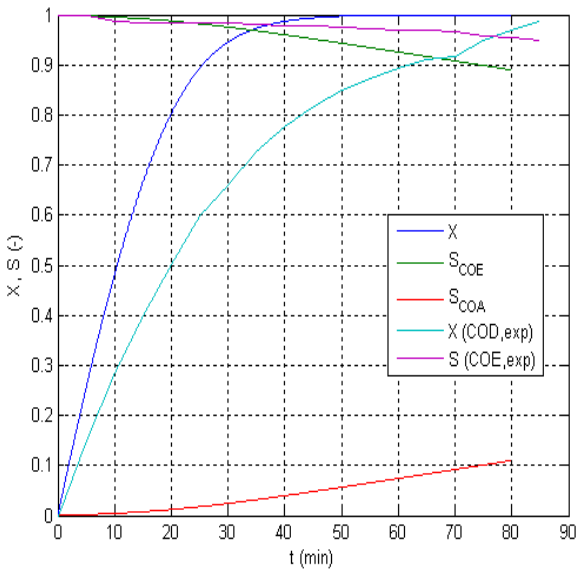

(b) Pd-content: 1.0 mg

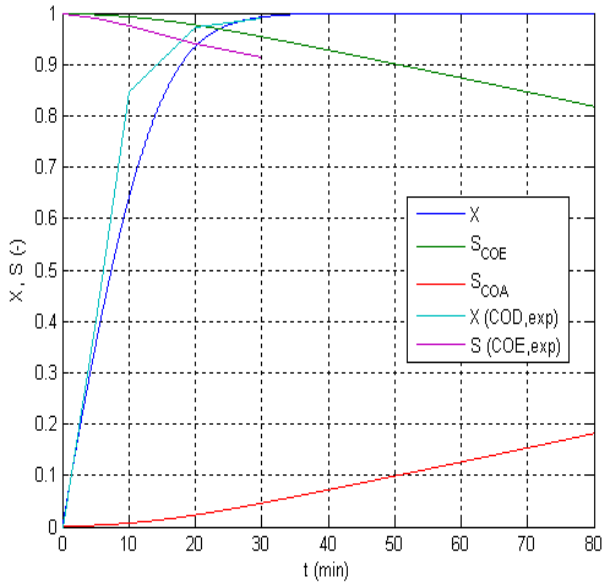

(c) Pd-content: 1.5 mg

Fig. 7.5: Time dependent COD conversion and COE selectivity (simulation and experimental data) at different Pd contents of the membranes during hydrogenation reaction in PFT-membrane reactor at 50°C, 10 bar hydrogen pressure and a circulation rate of 200 mL/min

7.6 References

[7.1] J. G. Sanchez Marcano, T. T. Tsotsis, *Catalytic Membranes and Membrane Reactors*, Wiley-VCH, Weinheim, Germany, 2002, p. 11

[7.2] F. Keil, U. Flügge, *High performance catalytic tubular membrane reactors owing to forced convective flow operation*, Hungarian Journal of Industrial Chemistry Veszprém, 33, 1-2, (2005) 31-42

[7.3] A. R. Garayhi, U. Flügge-Hamann, F. Keil, *Modeling of catalytic membrane reactors operated with liquids under nonstationary conditions*, Chem. Eng. Technol. 21 (1998) 1

[7.4] M. Torres, J. Sanchez, J. A. Dalmon, B. Bernauer, J. Lieto, *Modeling and simulation of a three-phase catalytic membrane reactor for nitrobenzene hydrogenation*, Ind. Eng. Chem. Res., 33 (1994) 2421-2425

[7.5] M. J. Vincent, R. D. Gonzalez, *Selective hydrogenation of acetylene through a short time reactor*, AIChE J. 48 (2002) 6

8 Partial hydrogenation of sunflower oil in PFT-membrane reactor

8.1 Introduction

The hydrogenation of vegetable oils is an important process in the modification of fats and oils. Typically, common vegetable oils contain a low percentage of saturated fatty acids and a high percentage of mono- and polyunsaturated fatty acids with the double bonds in the *cis*-configuration. The hydrogenation process saturates part of these double bonds which increases the melting point and the oxidative stability of the vegetable oil. The products are largely used in the alimentary industry and include margarines, shortenings, frying fats, salad and cooking oils [8.1]. There are also increasing industrial applications in pharmacy, cosmetics, lubricants, detergents, plastics etc. because of their low toxicity and their biodegradability and as they are renewable resources [8.2]. The degree of hydrogenation which leads to a hardening of the oil depends from the application but it is always desired to reduce the level of polyunsaturated fatty acids like linolenic and linoleic acid (C18:3 and C18:2) because they are very sensitive to oxidation [8.3]. From the nutritional point the level of the saturated fatty acids like stearic and palmitic acid in an edible fat should be as low as possible for they have an adverse influence on health. On the other hand a certain consistency and handling characteristics are required for functionality of the fat. An undesired product at the partial hydrogenation of oils are *trans*-isomers of fatty acids which increase the melting point and are suspected to correlate with cholesterol diseases as well [8.4]. For these reasons the demand and control for lower levels of *trans* fatty acids (<5%) in hydrogenated edible oils has increased.

In spite of a long history of hydrogenation processing of oils, its mechanism is not completely understood [8.5]. The chemistry is complex because of simultaneous reactions that occur: (1) saturation of double bonds, (2) *cis*-/*trans*-isomerization of double bonds and (3) shifts of double bonds. The hydrogenation of oils can be influenced by control of the operating variables temperature, hydrogen pressure, agitation and catalyst [8.1, 8.3]. Most commonly used in edible-oil industry are batch processes in slurry reactors (5-20 m^3), at high temperatures (140-225°C), low pressures (1-4 bar), long reaction times (2 h) and supported Ni catalysts or Raney nickel [8.3]. By varying the operation conditions it is possible to affect the selectivity of a hydrogenation process in order to form high-melting or low melting products. Selectivity means the saturation with hydrogen of the double bonds in the most

unsaturated fatty acid before that of a less unsaturated fatty acid [8.3]. However, it has not been possible to produce partially hydrogenated oil with a low *trans* fatty acid content in common industrial hydrogenation processes. A further problem is the difficult separation of the suspended catalyst from the product because the filtration of the catalyst is costly and time-consuming and results in a loss of the catalyst. Several alternatives to conventional hydrogenation processes have been proposed in the past few years. Most of them describe new catalyst development and modification [8.2, 8.6, 8.7, 8.8]. Some investigators study the hydrogenation process under supercritical conditions [8.9, 8.10]. Pintauro et al. reported soybean oil hydrogenation in a proton-exchange-membrane reactor resulting in partially hydrogenated products with low trans fatty acid content and moderately high concentration of saturated stearic acid [8.11]. Mathematical models were developed in order to predict the formation of *trans* isomers and unsaturated fatty acid changes during vegetable oil hydrogenation [8.12, 8.13]. A new reactor type for this reaction is the three-phase catalytic membrane reactor [8.14, 8.15]. Boger et al. proposed a monolithic catalyst as an attractive alternative to current technology [8.16].

One of the problems in the oil hydrogenation process is the low solubility of hydrogen in the oil which results in a low hydrogen concentration at the catalyst surface. Furthermore, the reaction is heavily limited by the hydrogen transfer to the catalyst surface due to diffusion within the catalyst pores. Zieverink et al. investigated how kinetic aspects and diffusion limitations determine the detailed composition of partially hydrogenated fatty acid methyl esters. They found that mass transfer limitations are a more likely explanation for the detailed product composition in fat hardening than previously reported kinetic arguments [8.17].

In this chapter the partial hydrogenation of sunflower oil in a membrane reactor in pore-flow-through (PFT) mode is described with the aim to improve the fatty acid selectivity for oleic acid and to prevent the *trans* fatty acid development. The reaction mixture (solvent, oil, saturated with hydrogen) was pumped through the pores of a catalytically active membrane with a convective flow in order to avoid mass transfer limitation by pore diffusion. Due to short contact times of the reactants at the catalyst it was expected to suppress the further hydrogenation to saturated fatty acids and to produce a partial hydrogenated oil with a high content of mono unsaturated fatty acid. The control of selectivities for partial hydrogenation reactions in a membrane reactor in pore-flow-through mode could be shown recently for a number of unsaturated olefines [8.18]. On the other hand, it was investigated how the use of Pd and Pt based membranes under high hydrogen pressures (3-20 bar) and low temperatures (50-80°C) would affect the *trans* level of the product. Because noble metals as catalysts are more active than Ni catalysts and allow mild reaction temperatures for the hydrogenation it was expected to control the isomerization to *trans* fatty acids. Furthermore, the immobilization of the noble metal as catalyst in the membrane structure makes a filtration

and recovery of the catalyst from the product needless. The catalyst lifetime with the application of noble metals is higher than with nickel catalysts which are prone to poisoning. Because of the passivity of Pt and Pd against atmospheric oxygen an evacuation before the reaction is not required. In the ideal case, the catalytic membrane can be reused directly in the next hydrogenation process without any catalyst loss. The elimination of process steps with the membrane reactor concept compared to conventional hydrogenation plants (Fig. 8.1) could reduce operation costs. On the other hand, emerging costs for recycling the reaction mixture by a pump have to be carefully considered.

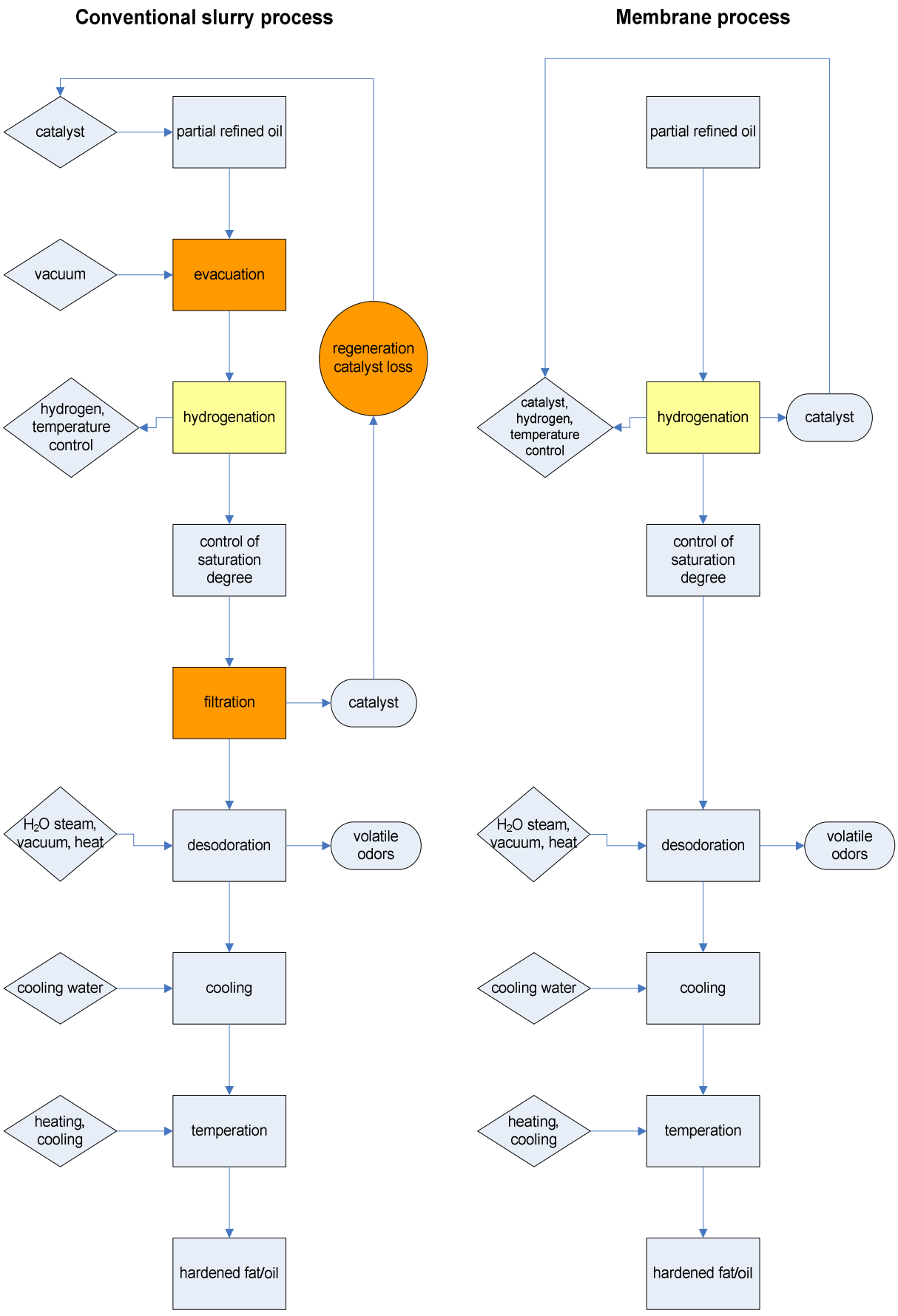

Fig. 8.1: Comparison of fat hardening process in conventional slurry and in membrane reactor

8.2 Experimental

Hydrogenation experiments in the PFT-membrane reactor were carried out at 50 and 80°C reaction temperature and hydrogen pressures in the range of 5 – 10 bar. The circulation rate of the reaction mixture (5 vol. % sunflower oil from a local supermarket in *n*-heptane as solvent) was 150 - 200 mL/min for all experiments. α-Al_2O_3 membranes with an average pore diameter of 3 µm were used as support for the catalyst. Palladium or platinum was deposited in the membrane by wet impregnation with an aqueous $PdCl_2$ (18.8 µmol) and H_2PtCl_6 (5.13 µmol/l) solution, respectively. Following, the membranes were activated with an aqueous reducing agent solution ($NaH_2PO_2 \cdot H_2O$). The preparation technique is described detailed in chapter 3. Samples of the reaction mixture were taken in 5 to 10 minutes interval and analyzed by gas chromatography (Siemens Sichromat 3, equipped with a Restek RTX 5 MS column). For GC anaylsis the reaction product has to be converted into their methyl esters by transesterification with the following procedure: 1 mL of the sample was mixed with 0.5 mL methanolic potassium hydroxide solution and stirred for 10 minutes. The mixture was left for 10 minutes for phase settling; then 1 mL HCl (1 mol/l) and one drop of methylorange was added. After centrifugation the organic phase could be separated and was applicable for the GC analysis.

For comparison reasons slurry experiments were carried out in a stirred stainless steel vessel with a liquid volume of 110 mL at 5 bar hydrogen pressure and 50°C with a commercial Pd/α-alumina catalyst (0.5 wt. % Pd) which was ground and sieved to a fine powder with 100 µm particle size in order to reduce any pore diffusion resistance. Samples were taken in intervals and prepared for GC analysis as described above.

8.3 Results and discussion

The activity of the catalytic membrane is depicted by the time dependent conversion of linoleic acid (C18:2). The development of stearic acid (C18:0) and elaidic acid (C18:1 *trans*) during the reaction is demonstrated as a function of linoleic acid conversion. The iodine value (IV) which expresses the degree of unsaturation in the oil is used for comparing different results. It was calculated from the composition determined by GC. The typical fatty acid composition in sunflower oil is 63 – 68 % linoleic acid (C18:2), 18 - 23 % oleic acid (C18:1 *cis*), 3 - 4.5 % stearic acid (C18:0) and 5 – 7 % palmitic acid (C16:0) [8.3, 8.17]. The composition of sunflower oils can vary from region to region and year to year. The level of linolenic acid (C18:3) in sunflower oil is very low (< 1%). Consequently, the hydrogenation reaction involves consecutive saturation of C18:2 *cis* to C18:1 *cis* and subsequent C18:1 *cis* to C18:0. The ratio of the reaction rate constants k_2 to k_1 controls the selectivity of the

monoene fatty acid. Parallel reactions are the isomerization of C18:2 *cis* to C18:2 *trans* and of C18:1 *cis* to C18:1 *trans* (Fig. 8.2). The aim of this study was to reduce the level of *trans* fatty acid below 5 % (a level consistent for butter [8.9]) and the level of stearic acid below 10 % through hydrogenation. This means selective hydrogenation of linoleic acid to oleic acid by suppressing the complete hydrogenation to stearic acid and the *trans* isomerization to elaidic acid.

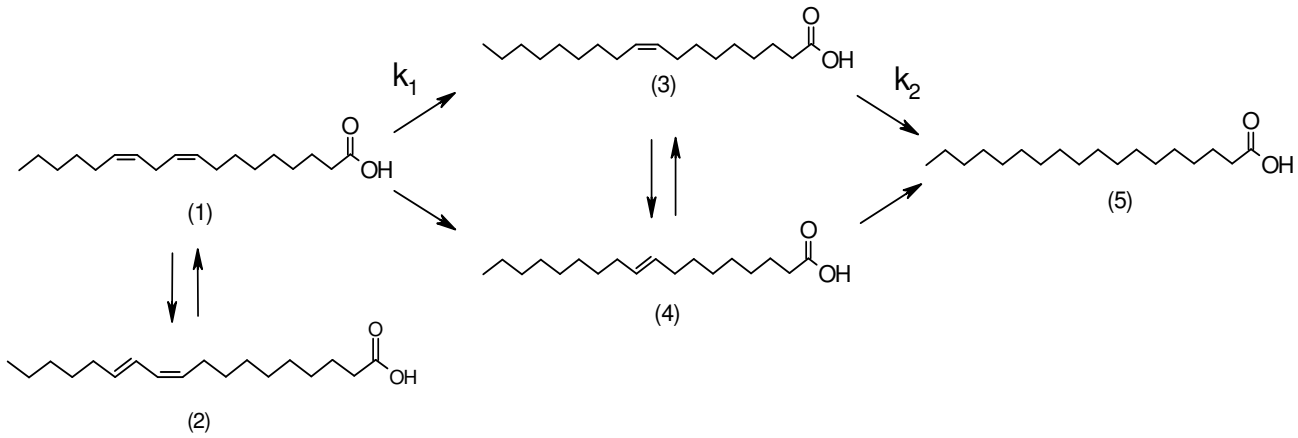

Fig. 8. 2: Reaction mechanism for the hydrogenation of fatty acids in sunflower oil (1) linoleic acid, (2) *trans* linoleic acid (3) oleic acid, (4) elaidic acid, (5) stearic acid

Fig. 8.3 represents an example of the change in fatty acid composition during the hydrogenation in the PFT- membrane reactor at 80°C and 10 bar hydrogen pressure for a Pd containing alumina membrane. Linoleic acid depletes within 60 minutes. The content of oleic acid initially increases first, then levels off, and subsequently decreases, while the elaidic acid content steadily increases to a final value of 42 %. The level of stearic acid increases from 4 % to 26 %. From this figure it becomes obvious that the parallel reaction, the isomerization to *trans* fatty acids, competes with the hydrogenation reaction. An experiment with a powder catalyst in a slurry reactor is performed in order to get insight into possible mass transfer limitations. The powder catalyst serves as benchmarking for the process in the membrane reactor. From Fig. 8.4 it becomes obvious that the consecutive reaction to stearic acid is strongly promoted in the slurry reactor. The increase of *trans* fatty acids during the hydrogenation, however, is smaller than in the membrane reactor. This is due to a better availability of hydrogen in the slurry reactor. The saturation of hydrogen in the liquid and the reaction take place in the same location while in the membrane reactor the hydrogen concentration decreases during every passage through the membrane. The reaction mixture has to be resaturated with hydrogen before passing it through the membrane again. The membrane reactor operates in a differential mode.

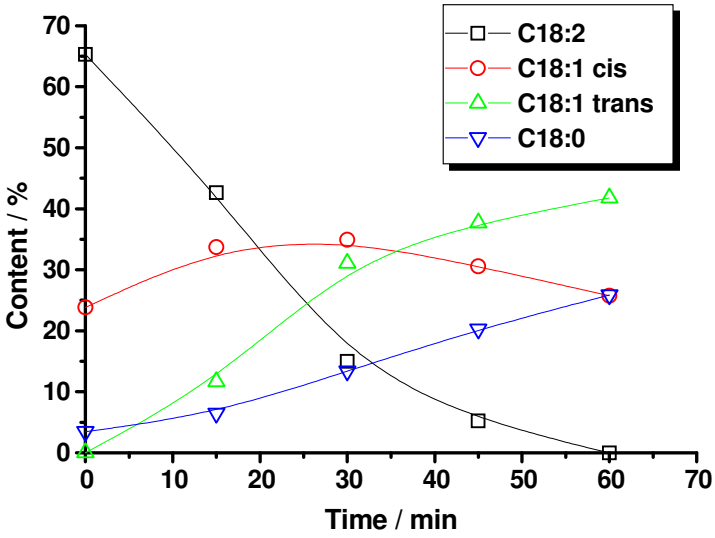

Fig. 8.3: Content of fatty acids in sunflower oil during hydrogenation in PFT- membrane reactor at 80°C, 10 bar H_2-pressure, 0.03 wt. % Pd, 200 mL/min circulation flow rate

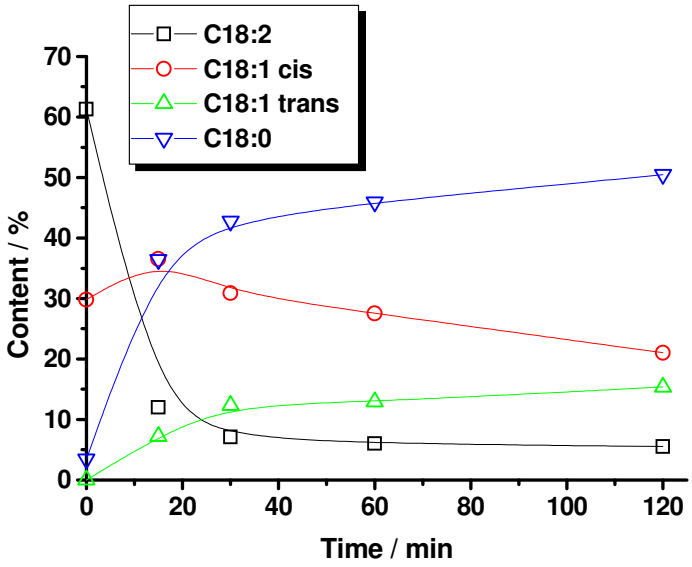

Fig. 8.4: Content of fatty acids in sunflower oil during hydrogenation in slurry reactor with powder catalyst at 50°C, 10 bar H_2-pressure, 0.03 wt. % Pd

As the consecutive reaction to the saturated fatty acids is also very pronounced in the membrane reactor it is assumed that the hydrogenation reaction of sunflower oil is subjected to different competitive impacts. Mass transfer by diffusion is not exclusively influencing the reaction rate to the stearic acid. The simultaneous occurrence of consecutive and parallel reactions makes it difficult to separate the effects on the reaction rate. Possibly, the

circulation velocity of the reaction mixture through the membrane is not high enough to suppress depletion of hydrogen in the pores. In this case, an increase of the circulation flow rate would at least reduce the stearic acid formation. Experiments with higher flows failed because of an increasing flow resistance at the membrane, which leads to a failure of the pump used. This is a problem of the membrane reactor that concerns especially substances with relatively high viscosities like natural oils.

8.3.1 Influence of H_2-pressure

The reaction rate of the hydrogenation is strongly limited by the hydrogen concentration in the oil. Because of the low solubility, the hydrogen concentration is substantially lower than the concentration of the unsaturated fatty acids. In order to obtain adequate conversions of linoleic acid in the PFT-membrane reactor, the reaction mixture has to be circulated through the reactor system and resaturated with hydrogen up to a hundred times. An important parameter in this context is the hydrogen pressure as the hydrogen solubility increases with increasing hydrogen pressure according to Henry's law. Therefore the reaction rate increases proportional to increasing hydrogen pressure. This is visible in Fig. 8.5 where the conversion of C18:2 is plotted versus time for different hydrogen pressures. At 80 °C reaction temperature, the linoleic acid is completely converted after 20 minutes at 20 bar and only after 60 minutes at 10 bar. At 5 bar 95 % conversion is obtained after 120 minutes. More important than the reaction time is the level of saturated fatty acids and of *trans* isomers, i.e. stearic acid and elaidic acid, respectively, when C18:2 is converted according to the desired level of iodine value (IV~ 80).

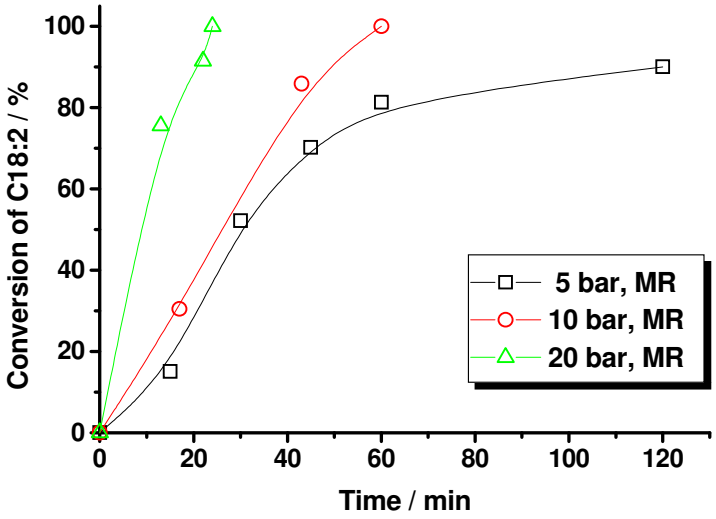

Fig. 8.5: Conversion of C18:2 during hydrogenation of sunflower oil in PFT- membrane reactor at 80 °C, 0.03 wt. % Pd and different H_2-pressure, 200 mL/min circulation flow rate

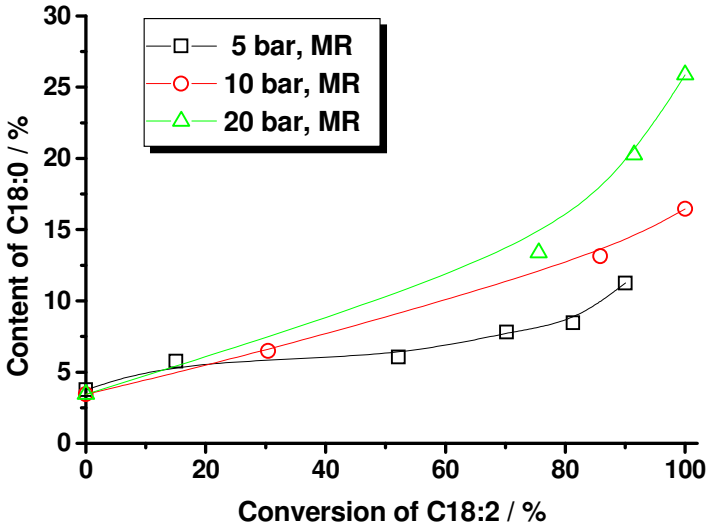

Fig. 8.6: Formation of C18:0 during hydrogenation of sunflower oil in PFT- membrane reactor at 80°C, 0.03 wt. % Pd and different H_2-pressure, 200 mL/min circulation flow rate

In Fig. 8.6 the formation of C18:0 during the reaction is plotted for 5, 10 and 20 bar hydrogen pressure at 80°C and the same membrane. The progress of the reaction is followed up to complete conversion of C18:2. A higher hydrogen pressure affects the selectivity for the monoene fatty acids negatively, which means more C18:0 is developed with increasing conversion of C18:2. While the reaction rate increases due to better supply of hydrogen, the complete hydrogenation to the saturated fatty acid is more promoted. At IV ≈ 80 the stearic acid content is 10 % (5 bar), 12 % (10 bar) and 15 % (20 bar).

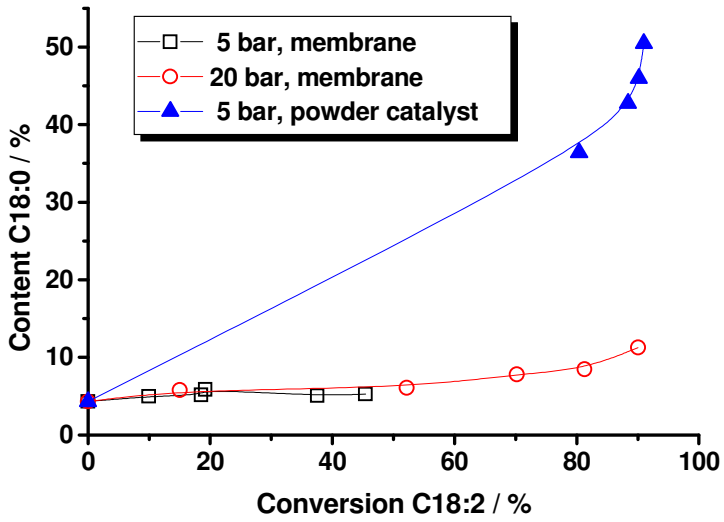

Fig. 8.7: Formation of C18:0 during hydrogenation of sunflower oil in PFT- membrane reactor and slurry reactor with powder catalyst at 50°C, 0.03 wt. % Pd and different H_2-pressure, 200 mL/min circulation flow rate

In Fig. 8.7 the content of stearic acid during the hydrogenation reaction in membrane and slurry reactor are compared for 5 and 20 bar at 50°C. It becomes obvious that in the slurry reactor the complete hydrogenation of C18:2 is more pronounced than in the membrane reactor at the same conditions. In the slurry reactor at 5 bar the stearic acid content is already 52 % at 90 % conversion of linoleic acid (45 % at IV ≈ 80) while in the membrane reactor at the same temperature and 20 bar the stearic acid content is only 11 %. The reaction at 50°C and 5 bar in the membrane reactor proceeded very slowly and was terminated at lower conversions. Therefore a comparison with the slurry reactor is possible only for smaller conversions. Up to 45% conversion the C18:0-content is still under 5 % in the membrane reactor.

A significant impact of the pressure was expected on the *trans* isomer development. In conventional hydrogenation processes which are performed at low pressures (1-3 bar) the low solubility of hydrogen in the oil and consequently, an insufficient hydrogen concentration at the catalyst surface promotes the formation of *trans* fatty acids. Therefore, the hydrogenation in the membrane reactor was performed at higher pressures. The expected results, however, were not obtained. The content of C18:1 *trans* increases linearly during the hydrogenation at 80°C up to 25 % for a C18:2- conversion of 60% for all three hydrogen pressures (Fig. 8.8). At IV ≈ 80 a *trans* isomer content of 30 % (20 bar), 35 % (10 bar) and 45 % (5 bar) is obtained. The reason for this impact of pressure on the *trans* isomer formation is accounted to the depletion of hydrogen within the membrane during every membrane passage of the reaction mixture. The higher concentration of hydrogen in the

liquid phase at higher pressures has only a little effect regarding the *trans* isomer prevention because the hydrogen is consumed very fast within the catalytic membrane during the hydrogenation reaction. This demonstrates also the comparison of membrane and slurry reactor at the same hydrogen pressure. In the slurry reactor the liquid phase is assumed to be saturated with hydrogen at any time of the reaction. Consequently, less C18:1 *trans* is produced in the slurry reactor (12 % at IV ≈ 80) at 5 bar and 50°C, compared to the membrane reactor at 20 bar (45 % at IV ≈ 80). In the membrane reactor no pressure impact is observed up to a linoleic acid conversion of 48 % (fig. 8.9).

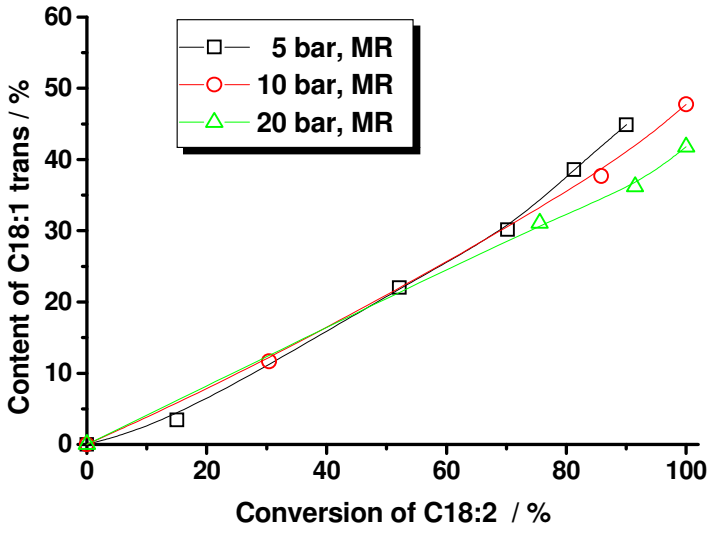

Fig. 8.8: Formation of C18:1 *trans* during hydrogenation of sunflower oil in PFT- membrane reactor at 80°C, 0.03 wt. % Pd and different H_2-pressure, 200 mL/min circulation flow rate

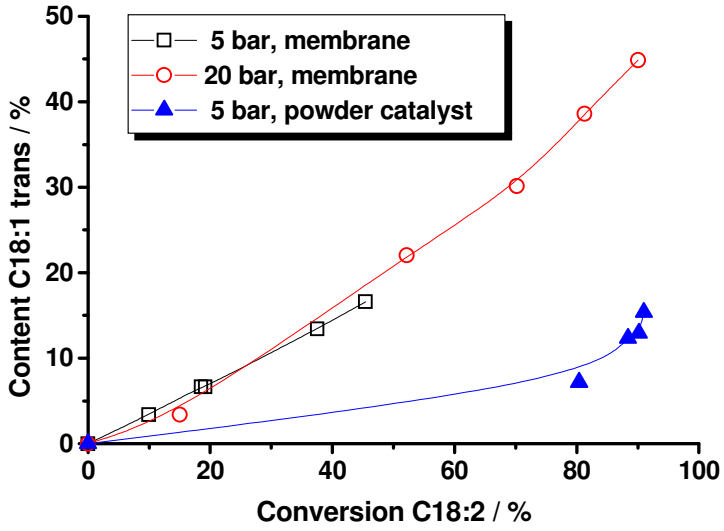

Fig. 8.9: Formation of C18:1 *trans* during hydrogenation of sunflower oil in PFT- membrane reactor and slurry reactor with powder catalyst at 50°C, 0.03 wt. % Pd and different H_2-pressure, 200 mL/min circulation flow rate

8.3.2 Influence of reaction temperature

The influence of the temperature on the activity and the product composition was determined in experiments with the same Pd membrane at 5 bar. The main effect was obtained for the reaction rate: at higher reaction temperature the reaction rate was substantially increased. The reaction at 50°C was very slow. After 225 minutes only 45% conversion of C18:2 were achieved. At 80°C 90% conversion was obtained after 120 minutes (Fig. 8.10).

The influence of temperature on the development of saturated and *trans* fatty acids, however, is low (Fig. 8.11). This is unexpected as in literature the temperature influence is described as follows: at low temperatures less *trans* fatty acids are formed [8.9, 8.13, 8.16, 8.20]. Up to a C18:2-conversion of 45% there is not much difference in the *trans* fatty acid and stearic acid content of the reaction runs at different temperatures in the membrane reactor. For higher conversions no statement can be given.

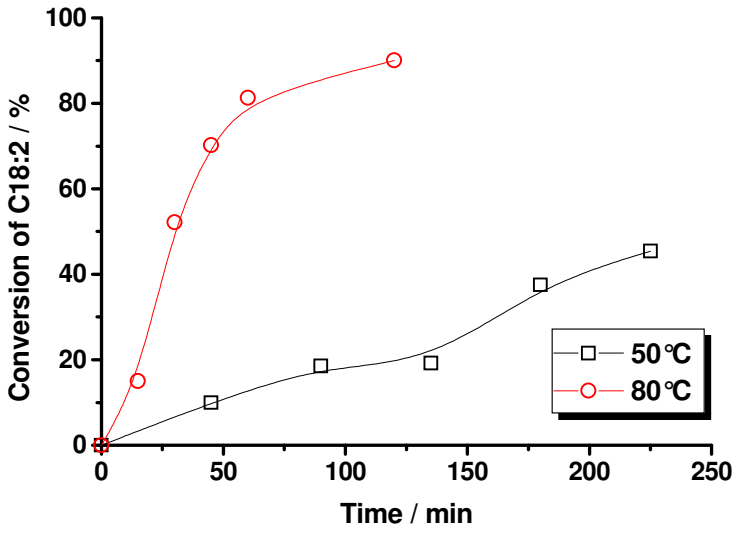

Fig. 8.10: Conversion of C18:2 during hydrogenation of sunflower oil in PFT- membrane reactor at 5 bar H_2-pressure, 0.03 wt. % Pd and different reaction temperatures, 200 mL/min circulation flow rate

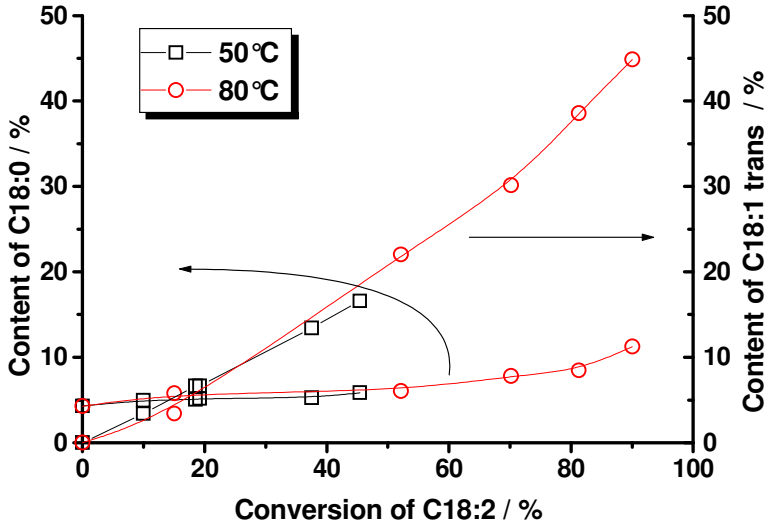

Fig. 8.11: Formation of C18:0 and C18:1 *trans* during hydrogenation of sunflower oil in PFT-membrane reactor at 5 bar H_2-pressure, 0.03 wt. % Pd and different reaction temperatures, 200 mL/min circulation flow rate

Pore blocking of the membrane is a technical problem with the PFT-membrane reactor that appears mainly at low temperatures during natural oil hydrogenation. The flow through the membrane decreases strongly and the reaction slows down, particularly when more

saturated fatty acids develop at the end. This may add to the bad results regarding *trans* fatty acid and stearic acid content because mass transport limitations cannot be excluded at low flow rates.

8.3.3 Influence of catalyst metal

The catalysts currently used on industrial scale contain nickel. These catalysts require reaction temperatures above 150°C in order to show adequate activity. There is some concern regarding the toxicity of traces of nickel leaching out in the oil. Noble metals like palladium or platinum exhibit an activity 100 times higher than that of nickel catalysts. They allow milder reaction conditions for the hydrogenation which should prevent the *trans* fatty acid production. The immobilization of the noble metal on the alumina membrane avoids the separation of the catalyst from the product by time-consuming and costly filtration steps. The hydrogenation of sunflower oil in a membrane reactor was tested with Pd- and Pt-containing membranes.

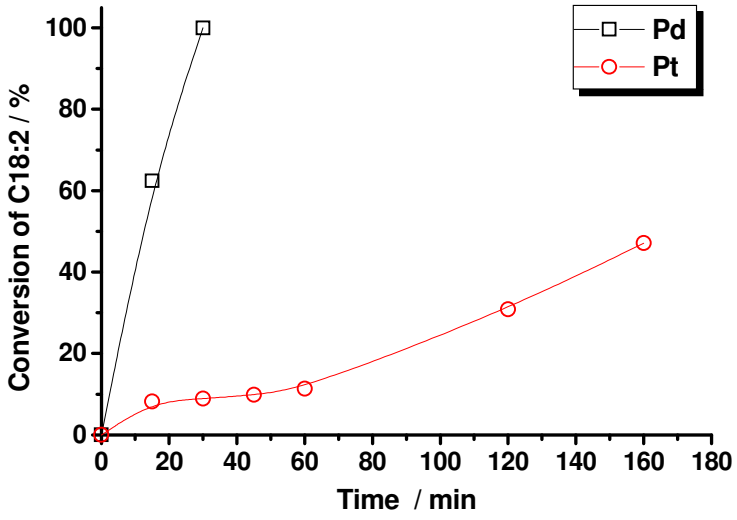

Fig. 8.12: Conversion of C18:2 during hydrogenation of sunflower oil in PFT-membrane reactor at 80°C, 20 bar H_2-pressure, 200 mL/min circulation flow rate and different metals as catalyst (1 mg)

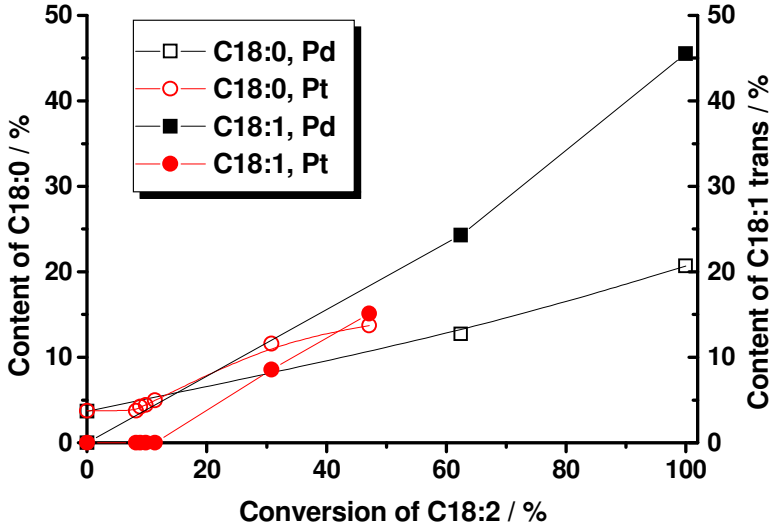

Fig. 8.13: Formation of C18:0 and C18:1 *trans* during hydrogenation of sunflower oil in PFT-membrane reactor at 80°C, 200 mL/min circulation flow rate, 20 bar H_2-pressure and different metals as catalysts

In Fig. 8.12 the conversion of linoleic acid is plotted for experiments with both metals as catalysts for a similar metal content in the membrane at 20 bar and 80°C. With Pd a complete conversion is obtained after 30 minutes. With Pt the reaction runs significantly slower than with Pd. After 160 minutes less than 50% of linoleic acid is converted. This is in good agreement with the published data of Nohair et al. [8.6]. With the Pt-containing membrane more C18:0 is developed at the same C18:2-conversion than with the Pd-membrane (Fig. 8.13). The *trans* isomer formation, however, is slightly less than with Pd (Pt: 15% and Pd: 18% at a C18:2-conversion of 48%).

8.4 Conclusion

The partial hydrogenation of sunflower oil was performed in a membrane reactor in pore flow though mode with Pd and Pt-containing α-alumina membranes. By forcing the reactants (hydrogen and oil) through the catalytically active membrane with a convective flow it was expected to suppress pore diffusion influence and reduce the residence time of the desired partially hydrogenated product at the catalyst. Consequently, the complete hydrogenation to the saturated fatty acid (C18:0) should be minimized and the selectivity for the monoene fatty acids (C18:1) improved. According to literature the *trans*-isomerization reaction as undesired side reaction is promoted at high reaction temperature (temperatures of ≥ 150°C which are

necessary in conventional oil hydrogenation processes with Ni catalysts). Therefore, it was expected to obtain less *trans*-isomer formation with noble metal catalysts at low temperatures (50-80°C). By performing the experiments at increased hydrogen pressures (3-20 bar) it was further expected to influence the *trans* fatty development because a low hydrogen solubility in liquid phase leads to insufficient supply of hydrogen at the catalyst surface which promotes the *trans* isomerization. The results aimed at were not obtained. The selectivity towards the monoene fatty acids in the membrane reactor was better than in the slurry reactor. The stearic acid content at an IV of 80 was 10 - 15 % in the membrane reactor and 45 % in slurry reactor. The strong development of saturated fatty acids in the slurry reactor was ascribed to a higher hydrogen supply at the catalyst at any time during the reaction. This promoted the consecutive reaction to C18:0. In the membrane reactor, however, the hydrogen concentration decreases while passing through the membrane. The reaction mixture had to be resaturated with every cycle. Because of the consumption of hydrogen per passage the consecutive reaction in the membrane reactor was reduced. Due to this fact, the selectivity towards the monoene fatty acids decreased with increasing hydrogen pressure. On the other hand, the lower hydrogen supply in the membrane promoted the isomerization to the *trans* fatty acids. In the slurry reactor with its high hydrogen concentration at the catalyst surface less *trans* fatty acid formation was obtained. The C18:1 *trans*-content at an IV of 80 was 30-45% in the membrane reactor, whereas in the slurry reactor 12% were obtained. For the *trans* isomer development, the influence of hydrogen pressure and temperature in the membrane reactor was rather low. This may be due to the low flow rate through the membrane at which the experiments were carried out. Technical limitations and pore clogging phenomena inhibited studies at higher flow rates. Further studies should be performed with membranes with larger pores that would allow adjusting higher flow velocities. Pd as catalyst showed a higher activity and selectivity compared to Pt, but promoted the *trans*-isomerization reaction in a greater extent.

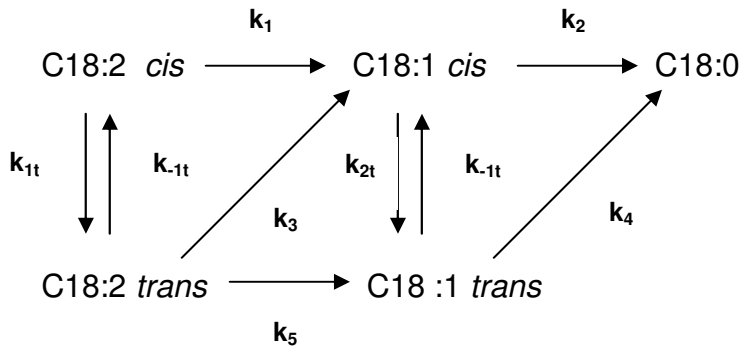

Fig. 8.14: Reaction pathway for the hydrogenation of sunflower oil

Recapitulating, the expected tendency concerning the improvement of oleic acid selectivity in the membrane reactor, compared to the slurry reactor, was observed in the experiments. However, the consecutive reaction to stearic acid in the membrane reactor was not controlled in an extent as desired. It is assumed from the slurry experiments with the Pd/α-alumina powder catalyst that mass transport by diffusion is not exclusively responsible for low selectivities of oleic acid and promotion of the *trans*-isomerization reaction in the oil hydrogenation process. The development of saturated fatty acids in the slurry reactor is already strongly advanced at lower conversions. This would not be the case if the reaction is exclusively limited by pore diffusion. The existence of intraparticle diffusion limitations in a slurry reactor can be almost excluded with a fine powder catalyst. In the membrane reactor, however, the complete hydrogenation is reduced compared to the slurry reactor, which indicates that the hydrogen supply has also an important impact. The temperature, the catalyst metal and the support may also affect the selectivity and *trans*-isomerization reaction as already described in numerous references. Table 8.1 summarizes the results of sunflower oil hydrogenation with different catalyst systems under similar reaction conditions collected from several references. It shows the difficulty of a control on selectivity to the monoene fatty acid without producing *trans* fatty acids in a greater extent during the hydrogenation process. A *trans* fatty acid content below 15 % at a IV of 80 was only achieved by adding amines to the reaction mixture which had the effect of a catalyst poison [8.2]. However, this method is only suitable for the non-food production. Veldsink [13] obtained a *trans* fatty acid contents of 25-26 % but at the expense of high stearic acid contents above 20 % and extremely long reaction times that are necessary for the desired IV (98-188 h). Veldsink reported further of severe catalyst deactivation. Fritsch et al. [14] produced a *trans* fatty acid content of 25 % and a stearic acid content of only 10 % at an IV of 90 but also after very long reaction times (8 h). Other references report of stearic acid contents in the range of 8 – 20 % but all at higher *trans* fatty acid contents (35 -48 %) in the product.

The mechanism of sunflower oil hydrogenation is a complex network of consecutive and parallel reactions, which has not been completely understood yet (Fig. 8.14). It was not the aim of this study to investigate the mechanism and the influences on the sunflower oil hydrogenation reaction but to test the application of the membrane reactor for this process. It was found that with the membrane reactor in pore-flow-through mode no improvement for the desired product composition can be obtained. Furthermore, some technical problems (pore blocking, deactivation) for this type of reaction in the membrane reactor have to be overcome for a further development.

Table 8.1: Comparison of catalyst systems for sunflower oil hydrogenation

Reference	Catalyst system	Reaction conditions	Content of C18:1 *trans* at IV~75 - 80	Content of C18:0 at IV ~ 75 - 80
Own results	Pd/ Al_2O_3-membranes	50 - 80°C; 5-20 bar	**30 - 45 %** after 20 - 120 min.	**10 -15 %**
D. Fritsch, G. Bengtson, *Catal. Today, 2006, 118, 1-2,121-127* [8.15]	Pt / polymer membranes (polyether-sulfone, polyamide-imide)	100°C; 4 bar	**25 %** after 8 h (IV= 90)	**10 %** (IV=90)
Plourde et al., *Ind. Eng. Chem. Res., 2004, 43,2382-2390* [8.8]	Pd/ SiO_2	110°C; 5 bar	**40 - 42 %** after 60 min.	**15- 20 %**
Fernández et al., *J. Mol. Catal. A: Chemical, 2005, 233, 133-139*,[8.7]	Pd/ Me/ Al_2O_3 (Me= Mo, V, Pb)	100°C; 4 bar	**35 - 48 %** after 60 min.	**8 – 14 %**
Nohair et al., *J. Mol. Catal. A: Chemical, 2005, 229, 117-126*, [8.2]	Pd/ SiO_2/ amine additives → nonfood	40°C; 10 bar	**10 - 15 %** after 20 -120 min.	**8 – 10 %**
Veldsink, *JAOCS, 2001, 78, 443-446*, [8.14]	Pd/ ZrO_2-membranes	74 – 86°C; 3-5 bar	**26 %** after 98 – 188 h	**25 %**

8.5 References

[8.1] M. Singer, *Gewinnung und Verarbeitung der pflanzlichen Fette und Öle*, Verlag für chemische Industrie (1992), p. 243-250

[8.2] B. Nohair, C. Especel, G. Lafaye, P. Marécot, L.C. Hoang, J. Barbier, *Palladium supported catalysts for the selective hydrogenation of sunflower oil*, J. Mol. Cat. A: Chemical 229 (2005) 117-126

[8.3] R. D. O'Brien, *Fats and Oils: Formulating and processing for applications*, 2nd ed. , CRC Press LLC (2004), p. 92-98

[8.4] A. Ascherio, W.C. Willett, *Health effects of trans fatty acids*, Am. J. Nutr. 66 (1997) 1006S

[8.5] K. K. Rajah, *Fats in food technology*, Sheffield Academic Press and CRC Press (2002), p.133

[8.6] B. Nohair, C. Especel, P. Marécot, C. Montassier, L. C. Hoang, J. Barbier, *Selective hydrogenation of sunflower oil over supported precious metals*, C. R. Chimie 7 (2004) 113-118

[8.7] M. B. Fernández, C. M. Piqueras, G. M. Tonetto, G. Crapiste. D. E. Damiani, *Hydrogenation of edible oil over Pd-Me/Al_2O_3 catalysts (Me=Mo, V and Pb)*, J. Mol. Cat. A: Chemical 233 (2005) 133-139

[8.8] M. Plourde, K. Belkacemi, J. Arul, *Hydrogenation of sunflower oil with novel Pd catalysts supported on structured silica*, Ind. Eng. Chem. Res. 43 (2004) 2382-2390

[8.9] M.-B. Macher, J. Högberg, P. Møller, M. Härröd, *Partial hydrogenation of fatty acid methyl esters at supercritical conditions*, Fett/Lipid 101(1999) Nr. 8, 301-305

[8.10] E. Ramírez, M. A. Larrayoz, F. Recasens, *Intraparticle diffusion mechanisms in sc sunflower oil hydrogenation on Pd*, AIChE Journal, 52 (2006) 4, 1539-1553

[8.11] M. Izadifar, *Neural network modeling of trans isomer formation and unsaturated fatty acid changes during vegetable oil hydrogenation*, J. Food Eng. 66 (2005) 227-232

[8.12] R. A. Holser, G. R. List, J. W. King, R. L. Holliday, W. E. Neff, *Modeling of hydrogenation kinetics from triglyceride compositional data*, J. Agric. Food Chem., 50 (2002), 7111-7113

[8.13] P. N. Pintauro, M. P. Gil, K. Warner, G. List, W. Neff, *Electrochemical hydrogenation of soybean oil with hydrogen gas*, Ind. Eng. Chem. Res. 44 (2005) 6188-6195

[8.14] J. M. Veldsink, *Selective hydrogenation of sunflower seed oil in a three-phase catalytic membrane reactor,* J. Am. Oil Chem. Soc., 78 (2001) 443-446

[8.15] D. Fritsch, G. Bengtson, *Development of catalytically reactive porous membranes for the selective hydrogenation of sunflower oil*, Catal. Today, 118, 1-2 (2006) 121-127

[8.16] T. Boger, M. M. P. Zieverink, M. T. Kreutzer, F. Kapteijn, J. A. Moulijn, W. P. Addiego, *Monolithic catalysts as an alternative to slurry systems: hydrogenation of edible oil*, Ind. Eng. Chem. Res. 43 (2004) 2337-2344

[8.17] M. M. P. Zieverink, M. T. Kreutzer, F. Kapteijn, J. A. Moulijn, *Combined hydrogenation and isomerization under diffusion limiting conditions*, Ind. Eng. Chem. Res. (2005), 44, 9668-9675

[8.18] A. Schmidt, R. Haidar, R. Schomäcker, *Selectivity of partial hydrogenation reactions performed in a pore-through-flow catalytic membrane reactor*, Cat. Today 104, 2-4 (2005) 305-312

[8.19] M. D. Guillén, A. Ruiz, *Edible oils: discrimination by ^{1}H nuclear magnetic resonance*, J. Sci. Food Agric. 83 (2003), 338-346

[8.20] M. O. Jung, S. H. Yoon, M. Yhung Jung, Effects of temperature and agitation rate on the formation of conjugated linoleic acids in soybean oil during hydrogenation process, J. Agric. Food Chem. 49 (2001) 3010-3016

9 Hydrogenation reactions of different substrates in PFT-membrane reactor

9.1 Introduction

Fine chemicals and their intermediates are often produced by heterogeneously catalyzed hydrogenation under mild reaction conditions in liquid phase. In the majority of cases the molecules are complex-structured, temperature-sensitive and contain of more than one functional group. Therefore, the formation of more than one product is possible. The choice of adequate catalysts and reaction conditions is essential for avoiding side products. But also process control can have strong impact on the selectivity of a reaction. Homogeneous catalysis is mostly highly selective for one product but at the expense of costly and time-consuming recovery of the catalyst. Therefore, fine chemicals and their intermediates are often produced with heterogeneous catalyst pellets in fixed-bed reactors. Lower selectivities for the desired product because of pore diffusion resistance are then accepted. A promising concept for selectivity improvement is the pore-flow-through (PFT) membrane reactor. The performance of this type of membrane reactor was already demonstrated for the partial hydrogenation of COD (chapter 6), the hydrogenation of α-methylstyrene to cumol [9.1] and the partial hydrogenation of phenylacetylene, 1-octyne and geraniol, carried out with polymeric membranes [9.3]. Higher space-time-yields and higher selectivities for the desired products in the case of the partial hydrogenation reactions were obtained in the PFT- reactor than in a fixed bed or a slurry reactor. In order to investigate the potential of ceramic membranes as support for the catalyst the partial hydrogenation of phenylacetylene to styrene, 1-octyne to 1-octene and geraniol to citronellol was studied in this chapter. Furthermore, the selective hydrogenation of cinnamaldehyde in the membrane reactor was investigated. In this case, the hydrogenation of the C-C double bond and of the carbonyl group is possible. Of particular interest is the unsaturated alcohol as product, however, thermodynamically constraints favor the formation of the saturated aldehyde [9.4]. Here, not only mass transfer limitations can influence activity and selectivity but also the type of catalyst metal, support and solvent which is reported in numerous literature data [9.5-9.13]. The hydrogenation of cinnamaldehyde and of geraniol yields important fragrance and flavor products for the fine chemical industry.

The hydrogenation experiments in this chapter represent a screening of different reactions with substrates containing different functional groups. Besides activity and selectivity the stability of the catalyst is an industrially important issue. Catalyst deactivation, in turn, can

affect reaction times and selectivity because the catalyst surface can change in several ways during the reaction. This is an aspect that also has to take into consideration for the evaluation of the PFT-membrane reactor performance in different reactions. Therefore, deactivation phenomena are also discussed in this chapter.

9.2 Experimental

Hydrogenation experiments in liquid phase were performed at different reaction temperatures and hydrogen pressures with Pd/alumina membranes. The catalytic membranes were obtained by wet impregnation with an aqueous solution of the Pd precursor ($PdCl_2$) and subsequent chemical reduction with $NaH_2PO_2 \cdot H_2O$-solution as described detailed in chapter 3. Wet impregnation with other noble metal precursor (Ru, Ag) resulted in very low metal amounts deposited in the membrane structure. Consequently, the activity of these catalytic membranes in hydrogenation experiments was significantly lower than with Pd membranes. For comparison reasons experiments with a fixed bed reactor and a slurry reactor with a commercial egg shell catalyst (Pd/α-Al_2O_3, 0.5 wt. % Pd) were carried out at similar reaction conditions (temperature, hydrogen pressure, circulation rate in fixed bed reactor, stirrer speed, Pd amount). For the experiments with the fixed bed the membrane module in the laboratory setup was replaced with a corresponding fixed bed reactor.

9.3 Results and discussion

9.3.1 Hydrogenation of alkynes

The partial hydrogenations of 1-octyne (OYN) to 1-octene (OEN) and phenylacetylene (PHAC) to styrene (STY) (Fig. 9.1) were performed at 50°C and 10 bar hydrogen pressure and a circulation rate of 200 mL/min in PFT-membrane and fixed bed reactor. The consecutive reaction to the alkane should be avoided. Pd/α-alumina membranes with an average pore diameter of 1.9 µm and different Pd amounts were used. For the fixed bed reactor an egg shell catalyst with pellets of approx. 1.5 mm diameter was employed. The concentration of the alkyne was 5 vol. % in *n*-heptane.

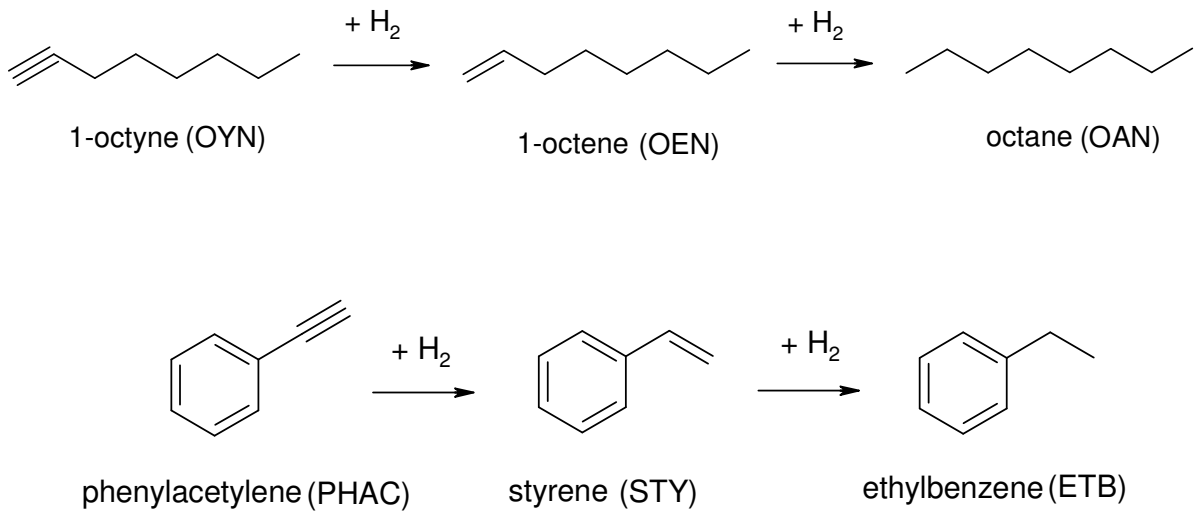

Fig. 9.1: Scheme of hydrogenation of 1-octyne and phenylacetylene

The performance of PFT- and fixed bed reactor was described with the following eq. 9.1 and 9.2 for conversion and selectivity:

$$\textit{Conversion of alkyne:} \quad X\,(\%) = \frac{C_{alkyne,0} - C_{alkyne,t}}{C_{alkyne,0}} \cdot 100 \qquad \text{(eq. 9.1)}$$

$$\textit{Selectivity for alkene:} \quad S\,(\%) = \frac{C_{alkene,t}}{C_{alkyne,0} - C_{alkene,t}} \cdot 100 \qquad \text{(eq. 9.2)}$$

The reaction rate of the alkyne hydrogenation increases with increased Pd amount (Fig. 9.2). Although the initial reaction rate in the fixed bed reactor with 1 mg Pd is higher than in the membrane reactor with 0.7 mg Pd, the reaction rate in the fixed bed reactor slows down strongly at the end of the reaction while the conversion in the PFT-reactor increases steadily until complete conversion is achieved. The selectivity for OEN is almost the same up to a conversion of 90 % for all catalysts; above that value the selectivity decrease in the fixed bed reactor is more pronounced than in the PFT-reactor. At complete conversion the selectivity in the fixed bed reactor is only 76 %. In the PFT-reactor selectivities of 95 % (0.7 mg Pd) and 92% (2.4 mg Pd), respectively, are obtained.

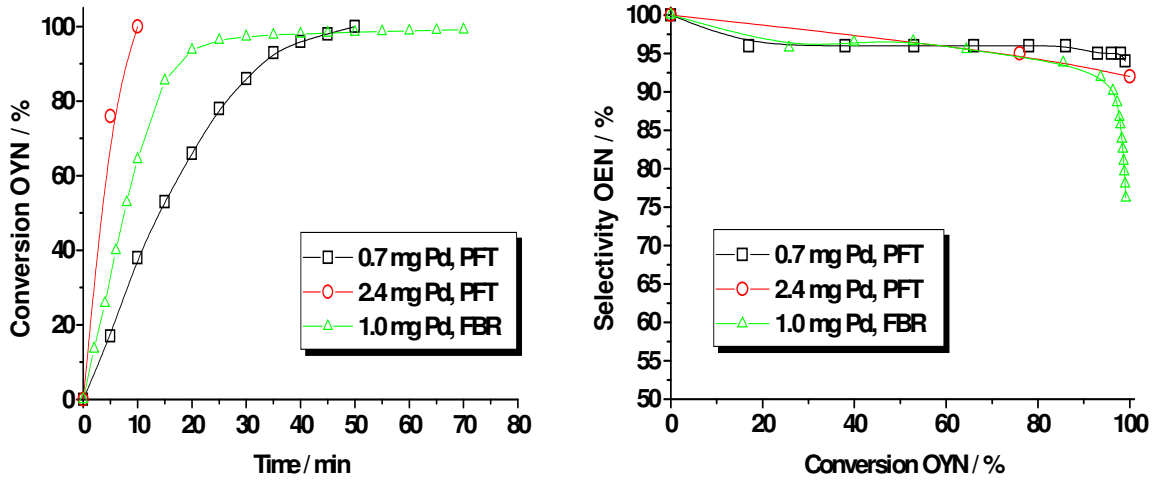

Fig. 9.2: OYN-conversion and OEN-selectivity in membrane (PFT) and fixed bed reactor (FBR) (50°C, 10 bar hydrogen pressure, circulation rate: 200 mL/min, pore size of membrane: 1.9 µm; initial OYN-concentration: 0.33 mol/L)

For the hydrogenation of PHAC membranes with 0.7 mg Pd and 2.1 mg Pd were compared to the egg shell catalyst (1 mg Pd) in the fixed bed reactor. The membrane with the higher Pd amount (2.1 mg) needs 20 minutes to obtain a complete conversion. With 0.7 mg Pd in the membrane a conversion of only 75% was achieved after 125 minutes (Fig. 9.3). The correlation between the activity and the Pd content of the membrane is not linear. The experiment shows that in spite of a higher Pd concentration within the membrane (which was determined by AAS after the experiments) the catalytic activity is the same as with the membrane with lower Pd content. This may be caused by a nonlinear increase of Pd surface with mass of Pd deposited in the membrane pores. It is assumed that at lower Pd concentrations within the membrane pore structure the Pd distribution is more uneven than in membranes with higher Pd contents. Pd cluster of larger size are responsible for a less catalytic activity of the membrane. The reaction rate in the fixed bed reactor with 1 mg Pd is comparable to the membrane reactor with even lower Pd amount.

The selectivity for STY did not differ in the PFT-membrane reactor for both Pd amounts (95 % up to a PHAC-conversion of 80 %). At complete PHAC-conversion a selectivity of 80 % was obtained in the PFT-membrane reactor. In the fixed bed reactor the STY-selectivity decreases faster to a value of 65 % at 90 % PHAC-conversion.

For both investigated hydrogenation reactions of alkynes the PFT-membrane reactor exhibits higher alkene selectivities than a fixed bed reactor at comparable reaction conditions which is attributed to the avoided pore diffusion limitation in the PFT-reactor.

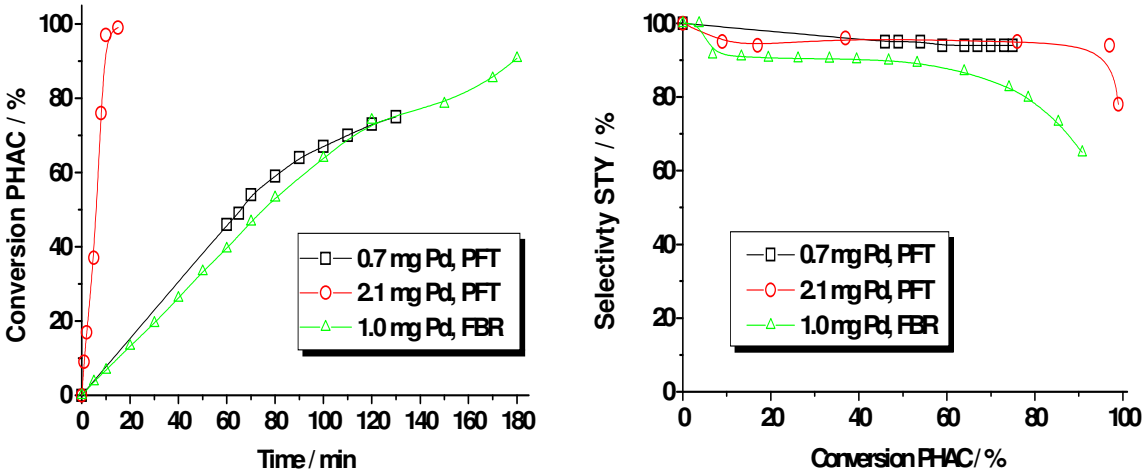

Fig. 9.3: PHAC-conversion and STY-selectivity in membrane (PFT) and fixed bed reactor (FBR) (50°C, 10 bar hydrogen pressure, circulation rate: 200 mL/min, pore size of membrane: 1.9 µm, initial PHAC-concentration: 0.46 mol/L)

9.3.2 Hydrogenation of an allylic alcohol

The hydrogenation of the terpenic allylic alcohol geraniol (GE) was performed in the membrane reactor at 50°C, 10 bar hydrogen pressure and Pd/α-alumina membranes with different Pd content. Terpenes are cheap precursors to flavors, fragrances, drugs and agrochemicals but because of their high reactivity a selective transformation is difficult. The target product in this study was the unsaturated alcohol citronellol (CL) which is one of the most widely used fragrance materials, particularly for floral compositions. Furthermore, it is starting material for numerous citronellyl esters and for hydroxydihydrocitronellol [9.14].

The selective catalytic hydrogenation of GE to CL has been widely investigated with homogeneous catalysts, particularly Ru- or Rh-based chiral catalysts, most frequently with the Noyori-BINAP-ligand [9.16, 9.17]. Heterogeneously catalyzed synthesis of CL was reported by Zaccheria et al. over Cu/Al_2O_3 catalysts with an unprecedented selectivity of 98% [9.18]. Still, a selective transformation with heterogeneous catalysts is complicated because several other reactions can occur on the catalyst surface [Fig. 9.4]: isomerization of GE to citronellal, complete hydrogenation to 3,7-dimethyloctanol (tetrahydrogeraniol, THG) or the formation of 3,7-dimethyl-2-octenol, although the hydrogenation of the 2,3-double bond is favored compared to the 6,7-double bond because of the activating presence of the OH-group [9.19].

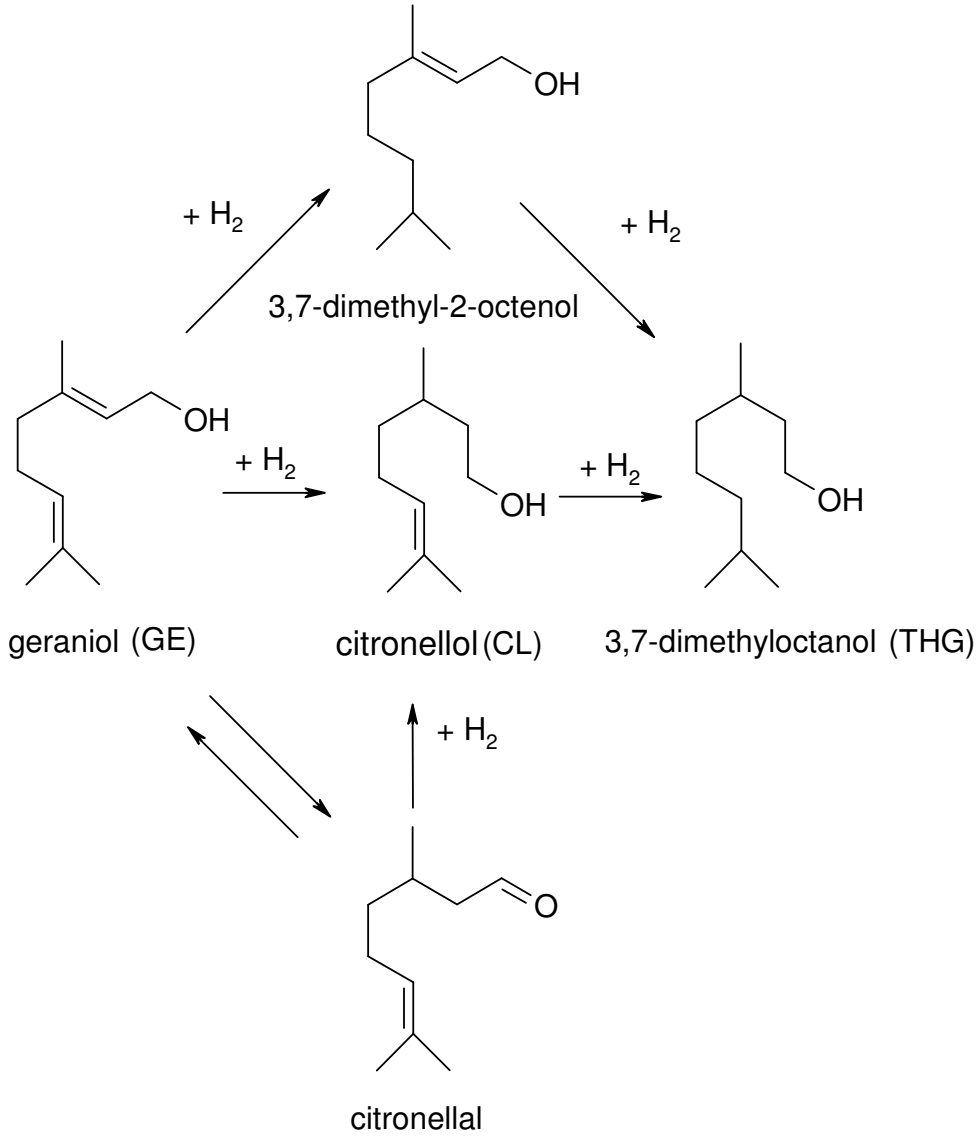

Fig. 9.4: Reaction scheme of geraniol hydrogenation

The main products of GE-hydrogenation in the PFT-membrane reactor are CL and THG. The other products are only obtained in small amounts (< 2%). The highest reaction rate of the GE-hydrogenation was observed with a Pd amount of 3 mg, a membrane pore size of 0.6 µm and a flow rate of 200 mL/min. A complete conversion is obtained after only 20 minutes (Fig. 9.5). The activity of a membrane with 2 mg Pd-content decreases strongly at the end of the reaction. In the fixed bed reactor with a higher Pd mass (5 mg) the reaction rate is even lower than in both PFT-membrane reactor experiments.

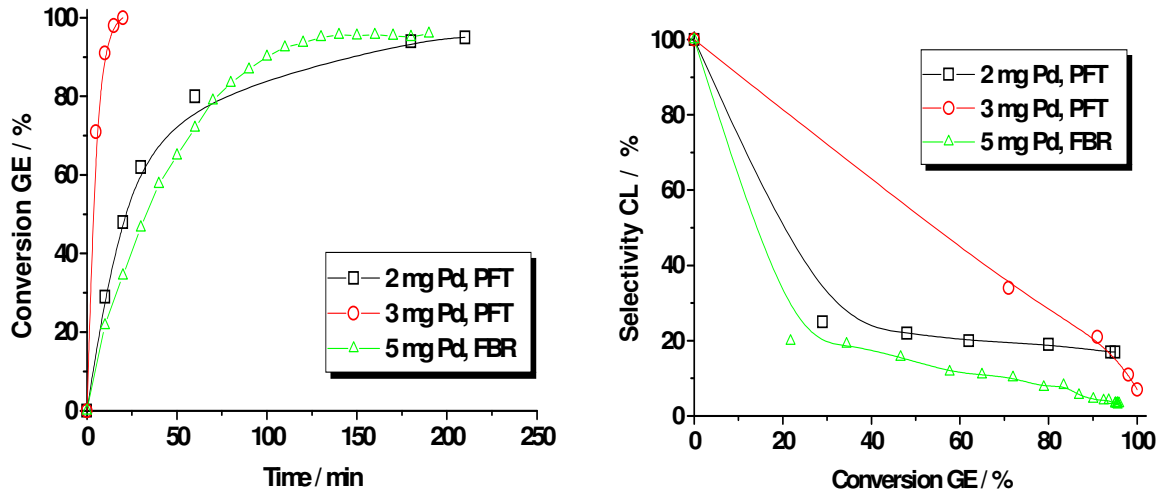

Fig. 9.5: GE-conversion and CI-selectivity at different Pd amounts in membrane (MR) and fixed bed reactor (FBR) (50°C, 10 bar hydrogen pressure, circulation rate: 200 mL/min, pore size: 0.6 µm, initial GE-concentration: 0.27mol/L)

The selectivity for CL decreases rapidly with conversion for the fastest experiment in the PFT-membrane reactor: at 70 % GE-conversion the selectivity is about 40 % and at complete conversion only the fully hydrogenated product is produced. With a lower reaction rate the selectivity decreases even faster at the beginning of the reaction but with increasing conversion the selectivity decline slows down. At 95 % conversion the selectivity for CI is 17 %. In the fixed bed reactor the selectivity increases even faster to value of 5 % for CI at almost complete GE-conversion.

Although maintaining the same reaction conditions the experiments were not reproducible very well. This is demonstrated in Fig. 9.6 where three experiments performed under the same operation conditions are compared. With two membranes two subsequent experiments were carried out (exp. A). In the second experiment (B) the reaction rate seems to slow down at a conversion of 50 %. Then, the reaction rate increases again and reaches the same final value as in the first experiment. Probably, a temporarily deactivation of the membrane by pore blocking which was removed by the reactant flow caused this unsteady run of the conversion curve. A further experiment (C) was carried out with two new membranes, containing the same Pd amount as the membranes in experiments A and B. Up to a conversion of 55 % the run of the conversion curve is comparable to the other experiments but then the reaction rate decelerates and the conversion curve reaches a plateau. The conversion does not exceed 74 %. This indicates a deactivation of the membrane during the reaction. The CL- selectivities for all experiments, however, are very well reproducible and are in the range of 17 % at 95 % conversion.

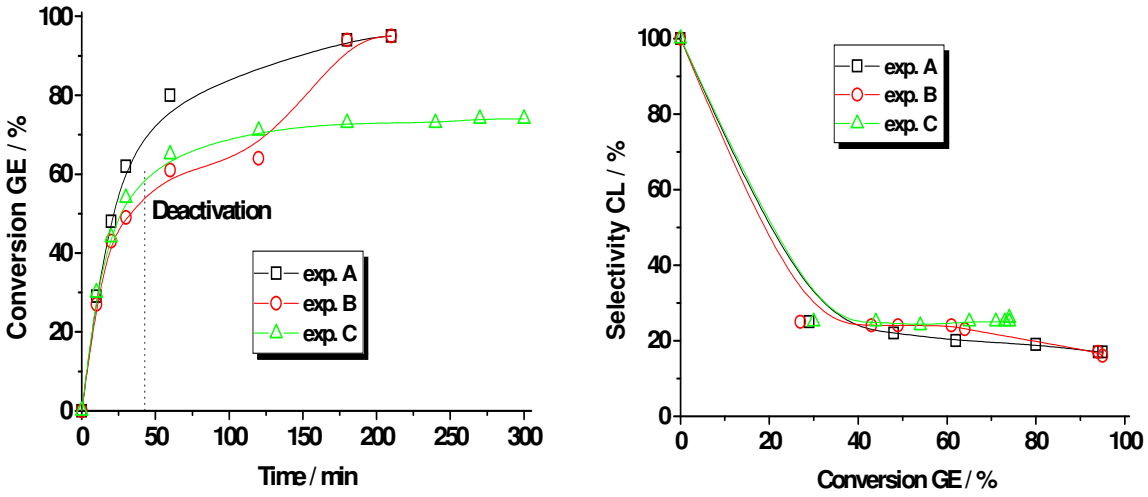

Fig. 9.6: Reproducibility of GE-hydrogenation experiments (50 °C, 10 bar hydrogen pressure, circulation rate: 200 mL/min, pore size: 0.6 µm, initial GE-concentration: 0.27mol/L)

The deactivation phenomenon was studied in detail for a series of experiments performed with the same membrane at a circulation rate of 150 mL/min and a pore diameter of 1.9 µm (fig. 9.7). The first experiment was performed at 10 bar hydrogen pressure and reached 90 % conversion at 150 minutes whereas the 3rd and 5th experiments which were carried out under the same hydrogen pressures reached only a conversion of 10-20 % in the same time. The 2nd and the 4th experiment were performed at 6 and 20 bar, respectively. For these experiments a conversion of 20 % was obtained. The curves of experiment 2-6 ended up in a plateau which indicates a catalyst deactivation.

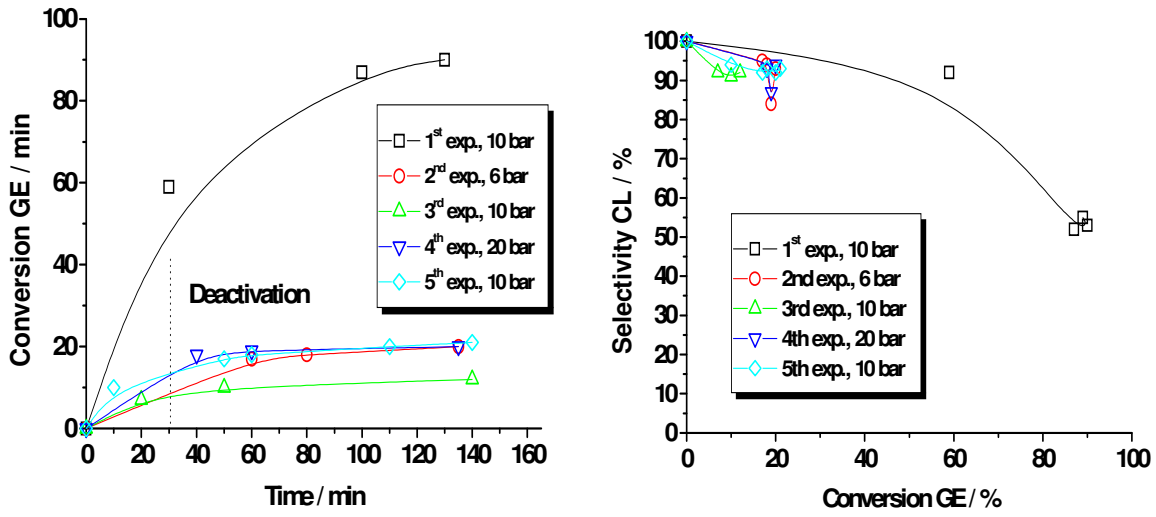

Fig. 9.7: A series of experiments for the hydrogenation of GE with the same membranes (50 °C, different hydrogen pressures, circulation rate: 150 mL/min, pore size: 1.9 µm, initial GE-concentration: 0.27 mol/L

Catalyst deactivation can have several causes: poisoning, sintering, leaching, fouling or mechanical degradation [9.19]. Catalyst poisoning occurs when strong adsorbents, e.g. sulphur, are present whereas sintering of catalyst particles to larger agglomerates happens at high temperatures (<500 °C). Both cases can be excluded in the experiments. AAS analysis of the product showed that no leaching of Pd was occurring during the reactions. However, an increase of the pressure drop at the membrane from 1 to 5 bar was observed during the experiments. This indicates a deactivation by pore blocking caused of carbon deposition in the membrane structure. This type of catalyst fouling reduces the activity because catalytic sites are occupied by different organic compounds formed during the reaction and adsorbed in different ways on the catalyst surface depending on their particular functional groups. The processes for the desired hydrogenation are hampered. This phenomenon takes place already at low temperatures and is specific for different substrates, catalyst metals and supports [9.20]. A regeneration of the catalytic membranes by simple rinsing of the membranes with different solvents is not successful because the adsorbents are bound strongly on the catalyst. As a further task, it has to be investigated, if calcination and a reduction of the deactivated catalytic membranes at temperatures of 200 – 400 °C lead to regeneration of the catalytic membranes. Alternatively, a washing treatment of the deactivated membranes with H_2O_2-solution at elevated temperatures is thinkable.

9.3.3 Hydrogenation of an α,β-unsaturated aldehyde

Hydrogenation of cinnamaldehyde (CA) was investigated in the membrane reactor at different hydrogen pressures (10 – 20 bar), reaction temperatures (50 – 80°C) and catalysts (Pd/alumina membrane, Pd/alumina catalyst as 3-5 mm pellets and 100-200 µm particles). The cinnamaldehyde hydrogenation pathway is depicted in Fig. 9.8. Each of the two functionalities present in the molecule, the C-C double bond and the carbonyl group, can be selectively hydrogenated by a suitable choice of catalyst. The C-C double bond is hydrogenated selectively in the presence of Pd and Pt which yields the saturated aldehyde hydrocinnamaldehyde (HCA, 3-phenylpropanal) and the carbonyl group is hydrogenated in the presence of modified Pt, Ru, or Os catalysts which yield the α,β-unsaturated alcohol cinnamylalcohol (COL). The saturated alcohol hydrocinnamylalcohol (HCOL, 3-phenylpropanol) is selectively obtained by hydrogenation over nickel or copper catalysts [9.21]. A key problem in carrying out these multiphase reactions involving hydrogen is mass transfer limitation due to a low solubility of hydrogen in the liquid phase. Therefore, cinnamaldehyde is conventionally hydrogenated in slurry reactors with powdered catalysts under high pressures and intensive stirring in order to improve the contact of the gaseous, liquid and solid phase [9.22]. A serious disadvantage here is the difficulty of the catalyst separation from the product. The membrane reactor in PFT-mode with the catalyst immobilized in a membrane support could provide several advantages: intimate contact of gas-liquid-solid phases, no catalyst separation from the product and necessity of only low catalyst amounts because of good catalyst accessibility.

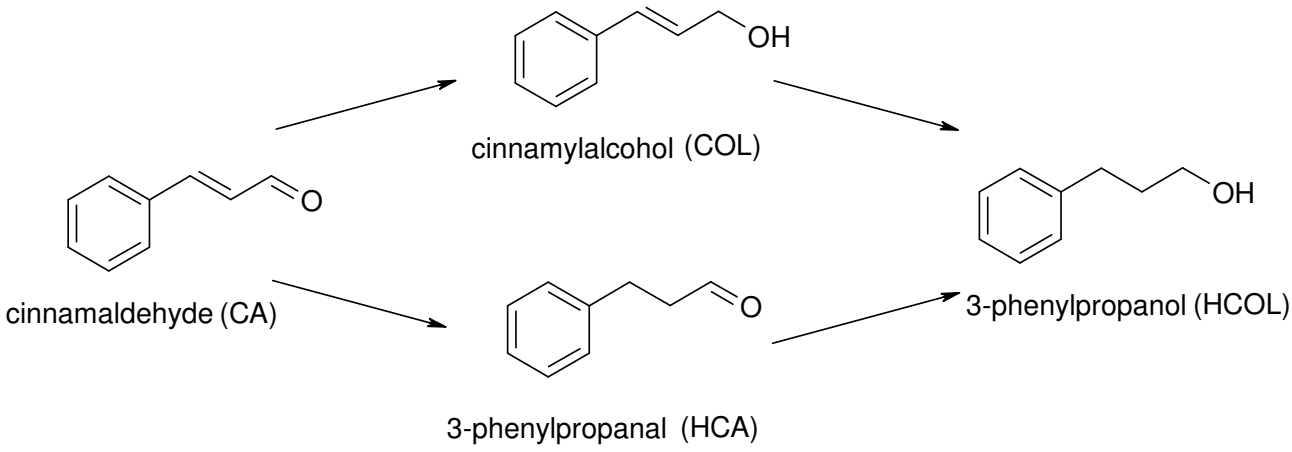

Fig. 9.8: Reaction scheme of cinnamaldehyde hydrogenation

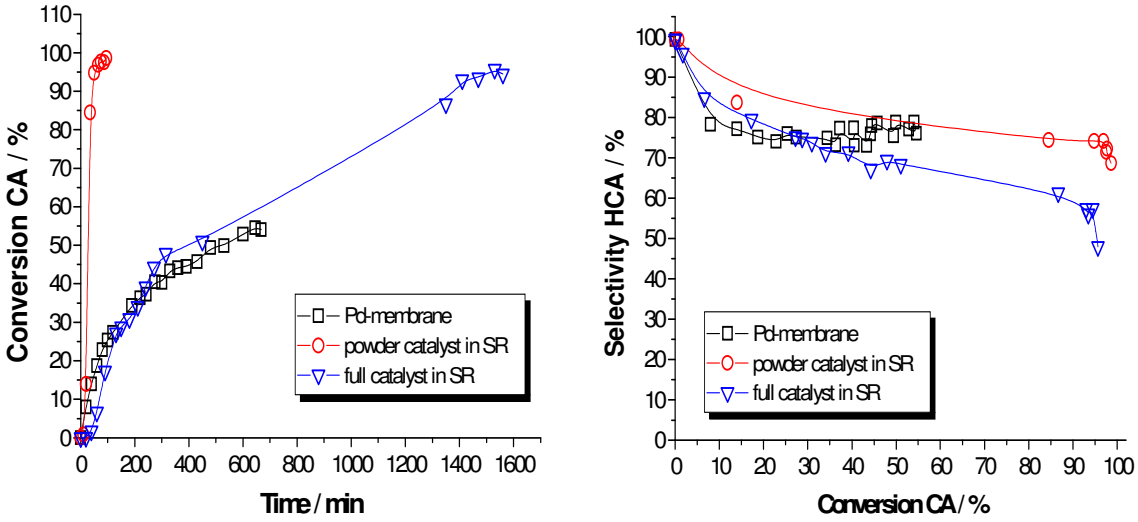

Fig. 9.9: Hydrogenation of cinnamaldehyde with different catalysts (70 °C, 20 bar hydrogen pressure and 3 mg Pd, circulation rate in membrane reactor 470 mL/min, 5 vol. % CA in isopropanol), (a) CA conversion, (b) HCA selectivity

A comparison of different catalysts for the hydrogenation of CA at similar reaction conditions is depicted in Fig. 9.9. The Pd-membrane and the spherical full catalyst (Pd/alumina 0.5 wt. Pd, pellet size: 3-5 mm diameter) in the slurry reactor show comparable reaction rates. The experiment in the PFT-membrane reactor was abandoned after 700 minutes; the reaction in the slurry reactor was followed up to complete conversion (1600 minutes). With the powder catalyst (Pd/alumina 0.5 wt. Pd, particle size: 100 – 200 µm) in the slurry reactor the reaction proceeds much faster; a complete conversion is obtained in 100 minutes. The main product was HCA, as side product HCOL was formed with all Pd-catalysts; COL was not produced. The selectivity for HCA decreases in the same way up to a conversion of 30 % with the membrane and the full catalyst. Then, the selectivity with the full catalyst decreases further whereas with the membrane the selectivity remains constant at a value of 80%. However, for conversions above 50 % no evaluation can be given. With the powder catalyst the selectivity at 50 % conversion is comparable to the PFT- reactor.

Tab. 9. 1: Comparison of PFT- membrane reactor with Pd- catalyst in fixed bed and slurry reactor for different hydrogenation reactions

		S at X=100 %	time needed for X=100%
1-octyne → 1-octene	PFT	92%	55 min.
	FBR (egg shell)	76 %	100 min.
phenylacetylene → styrene	PFT	80%	20 min.
	FBR (egg shell)	>65%	100 min.
geraniol → citronellol	PFT	7 %	60 min.
	FBR (egg shell)	5 %	100 min.
cinnamaldehyde→	PFT	80% (at X=50%)	630 min. (for X=50 %)
3-phenylpropanal	SR (powder)	85% (at X=50%)	50 min. (for X=50 %)

A summary of the results for the hydrogenation of different substrates in the PFT-reactor compared to fixed bed and slurry reactor gives Tab. 9.1. In the PFT-reactor higher reaction rates and selectivities for the desired product are obtained in the case of alkyne hydrogenation but comparable or even worse results in the case of GE and CA-hydrogenation.

Deactivation is observed with increasing number of experiment with CA for catalytic membrane and full catalysts but for the membrane this behaviour is pronounced. The second experiment in the PFT-reactor is already much slower than the first one whereas the egg shell catalyst in the slurry reactor shows deactivation not until the third experiment (Fig. 9.10). As already shown by the experiments with GE the membrane is prone to deactivation when using reactants with OH- and CO-functional groups in the molecule. Ideas for membrane regeneration are already discussed in the section on GE hydrogenation. An easy and low-priced regeneration technique that is also applicable in larger scale is necessary for further development of the membrane reactor. Further investigations should focus on this topic.

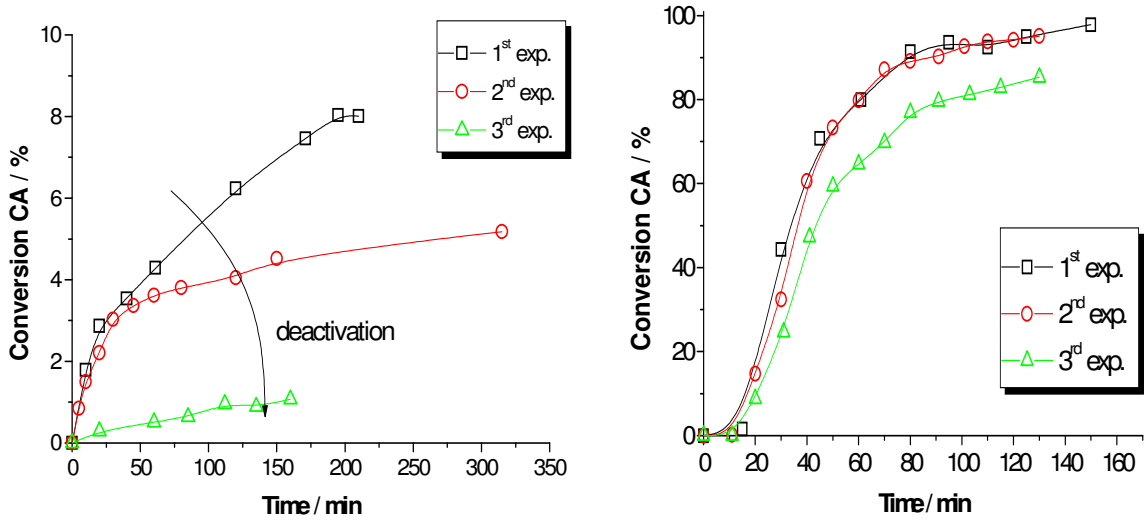

(a) **(b)**

Fig. 9.10: A series of experiments for hydrogenation of CA (a) with the same Pd-membrane (60°C, 10 bar hydrogen pressure and 9 vol. % CA in isopropanol, 3 mg Pd); (b) with the same Pd-catalyst (80°C, 20 bar hydrogen pressure and 5 vol. % CA in isopropanol, 3 mg Pd)

9.4 References

[9.1] H. Purnama, P. Kurr, A. Schmidt, I. Voigt, A. Wolf, R. Warsitz, R. Schomäcker, *α-Methylstyrene hydrogenation in a flow-through membrane reactor*, AIChE J., 52, 8, 2006, 2805-2811

[9.2] A. Schmidt, R. Haidar, R. Schomäcker, *Selectivty of partial hydrogenation reactions performed in a pore-through-flow catalytic membrane reactor*, Catal. Today 104, 2-4 (2005) 305-312

[9.3] R. Schomäcker, A. Schmidt, B. Frank, R. Haidar, A. Seidel-Morgenstern, *Membranen als Katalysatorträger*, Chem. Ing. Tech. 77 (2005), 5, 549-558

[9.4] J. Hájek, D. Murzin, *Liquid-phase hydrogenation of cinnamaldehyde over a Ru-Sn sol-gel catalyst. 1. evaluation of mass transfer via a combined experimental/theoretical approach*, Ind. Eng. Chem. Res. 43 (2004) 2030-2038

[9.5] M. Lashdaf, A. O. I. Krause, M. Lindblad, M. Tiitta, T. Venäläinen, *Behaviour of palladium and ruthenium catalysts on alumina and silica prepared by gas and liquid phase deposition in cinnamaldehyde hydrogenation*, Appl. Catal. A: General 241 (2003) 65-75

[9.6] M. Lashdaf, M. Tiitta, T. Venäläinen, H. Österhol, A. O. I. Krause, *Ruthenium on beta zeolite in cinnamaldehyde hydrogenation,* Cat. Lett. , 94, Nos. 1-2, (2004) 7-14

[9.7] B. Coq, P. S. Kumbhar, C. Moreau, P. Moreau, M. G. Warawdekar, *Liquid phase hydrogenation of cinnamaldehyde over supported ruthenium catalysts : influence of particle size, bimetallics and nature of support,* J. Mol. Catal. 85 (1993) 215-228

[9.8] B. Coq, P. S. Kumbhar, C. Moreau, P. Moreau, F. Figuéras, *Zirconia-supported monometallic Ru and bimetallic Ru-Sn, Ru-Fe Catalysts: role of metal support interaction in the hydrogenation of cinnamaldehyde,* J. Phys. Chem., 98 (1994) 10180-10188

[9.9] G. Neri, L. Bonaccorsi, L. Mercadente, S. Galvagno, *Kinetic analysis of cinnamaldehyde hydrogenation over alumina-supported ruthenium catalysts*, Ind. Eng. Chem. Res., 36 (1997) 3554-3562

[9.10] L. Zhang, J. M. Winterbottom, A. P. Boyes, S. Raymahasay, J. Chem. Technol. Biotechnol. 72 (1998) 264-272

[9.11] M. Guisnet et. al., Heterogenous Catalysis and Fine chemicals, 1988, Elsevier Science Publishers, 123-129

[9.12] A. Giroir-Fendler, D. Richard, P. Gallezot, *Chemioselectivity in the catalytic hydrogenation of cinnamaldehyde. Effect of metal particle morphology,* Cat. Lett. 5 (1990) 175-182

[9.13] A. B. da Silva, E. Jordão, M. J. Mendes, P. Fouilloux, *Selective hydrogenation of cinnamaldehyde with Pt and Pt-Fe catalysts: effects of the support*, Braz. J. Chem. Eng., 15, no. 2 (1998)

[9.14] Ullmann's Encyclopedia of Industrial Chemistry, *Flavors and Fragrances*, Wiley Interscience, online release 2005, 7th edition

[9.15] H. Takaya, T. Ohta, N. Sayo, H. Kumobayashi, S. Akutagawa, S. Inoue, I. Kasahara, R. Noyori, *Enantioselective hydrogenation of allylic and homoallylic alcohols*, J. Am. Chem. Soc. 109 (1987) 1596-1597

[9.16] Y. Sun, C.LeBlond, J. Wang, D. G. Blackmond, *Observation of a [RuCl2((S)-(-)-tol-binap)]-N(C2Hs)-catalyzed isomerization-hydrogenation network*, J. Am. Chem. Soc. 117 (1995) 12647-12648

[9.17] F. Zaccheria, N. Ravasio, A. Fusi, M. Rodondi, R. Psaro, *Tuning selectivity in terpene chemistry: selective hydrogenation versus cascade reactions over copper catalysts*, Adv. Synth. Catal. 347 (2005) 1267-1272

[9.18] P. Mäki-Arvela, N. Kumar, A. Nasir, T. Salmi, D. Yu. Murzin, *Selectivity enhancement by catalyst deactivation in three-phase hydrogenation of nerol*, Ind. Eng. Chem. Res. 44 (2005) 9376-9383

[9.19] C. H. Bartholomew, *Mechanisms of catalyst deactivation*, Appl. Catal. A 212 (2001) 17

[9.20] Ullmann's Encyclopedia of Industrial Chemistry, *Aldehydes, Aliphatic and Araliphatic*, Wiley Interscience, online release 2005, 7th edition

[9.21] X. L. Pan, G. X. Xiong, S. S. Sheng, W. S. Yang, *Exploration of cinnamaldehyde hydrogenation in Co–Pt/γAl_2O_3 catalytic membrane reactors*, Catal. Lett. 66 (2000) 125-128

10 Conclusion and outlook

The object of this thesis was the development and construction of a catalytic membrane reactor for selective hydrogenation reactions in three phases. Based on previous investigations with catalytic membranes it was expected to attain two main advantages compared to the conventional, at present in industry applied fixed bed and slurry reactors. Pore diffusion frequently occurs in porous catalyst pellets in fixed beds and causes side reactions resulting in decreased selectivities and decreased effective reaction rates. In slurry reactors this problem is reduced by using fine powder catalysts; however due to their small size the catalyst particles are difficult to separate from the product and make costly and time consuming filtration steps necessary. The proposed membrane reactor in pore-flow-through mode combines a solution for both problems: by forcing the reactants through the pores of a catalytic membrane the contact time with the catalyst is short and the developed product is removed quickly by a convective flow. A consecutive reaction consuming the desired product is almost avoided. High selectivities for the desired product in complex reactions can be expected. A separation of the catalyst from the product is not required as the catalyst is immobilized as nanoparticles in pore structure of the membrane.

An easy preparation technique was developed in order to deposit palladium and other noble metal nanoparticles homogeneously distributed inside the pores of alumina membrane tubes. The membrane tubes were impregnated with an aqueous metal salt solution by pumping the impregnation solution through the membrane pores for 24 h. Subsequently, a reducing agent was pumped likewise through the membrane in order to activate the catalyst. After drying catalytically active membranes with a metal content of about 1 mg per membrane (0.03 wt. %) were obtained. SEM, TEM and EPMA analysis revealed a homogeneously dispersion of the catalytic metal in nanometer size in the whole membrane matrix. A good adhesion between active component and support was obtained even without calcination steps. However, the technique could be improved by a better control of the Pd amount deposited in the membrane during the impregnation process and a better reproducibility of the produced Pd-membranes.

Before starting hydrogenation experiments with 1,5-cyclooctadien as model substrate in the membrane reactor the intrinsic kinetics of this reaction was determined with a powder of a Pd/α-alumina catalyst in a slurry reactor in a wide range of operating conditions (chapter 5). The reaction rate was increased with increasing reaction temperature, increasing hydrogen pressure and decreasing initial COD concentration. The selectivity for COE was 92-95 % and was slightly decreased with increasing hydrogen pressure and increasing temperature.

Reaction rates were found to depend on COD, COE and hydrogen concentration according to Langmuir-Hinshelwood kinetics. Rate constants and activation energy were determined by fitting experimental data to the proposed model.

The operating conditions for the COD hydrogenation in the membrane reactor were defined as 50°C reaction temperature, 10 bar hydrogen pressure and 5 vol. % COD concentration.

The partial hydrogenation of COD in the PFT-membrane reactor was investigated in detail in chapter 6. The influence of the process parameters flow velocity through the membrane, membrane pore size and membrane Pd amount on reaction rate and selectivity for COE was studied. The reaction rate was increased with increasing flow rate, decreasing membrane pore diameter and increasing Pd amount. Reasons for the pore size impact are not yet clear. In order to explain this influence, further investigations in the characterization of the Pd membranes (Pd dispersion and Pd particle size in pores of different diameter) as well as a simulation of convection and diffusion in the pores have to be carried out in future.

The influence of these parameters on the COE selectivity was notably small; the selectivity was always in a range of 92-95 %. These values comply with the selectivities obtained with the powder catalyst in the slurry reactor and indicate that indeed no pore diffusion resistance occur in the membrane reactor for COD and COE. Experiments with commercial catalyst pellets in a fixed bed reactor that were performed for comparison reasons, showed significantly lower COE selectivities (down to 45 %).

A successful scale-up of the PFT-reactor in lab scale to a pilot plant was carried out by multiplication of the membrane area, the liquid volume and the circulation rate. For this, bundles of 27-membrane tubes were loaded with Pd and were applied to the COD hydrogenation under similar conditions as in the laboratory. Complete COD conversions were obtained in about 20 minutes with COE selectivities of 92-95 %. Long-term stability of the membranes was proved for the hydrogenation of COD in a series of 11 subsequent experiments. By this, the performance of the PFT-membrane reactor was also demonstrated in a technical scale. Further scale-up can be performed by numbering up, e.g. multiple membrane capillary bundles assembled in one membrane module.

In chapter 7 the study was focussed on the development of a mathematical model for the COD hydrogenation in the membrane reactor. The model is based on the assumption that the liquid flow through the membrane pores is “plug-flow”. Concentration profiles of hydrogen through the membrane pores were simulated by solving mass balances including kinetic rate laws obtained from the slurry experiments. The model represents the effects of circulation flow rate and Pd amount on the hydrogenation process as experimentally found. The influence of the membrane pore size cannot be described. As a first approach the model can be used for prediction of the reaction progress under different operation conditions. For a detailed description of the processes inside the membrane the model has to be advanced.

Chapter 8 and 9 were devoted to application examples for the membrane reactor that may be interesting for an industrial operation. The partial hydrogenation of sunflower oil was tested in the membrane reactor. The aim was to hydrogenate the polyunsaturated fatty acids (linolenic acid) in the oil to the monoene fatty acid (oleic acid) and control the consecutive saturation to stearic acid. Simultaneously, the isomerization to *trans* fatty acids, an undesired concomitant phenomenon at partial hydrogenations of fats, should be prevented by adjusting mild reaction conditions. The stearic acid content in the product obtained in the membrane reactor was significantly lower (10-15%) than in the products obtained in a slurry reactor with a powder catalyst (45%) at the same iodine value of 80 but the *trans* fatty acid development could not be prevented in the membrane reactor (30-45% *trans* fatty acids at IV= 80). In the slurry reactor, however, the fatty acid content was only 12 % at IV= 80. This was ascribed to the different hydrogen supply in slurry and membrane reactor. Furthermore, pore blocking of the membrane was a problem, particularly at the end of the reaction. The performance of the fat hardening process in the pore-flow-through-membrane reactor was considered not to be appropriate as no improvement in the product composition was obtained and technical problems complicate the hydrogenation process.

Further selective hydrogenation reactions in the membrane reactor are discussed in chapter 9. The partial hydrogenation of alkynes to alkenes proceeded well in the membrane reactor. The selectivity for the target products octene and styrene was 92-95 % and 80 %, respectively, at complete conversions of the alkynes. In the fixed bed reactor only selectivities of 76 % and <65 % were obtained under similar conditions.

The selective hydrogenation of geraniol, a terpenic allylic alcohol, to citronellol, an important product for flavors and fragrances, was tested. The experiments did not yield the expected results: as main product the saturated alcohol 3,7-dimethyloctanol was obtained. Furthermore, severe deactivation of the catalytic membranes by pore blocking interfered with the reaction.

The selective hydrogenation of cinnamaldehyde, an α,β-unsaturated aldehyde, was investigated with a Pd/alumina membrane and was compared to other Pd/alumina catalysts (egg shell, full and powder catalysts). With the membrane as catalyst support the reaction was carried out with selectivities of 80 % for the saturated aldehyde 3-phenylpropanal. The side product was the completely saturated alcohol 3-phenylpropanol. The unsaturated alcohol (cinnamylalcohol) was not obtained. The reaction rates were extremely lower than with an egg shell and a powder catalyst in a slurry reactor but similar to a full catalyst in the slurry reactor under the same reaction conditions. This was ascribed to a pronounced deactivation by fouling within the pore structure of the membrane and the porous full catalyst. The deactivation of the catalytic membranes is a disadvantage of the PFT-concept because of the unity of catalyst and membrane support. The replacement of catalytic membrane

capillary bundles after deactivation would be very expensive. The development of an easy and low-priced regeneration technique of the deactivated membranes is necessary.

The results in this work show that the application of a PFT-membrane reactor is beneficial when pore diffusion limitations have an impact on reaction kinetics. This is the case for fast reactions like the hydrogenation of alkadienes and alkynes. The control on selectivity for the desired product in the PFT-membrane reactor results in an efficient use of feedstock and in reduced energy costs by eliminating distillation or other separation steps. Furthermore, it was demonstrated that due to a good accessibility of the reactants to the active centers only small amounts of the catalytically active noble metal are required for acceptable reaction rates. On the other hand, energy cost for circulating the reactants by a pump and relatively high costs for the ceramic membrane supports have to be considered. For reactions where the reactants or the developed products tend to adsorb strongly on the catalyst as well as for reactant mixtures with high viscosities deactivation phenomena and pore blocking have to be expected. Methods to regenerate the deactivated catalytic membranes in-situ without dismantling the reactor still have to be developed. Thinkable are closed loops in the reactor system in which the membranes are regenerated (e. g. by rinsing them with a solvent or H_2O_2-solution) while the process is directed to a loop with a new or regenerated membrane.

11 Appendix

11.1 Chemicals

- α-Al_2O_3 capillary membranes (Hermsdorfer Institut für Technische Keramik-HITK, Germany)
- Pd-(II)-acetate (98 %, Aldrich)
- $PdCl_2$ (99.9%, Alfa Aesar)
- NaCl (99.5, Fluka)
- $H_2PtCl_6 \cdot xH_2O$ (Aldrich)
- $RuCl_3 \cdot xH_2O$ (purum, Fluka)
- $NaH_2PO_2 \cdot H_2O$ (≥ 99.0 %, Fluka)
- toluene (≥ 99.5 %, Roth)
- n-heptane (≥ 99.5 %, Roth)
- 2-propanol (≥ 99.5, Roth)
- 1,5-cyclooctadiene (99 %, Aldrich)
- 1-octyne (97 %, Aldrich)
- phenylacetylene (≥ 97 %, Fluka)
- geraniol (98 %, Aldrich)
- cinnamaldehyde (99%, Fluka)
- sunflower oil (customary from local supermarket)
- hydrogen 5.0 (Messer Griesheim)
- Pd/α-Al_2O_3 egg-shell catalyst, 0.5 wt. % Pd, K-0242 (W. C. Heraeus GmbH)
- Pd/α-Al_2O_3 full catalyst, 0.5 wt. % Pd, K-0264 (W. C. Heraeus GmbH)

11.2 Equipment

Characterization of catalytic membranes:

- Flame atomic absorption spectroscope – AAS (Perkin Elmer 3500)
- Graphite furnace atomic absorption spectroscope (Perkin Elmer 1100B)
- Scanning electron microscope – SEM (Hitachi S-4000) with energy dispersive X-ray – EDX (IDFix, SamX)

Membrane reactor system:

- membrane reactor module (volume 50 ml, HITK, Germany)
- gear pump (BVP-Z, Ismatec)
- stirrer motor (Eurostar, IKA)
- magnetic stirrer head (MRK Mini 100, Buddeberg)
- thermostat (Polystat CC3, Huber)
- heating jacket (HT MC1, Horst GmbH)
- pressure transmitter (S-10, WIKA)
- digital thermometer (GTH 1170, Greisinger)
- O – rings, 50 x 2.5 mm and 2.75 and 1.6 mm, Viton and Kalrez (Westring)

Product analysis:

- gas chromatograph (Sichromat, Siemens) with column RTX5 MS (Restek)

Tab. 11.1.: Data of gas chromatograph

column	RTX 5 MS
	length: 30 m
	inner diameter: 0.25 mm
	layer thickness: 0.25µm
carrier gas	N_2, 1bar
detector gas	H_2, 0.6 bar
	air, 1.8 bar

Tab. 11.2.: Temperature programs for gas chromatography

Product	retention time [min]	oven temperature [°C]
1,5-cyclooctadiene	7.4 – 7.5	
cyclooctene	5.9 – 6.2 und 6.3 – 6.5	55, isotherm
cyclooctane	6.7 - 6.8	
1-octyne	5.9 – 6.6	
1-octene	4.9 – 5.0	40, isotherm
octane	5.1 – 5.5	
phenylacetylene	5.0 – 5.3	
styrene	5.4 – 5.6	60, isotherm
ethylbenzene	4.5 – 4.6	
geraniol	12.5 – 13.0	
citronellol	10.5 – 11.2	100, isotherm
3,7-dimethyloctanol	8.2 – 8.9	
cinnamaldehyde	12.0-13.0	5 min. isotherm at 60°C, with
cinnamylalcohol	15.0-16.0	a rate of 25°C at 125°C, 10
3-phenylpropanal	10.0-10.5	min. isotherm at 125°C
3-phenylpropanol	11.0-12.0	
linoleic acid methyl ester	58.0 – 60.0	
oleic acid methyl ester	60.0 – 62.0	
elaidic acid methyl ester	61.0 – 64.0	160, isotherm
stearic acid methyl ester	66.0 – 68.0	
palmitic acid methyl ester	25.0 – 28.0	

11.3 Simulation of COD kinetics by Berkeley Madonna

Simulation of COD hydrogenation at different initial COD concentrations at 50°C and 10 bar hydrogen pressure

```
KCOD=17.5e-03                ; equilibrium constant COD [m³/mol]
KCOE= 10e-03                 ; equilibrium constant COE [m³/mol]
KH=4e-03                     ; equilibrium constant hydrogen [m³/mol]
H=58                         ; saturation concentration of hydrogen [mol/m³]

INIT COD1= 410               ; initial COD concentration in exp.1 [mol/m³]
INIT COD2=820                ; initial COD concentration in exp.2 [mol/m³]
INIT COD3=610                ; initial COD concentration in exp.2 [mol/m³]
INIT COE1=0.1                ; initial COE concentration in exp.1 [mol/m³]
INIT COE2=0.1                ; initial COE concentration in exp.2 [mol/m³]
INIT COE3=0.1                ; initial COE concentration in exp.3 [mol/m³]

k1=0.108e03                  ; rate constant for COD hydrogenation [mol/gPd*min]
k2=0.002e03                  ; rate constant for COE hydrogenation [mol/gPd*min]

mcat=0.002                   ; Pd amount [gPd]
V=0.11e-03                   ;liquid volume [m³]
ccat=mcat/V                  ; catalyst concentration [gPd/m³]

d/dt(COE1)=ccat*k1*KH*H*KCOD*COD1/(1+KH*H+KCOD*COD1+KCOE*COE1)^2-
ccat*k2*KH*H*KCOE*COE1/(1+KH*H+KCOD*COD1+KCOE*COE1)^2
d/dt(COD1)=-(ccat*k1*KH*H*KCOD*COD1/(1+KH*H+KCOD*COD1+KCOE*COE1)^2)

d/dt(COE2)=ccat*k1*KH*H*KCOD*COD2/(1+KH*H+KCOD*COD2+KCOE*COE2)^2-
ccat*k2*KH*H*KCOE*COE2/(1+KH*H+KCOD*COD2+KCOE*COE2)^2
d/dt(COD2)=-(ccat*k1*KH*H*KCOD*COD2/(1+KH*H+KCOD*COD2+KCOE*COE2)^2)

d/dt(COE3)=ccat*k1*KH*H*KCOD*COD3/(1+KH*H+KCOD*COD3+KCOE*COE3)^2-
ccat*k2*KH*H*KCOE*COE3/(1+KH*H+KCOD*COD3+KCOE*COE3)^2
d/dt(COD3)=-(ccat*k1*KH*H*KCOD*COD3/(1+KH*H+KCOD*COD3+KCOE*COE3)^2)


X1=((410-COD1)/410)*100      ; COD conversion in exp.1  [%]
X2=((820-COD2)/820)*100      ; COD conversion in exp. 2 [%]
X3=((610-COD3)/610)*100      ; COD conversion in exp. 3 [%]

S1=COE1/(410.1-COD1)*100     ; COE selectivity in exp. 1 [%]
S2=COE2/(820.1-COD2)*100     ; COE selectivtiy in exp. 2 [%]
S3=COE3/(610.1-COD3)*100     ; COE selectivity in exp. 3 [%]

METHOD RK4                   ; integration method: Runge-Kutta
STARTTIME = 0
STOPTIME=100
DT =0.2                      ; integration time interval
```

Simulation of COD hydrogenation at different hydrogen pressures at 50°C and 0.41 mol/l initial COD concentration

```
KCOD=17.5e-03                ; equilibrium constant COD [m³/mol]
KCOE= 10e-03                 ; equilibrium constant COE [m³/mol]
KH=4e-03                     ; equilibrium constant hydrogen [m³/mol]
```

```
H1=12                    ; saturation concentration of hydrogen at 2 bar [mol/m³]
H2=29                    ; saturation concentration of hydrogen at 5 bar [mol/m³]
H3=58                    ; saturation concentration of hydrogen at 10 bar [mol/m³]


INIT COD1= 410           ; initial COD concentration at 2 bar [mol/m³]
INIT COD2=410            ; initial COD concentration at 5 bar [mol/m³]
INIT COD3=410            ; initial COD concentration at 10 bar [mol/m³]
INIT COE1=1              ; initial COE concentration at 2 bar [mol/m³]
INIT COE2=1              ; initial COE concentration at 5 bar [mol/m³]
INIT COE3=1              ; initial COE concentration at 10 bar [mol/m³]

k1=0.108e03              ; rate constant for COD hydrogenation [mol/gPd*min]
k2=0.002e03              ; rate constant for COE hydrogenation [mol/gPd*min]

mcat=0.002               ; Pd amount [gPd]
V=0.11e-03               ;liquid volume [m³]
ccat=mcat/V              ; catalyst concentration [gPd/m³]


d/dt(COE1)=ccat*k1*KH*H1*KCOD*COD1/(1+KH*H1+KCOD*COD1+KCOE*COE1)^2-
ccat*k2*KH*H1*KCOE*COE1/(1+KH*H1+KCOD*COD1+KCOE*COE1)^2
d/dt(COD1)=-(ccat*k1*KH*H1*KCOD*COD1/(1+KH*H1+KCOD*COD1+KCOE*COE1)^2)
d/dt(COE2)=ccat*k1*KH*H2*KCOD*COD2/(1+KH*H2+KCOD*COD2+KCOE*COE2)^2-
ccat*k2*KH*H2*KCOE*COE2/(1+KH*H2+KCOD*COD2+KCOE*COE2)^2
d/dt(COD2)=-(ccat*k1*KH*H2*KCOD*COD2/(1+KH*H2+KCOD*COD2+KCOE*COE2)^2)
d/dt(COE3)=ccat*k1*KH*H3*KCOD*COD3/(1+KH*H3+KCOD*COD3+KCOE*COE3)^2-
ccat*k2*KH*H3*KCOE*COE3/(1+KH*H3+KCOD*COD3+KCOE*COE3)^2
d/dt(COD3)=-(ccat*k1*KH*H3*KCOD*COD3/(1+KH*H3+KCOD*COD3+KCOE*COE3)^2)


X1=((410-COD1)/410)*100      ; COD conversion at 2 bar [%]
X2=((410-COD2)/410)*100      ; COD conversion at 5 bar [%]
X3=((410-COD3)/410)*100      ; COD conversion at 10 bar [%]

S1=COE1/(411-COD1)*100       ; COE selectivity at 2 bar [%]
S2=COE2/(411-COD2)*100       ; COE selectivity at 5 bar [%]
S3=COE3/(411-COD3)*100       ; COE selectivity at 10 bar [%]

METHOD RK4
STARTTIME = 0
STOPTIME=100
DT = 0.2
```

Simulation of COD hydrogenation at different initial COD concentrations at 40°C and 10 bar hydrogen pressure

```
KCOD=20e-03              ; equilibrium constant COD [m³/mol]
KCOE= 15e-03             ; equilibrium constant COE [m³/mol]
KH=7.4e-03               ; equilibrium constant hydrogen [m³/mol]
H=58                     ; hydrogen concentration [mol/m³]

INIT COD1= 410           ; initial COD concentration in exp. 1 [mol/m³]
INIT COE1=1              ; initial COE concentration in exp. 1 [mol/m³]
INIT COD2= 820           ; initial COD concentration in exp. 2 [mol/m³]
INIT COE2=1              ; initial COE concentration in exp. 2 [mol/m³]

k1=0.054e03              ; rate constant of COD hydrogenation [mol/gPd*min]
k2=0.00035e03            ; rate constant of COE hydrogenation [mol/gPd*min]
```

```
mcat=0.002                          ; Pd amount [gPd]
V=0.11e-03                          ;liquid volume [m³]
ccat=mcat/V                         ; catalyst concentration [gPd/m³]

d/dt(COE1)=ccat*k1*KH*H*KCOD*COD1/(1+KH*H+KCOD*COD1+KCOE*COE1)^2-
ccat*k2*KH*H*KCOE*COE1/(1+KH*H+KCOD*COD1+KCOE*COE1)^2
d/dt(COD1)=-(ccat*k1*KH*H*KCOD*COD1/(1+KH*H+KCOD*COD1+KCOE*COE1)^2)
d/dt(COE2)=ccat*k1*KH*H*KCOD*COD2/(1+KH*H+KCOD*COD2+KCOE*COE2)^2-
ccat*k2*KH*H*KCOE*COE2/(1+KH*H+KCOD*COD2+KCOE*COE2)^2
d/dt(COD2)=-(ccat*k1*KH*H*KCOD*COD2/(1+KH*H+KCOD*COD2+KCOE*COE2)^2)

X1=((410-COD1)/ 410)*100            ; COD conversion in exp.1 [%]
X2=((820-COD2)/ 820)*100            ; COD conversion in exp.2 [%]

S1=COE1/(411-COD1)*100              ; COE selectivity in exp. 1 [%]
S2=COE2/(821-COD2)*100              ; COE selectivity in exp. 2 [%]

METHOD RK4
STARTTIME = 0
STOPTIME=100
DT =0.2
```

Simulation of COD hydrogenation at different initial COD concentrations at 70°C and 10 bar hydrogen pressure

```
KCOD=17e-03                         ; equilibrium constant COD [m³/mol]
KCOE=9e-03                          ; equilibrium constant COE [m³/mol]
KH=1.1e-03                          ; equilibrium constant hydrogen [m³/mol]
H=58                                ; hydrogen concentration [mol/m³]

INIT COD1= 410                      ; initial COD concentration in exp. 1 [mol/m³]
INIT COE1=1                         ; initial COE concentration in exp. 1 [mol/m³]
INIT COD2= 820                      ; initial COD concentration in exp.2 [mol/m³]
INIT COE2=1                         ; initial COE concentration in exp. 2 [mol/m³]

k1=0.72e03                          ; rate constant of COD concentration [mol/gPd*min]
k2=0.0138e03                        ; rate constant of COE hydrogenation [mol/gPd*min]

mcat=0.002                          ; Pd amount [gPd]
V=0.11e-03                          ;liquid volume [m³]
ccat=mcat/V                         ; catalyst concentration [gPd/m³]

d/dt(COE1)=ccat*k1*KH*H*KCOD*COD1/(1+KH*H+KCOD*COD1+KCOE*COE1)^2-
ccat*k2*KH*H*KCOE*COE1/(1+KH*H+KCOD*COD1+KCOE*COE1)^2
d/dt(COD1)=-(ccat*k1*KH*H*KCOD*COD1/(1+KH*H+KCOD*COD1+KCOE*COE1)^2)
d/dt(COE2)=ccat*k1*KH*H*KCOD*COD2/(1+KH*H+KCOD*COD2+KCOE*COE2)^2-
ccat*k2*KH*H*KCOE*COE2/(1+KH*H+KCOD*COD2+KCOE*COE2)^2
d/dt(COD2)=-(ccat*k1*KH*H*KCOD*COD2/(1+KH*H+KCOD*COD2+KCOE*COE2)^2)

X1=((410-COD1)/410)*100             ; COD conversion in exp. 1 [%]
X2=((820-COD2)/ 820)*100            ; COD conversion in exp. 2 [%]

S1=COE1/(411-COD1)*100              ; COE selectivity in exp. 1 [%]
S2=COE2/(821-COD2)*100              ; COE selectivity in exp. 2 [%]

METHOD RK4
STARTTIME = 0
STOPTIME=100
DT = 0.2
```

11.4 Simulations of COD-hydrogenation in PFT- membrane reactor

```
%
%       saturation vessel   Recycle cr(t)
% Feed |----|----|<------------------------|
% ---->|    |    | M-Feed |----------|     |
% cf   |   o|o   |------->|membrane  |-----|
%      |--------|        |----------|     |------>
%         c0(t)              c(x,t)         product
%
% operational mode: semibatch or continuously
% Assumptions:
% - the whole liquid volume of the system is in the saturation vessel and
%   regarded as ideally mixed
% - constant liquid volume in the saturation vessel, i.e.
%   a) the optional feed- und product volume flows are identical
%   b) M-Feed = Feed + Recycle
% - capillary geometry: (da/di = 2.9/1.9 mm, length: 220mm)
% - no balancing of the gas phase in the saturation vessel, i.e.
%   the hydrogenation supply results from the H2-(partial) pressure, the
%   Henry-constant, the kla-value and the H2-concentration in the liquid
%   phase
% - the calculation is carried out quasi-stationary, the change of the
%   concentrations during passing the pores is determined by integration
%   over the average residence time
%   Following the concentration change in the saturation vessel is
%   calculated iteratively for a given time interval.

% Program by R. Dittmeyer, KWI/DECHEMA, Frankfurt

% Subprogram: rrate (concentration change of COD, COE, COA and H2)
%
% Capillary parameters
mCat = 1.0e-03;           % Pd-amount per capillary, g
por = 0.3;                % porosity of capillaries, -
Lm = 22.0e-02;            % active length of capillaries, m
dka = 2.9e-03;            % external diameter of capillaries, m
dki = 1.9e-03;            % inner diameter of capillaries, m
ageo = (dka+dki)/2*pi*Lm; % geometric surface of one capillary, m2
dp = 1.9e-06;             % pore diameter, m
ap = dp^2*pi/4;           % cross-sectional area of pore, m2
zahl = ageo*por/ap;       % number of pores per capillary, -
tau = 2.0;                % tortuosity factor of pores, -
Lp = (dka-dki)/2*tau;     % effective length of pores, m
Vp = Lp*dp^2*pi/4;        % effective volume of one Pore, m3
cCat = mCat/(zahl*Vp);    % Pd-amount in pore volume, g/m3

% circulation volume flow
recycle = 0.2e-03/1/60;  % m3/s (correspond to 0.2 L/min through 1
% capillary)

% Feed-volume flow (optional)
feed = 0.0e-09/60;        % m3/s (for continuous operation mode)

% volume flow from saturation vessel to membrane module
mfeed = recycle + feed;   % m3/s
```

```
% average flow velocity and residence time in the pores
w = mfeed/(ageo*por);     % flow velocity, m/s
vwz = Lp/w;               % residence time, s
tspan = linspace(0,vwz); % integration boundaries, s

% temperature
T = 273.15 + 50;          % K

% parameters of the saturation vessel
V = 0.116e-03;            % liquid volume, m3
P = 10*1.0e+05;           % gas pressure, Pa
kla = 1.5e-01;            % kla-value, 1/s
H = 6.6e-05;              % Henry-coeffizient, mol/m3Pa (DETHERM, H2 in n-
Heptan, 50°C)
cf = [410.0 0 0 0];       % feed concentrations and initial concentrations
in saturation vessel, respectively
% (COD, COE, COA, H2), mol/m3 (given values, the hydrogen concentration is
determined iteratively
% transfer of initial concentrations
c0 = cf;                  % in saturation vessel, mol/m3
cr0 = cf;                 % in circulation, mol/m3

% options for ODE-integration routine
options = odeset('RelTol',1.0e-05); % rel. accuracy

% parameters for determination of H2-concentration in circulation at t = 0
lim = 1.0e-06;
change = 1;

% parameters for time loop
j = 1;            % counter for tp
js = 1;           % counter for tps
tp(j) = 0;        % starting point, s
tps(j) = 0;       % starting point, s
cp(j,1:4) = c0;   % concentration in saturation vessel at t = 0, mol/m3
tpmx = 80;        % end point of time loop, min (given endpoint of
calculation)
dt = 0.2;         % time interval for integration, s (given desired time
pattern)
jd = 10;          % time interval for surface-plot, s (given time pattern
for the 3-D-Plot of the H2-concentration, figure 3)

% initialization of the display of processing progress
h = waitbar(0,'Integration läuft...');

% loop for determination of H2-concentration in circulation at t = 0
while (change > lim)
  % concentration at outlet of saturation vessel, mol/m3
  c0(1:3) = (feed*cf(1:3) + recycle*cr0(1:3))/mfeed;
  c0(4) = (recycle*cr0(4) + feed*cf(4) + V*kla*P*H)/(recycle + V*kla);
  % concentration profile along the pore in membrane modul, mol/m3
  [t,c] = ode45(@rrate,tspan,c0,options,T,cCat);
  % new concentration in circulation, mol/m3
  cr = c(length(t),:);
  % criterion of abort
  change = abs(cr(4)-cr0(4))/cr(4);
    % transfer of values H2-concentration in circulation at t = 0
  cr0(4) = cr(4);
end

% save concentration profile at t = 0 in array cxt
```

```
cxt = c(:,4);
 % translation of (residence-) time- in coordinate of space (pore)
x = w*t;

% loop for calculation of time dependent concentration progress in
saturation vessel
while (tp(j) < tpmx)

  % update of concentrations in saturation vessel (Euler-method, time step
  dt)
  c0(1:3) = c0(1:3) + dt*(recycle*cr(1:3) - mfeed*c0(1:3) +
  feed*cf(1:3))/V;
  c0(4) = c0(4) + dt*(recycle*cr(4) - mfeed*c0(4) + V*kla*(P*H-c0(4)))/V;

  % transfer of values
  tp(j+1) = j*dt/60;      % time, min
  cp(j+1,1:4) = c0(1:4); % concentrations, mol/m3
  j = j+1;               % array index

  % concentration profile along the pore in membrane modul, mol/m3
  [t,c] = ode45(@rrate,tspan,c0,options,T,cCat);

  % update of concentrations in circualtion, mol/m3
  cr = c(length(t),:);

  % save concentration profile in cxt (only every jd/j-te value)
  if (j/jd - round(j/jd)) == 0
      tps(js+1) = tp(j);
      cxt(:,js+1) = c(:,4);
      cxt1(:,js+1) = c(:,1);
      js = js + 1;
  end

  % display of processing progress
  ff = tp(j)/tpmx;
  waitbar(ff);
end

% close display of processing progress
close(h);

% calculation of COD-conversion and COE- and COA-selectivity, respectively
im = length(tp);

% conversion and selectivity at t = 0
X(1) = 0;
S(1,1) = 1;
S(2,1) = 0;

% conversion and selectivity at t > 0
for i=2:im
    X(i) = 1 - cp(i,1)/cp(1,1);                    % conversion
    S(i,1) = (cp(i,2)-cp(1,2))/(cp(1,1)-cp(i,1)); % selectivity COE
    S(i,2) = (cp(i,3)-cp(1,3))/(cp(1,1)-cp(i,1)); % selectivity COA
end
```

```
% experimental data at 50°C, 10 bar, 5 vol.% COD, 200 mL/min circulation
rate, 1 mg Pd
t_exp = [0   5        10        15          20      25         30       35
40          45          50          55          60          65          70
75          80          85];
X_exp = [0  15.1471  28.60063  39.99395    50.2343 59.70118   65.91496
72.56648    77.51747    81.63237    84.85837    87.36546    89.20646
91.09855    91.74578    94.76402    96.79627    98.62901];
S_exp = [100 100     98.56699  98.27591    98.33   98.3206    98.37415
98.01031    97.84158    97.83559    97.56711    97.14442    96.89359
96.83565    96.71357    95.79045    95.35157    94.87703];

% experimental data at 50°C, 10 bar, 5 vol.% COD, 80 mL circulation rate,
1.5 mg Pd
%t_exp = [0 5   10  15  20  25  30  35  40  45  55  75];
%X_exp = [0     37.42645    56.44583    73.74744    84.94952    92.10639
95.72552    97.64941    97.64941    98.6808     99.14803    99.7421];
%S_exp = [100   99.01866    98.99401    98.81946    98.46142    97.86242
97.15662    96.39207    96.39207    95.58534    94.78259    93.18809];

% experimental data at 50°C, 10 bar, 5 vol.% COD, 100 mL/min, 1.5 mg Pd
%t_exp = [0  5  10  15  20  25  30  35  40];
%X_exp = [0  34.81207   60.75131    77.56301  88.25474  94.12301
97.13846    98.63911    100];
%S_exp = [100 100       99.99998    100       98.08519  97.30902
96.36092    95.28537    94.08072];

% experimental data at 50°C,10 bar,5 vol.% COD, 120 mL/min,1.5 mg Pd
%t_exp = [0 5   10  15  20  30  40];
%X_exp = [0  48.29326   75.32277    89.50467    95.53804    99.15152
100];
%S_exp = [100 98.65288  98.72468    97.95959    96.99201    94.52355
93.75218];

% experimental data at 50°C,10 bar, 5 vol.% COD, 260 mL/min, 1.5 mg Pd
%t_exp = [0 5   10  15  20  25  30  35];
%X_exp = [0  62.32053   83.88208    97.55291    98.82424    99.1426
99.56581    99.59956];
%S_exp = [100 98.9029   98.26957    96.49229    95.63672    95.12619
94.41832    93.75165];

% experimental data at 50°C, 10 bar, 5 vol.% COD, 200mL/min,1.5 mg Pd
%t_exp = [0  5   10  20  30];
%X_exp = [0  40.21607    84.71086   97.33359    98.99994];
%S_exp = [100 99.11672125 97.5068604    93.89932088 91.44895441];

% experimental data at 50°C, 10 bar, 5 vol.% COD, 200 mL/min, 0.7 mg Pd
%t_exp = [0  5  10  20  30  40  50  60  70  80  90  100];
%X_exp = [0  12.39176 19.12787    31.1582 39.38668     46.80288
53.76894    56.91425    63.36806    68.28723    73.26919    76.86181];
%S_exp = [100 100     99.99994772 100     99.00156601  98.68206828
98.51918226 98.2666204  98.11294523 97.91272834 97.78288801 97.5842099];


% graphical display of the results
% plot 1: concentration profile versus time
figure(1)
plot(tp,cp(:,1),tp,cp(:,2),tp,cp(:,3),tp,cp(:,4))
xlabel('t (min)')
ylabel('c (mol/m3)')
legend('COD','COE','COA','H_2')
```

```
grid on

% plot 2: conversion and selectivity versus time
figure(2)
plot(tp,X,tp,S(:,1),tp,S(:,2), t_exp, X_exp/100, t_exp, S_exp/100)
xlabel('t (min)')
ylabel('X, S (-)')
legend('X','S_{COE}','S_{COA}','X (COD,exp)', 'S (COE,exp)' )
grid on

% plot 3: H2-profile in the pore
figure(3)
surfc(tps,x,cxt)
shading interp
colormap jet(128)
colorbar
title('c(H_2) (x,t)')
xlabel('t (min)')
ylabel('x (m)')
 function Ri = rrate(t,c,T,cCat)

% subroutine for definition of kinetics of COD-hydrogenation for program
pft.m
% input variables
% c: concentrations in liquid phase, mol/m3
%    order: COD, COE, COA, H2
% T: temperature
% cCat: catalyst concentration (relating to the pore volume), g/m3

% (implemented are the reaction rate constants at 50°C)

% overall gas constant, J/molK
R = 8.314;
rti = 1/(R*T);

% reaction 1: COD + H2 -> COE
% reaction 2: COE + H2 -> COA

E1 = 0.0e+00;                    % activation energy reaction 1, J/mol
E2 = 0.0e+00;                    % activation energy reaction 2, J/mol
k1 = 0.0017e+03*exp(-E1*rti);    % rate constant 1, m3gPd/mol
k2 = 0.000034e+03*exp(-E2*rti);  % rate constant 2, m3gPd/mol

KCOD = 17.5e-03; % adsorption constant COD, m3/mol
KCOE = 10.0e-03; % adsorption constant COE, m3/mol
KH2 = 4.0e-03;   % adsorption constant H2, m3/mol

% reaction rates, mol/m3s
r1 = cCat*k1*KCOD*c(1)*KH2*c(4)/(1+KCOD*c(1)+KCOE*c(2)+KH2*c(4))^2;
r2 = cCat*k2*KCOE*c(2)*KH2*c(4)/(1+KCOD*c(1)+KCOE*c(2)+KH2*c(4))^2;

% rate of concentration change, mol/m3s
Ri = [-r1; r1 - r2; r2; -r1 - r2];
```